Original Article

Network analyses unveil ageing-associated pathways evolutionarily conserved from fungi to animals

Jérôme Teulière[1], Charles Bernard[1], Eduardo Corel[1], François-Joseph Lapointe[2], Johannes Martens[3], Philippe Lopez[1], and Eric Bapteste[1]*

[1]Institut de Systématique, Evolution, Biodiversité (ISYEB), Sorbonne Université, CNRS, Museum National d'Histoire Naturelle, EPHE, Université des Antilles, Paris, France

[2]Département de Sciences Biologiques, Complexe des Sciences, Université de Montréal, Montréal, QC, Canada

[3]Sciences, Normes, Démocratie (SND), Sorbonne Université, CNRS, Paris, 75005, France

*Corresponding author : Eric Bapteste, eric.bapteste@mnhn.fr

Keywords: Protein-Protein Interaction, longevity, senescence, antagonistic pleiotropy, phylosystemics, Evolution of ageing

Abstract

The genetic roots of the diverse paces and shapes of ageing and of the large variations in longevity observed across the Tree of Life are poorly understood. Indeed, pathways associated with ageing/longevity are incompletely known, both in terms of their constitutive genes/proteins and of their molecular interactions. Moreover, there is limited overlap between the genes constituting these pathways across mammals. Yet, dedicated comparative analyses might still unravel evolutionarily conserved, important pathways associated with longevity or ageing. Here, we used an original strategy with a double evolutionary and systemic focus to analyse protein interactions associated with ageing or longevity during the evolution of five species of Opisthokonta. We ranked these proteins and interactions based on their evolutionary conservation and centrality in past and present protein-protein interaction networks (PPI), providing a big systemic picture of the evolution of ageing and longevity pathways, that identified which pathways emerged in which Opisthokonta lineages, were conserved and/or central. We confirmed that longevity/ageing associated proteins (LAPs), be they pro- or anti-longevity, are highly central in extant PPI, consistently with the Antagonistic Pleiotropy theory of ageing, and identified key antagonistic regulators of ageing/longevity, 52 of which with homologs in humans. While some highly central LAPs were evolutionarily conserved for over a billion years, we report a clear transition in the functionally important components of ageing/longevity within Bilaterians. We also predicted 487 novel evolutionarily conserved LAPs in humans, 54% of which are more central than mTOR, and 138 of which are druggable, defining new potential targets for anti-ageing treatments in humans.

Introduction

Ageing and longevity are critical components of organismal fitness, both characterised by their remarkable heterogeneity between, and sometimes even within, species across the Tree of Life. For instance, there is a 100-fold variation of longevity across mammals (Tacutu et al. 2018), and studies have revealed a diversity of paces and shapes of ageing across metazoans, even though all these taxa come from a last common ancestor (Baudisch and Vaupel 2012; Jones et al. 2014; Treaster et al. 2021; da Silva et al. 2022). Importantly, the genetic mechanisms that contribute to this heterogeneity are still poorly understood. While there is no doubt that ageing and longevity are in part genetically determined (Kenyon 2010), the pathways associated with ageing and longevity are incompletely known, both in terms of their constitutive genes/proteins and of their molecular

interactions. Indeed, genomic and transcriptomic analyses of organisms with high quality genomes, informed by careful considerations of molecular evolution, have uncovered sets of genes associated with ageing or longevity (Li and de Magalhães 2013; Gorbunova et al. 2014; Keane et al. 2015; Doherty and de Magalhães 2016; Foley et al. 2018; Sahm et al. 2018; Huang et al. 2019; Toren et al. 2020; Farré et al. 2021; Irving et al. 2021; Kacprzyk et al. 2021; Kolora et al. 2021; Orkin et al. 2021; Lu et al. 2022; Tejada-Martinez et al. 2022) with little overlap, even across mammalian species (Farré et al. 2021). This observation of a diversity of genetic bases of longevity and ageing across species is consistent with Darwinian theory, which predicts that longevity can be selected for, yet does not imply that homologous genes should be involved in longevity in different populations or species. Like extant organismal lineages, whose members thrive in very diverse environments and niches, members from ancestral organismal lineages from different clades and from different populations were not all exposed to the same ecological challenges during the course of evolution. For example, some organisms belong to lineages that can fly, while others can live in caves, or must face their predators on the ground (Lunghi and Bilandžija 2022). Similarly, some organisms are solitary, whereas other live in societies (Keller and Genoud 1997), and evolution of their longevities and ageing can thus be affected by social organisation and kin selection, etc. Such differences in past and present selective pressures likely explain the considerable variations in ageing and longevity observed throughout the Tree of Life, and since the effect of each gene variant on the longevity in individual species can be small, as is the case for humans (Singh et al. 2019) different combinations of different genes are possibly associated with the variability of lifespan within and between species.

More precisely, mainstream evolutionary theories of ageing, namely the Mutation Accumulation theory (MA) (Medawar 1952), the Antagonistic Pleiotropy theory (AP) (Williams 1957) and the Disposable Soma theory (DS) (Kirkwood and Holliday 1979), hold that ageing is not genetically programmed *per se* but occurs as a side-effect due to the existence of a selection shadow (Johnson et al. 2019). As a result, AP and MA do not make strong predictions regarding whether the same genes should be collaterally associated with ageing across populations and species, while DS predicts that the functions of the genes associated with ageing are likely related with repair/maintenance and energy allocation to trade-offs between reproduction and survival, mediated by a network of interacting, possibly synergistic processes, rather than by a single mechanism (Kirkwood 1997). In addition, reknown experts on aging consider that aging is a programmed process (Rando and Chang 2012). While more aging-associated genes or proteins than appreciated could be conserved (consistent with either AP theory or programmed theory), this is

not necessarily the case for longevity. Thus, although theoretically plausible, the limited overlap in genes associated with ageing and longevity across species nonetheless raises important conceptual and practical challenges (Farré et al. 2021). On the one hand, this limited overlap may reflect some limits of current methods of detection of longevity- and ageing-associated genes. On the other hand, this genetic heterogeneity does not preclude a form of functional unity at a higher level than genes: even though different gene families are associated with longevity or ageing across species, some belong to pathways (e.g. proteostasis, immune and inflammatory response, hemostasis, development, metabolism) that appear to be shared across species (Muntané et al. 2018; Farré et al. 2021; Treaster et al. 2021).Therefore, updated or enhanced comparative analyses may still unravel evolutionarily conserved pathways associated with longevity or ageing. To reach this goal, however, technical developments that enhance the predictive power of genomics and comparative genomics to detect longevity- and ageing- associated genes appear warranted.

Around twenty years ago, several pioneering ageing studies focusing on interactome data (e.g. (Promislow 2004; Ferrarini et al. 2005; Witten and Bonchev 2007; Fortney et al. 2010)) seeded an original path in this direction. They sought to identify not only the molecular components of pathways associated with ageing and longevity, but also the molecular interactions that compose these pathways. In brief, these approaches relied upon prior experimental evidence defining sets of genes associated with longevity or ageing, hereafter called longevity-associated genes (LAGs), such as those forming the mTOR nutrient-sensing signalling network (Kenyon 2010; Templeman and Murphy 2018; Papadopoli et al. 2019). mTOR is noteworthy because it has been shown to regulate many ageing-associated processes (including cellular senescence, immune responses, stem cell regulation, autophagy, mitochondrial function, and proteostasis) and to mediate caloric restriction-induced lifespan extension in model organisms. For some species, LAGs were further classified as pro- or anti-longevity (pro-LAG, anti-LAG), according to the altered lifespan phenotypes resulting from their genetic loss or gain of function in model organisms (Kenyon 2010; Tacutu et al. 2018). These phenotypic labels were then conjugated with additional, independent information from interactome databases (Szklarczyk et al. 2019) to perform protein-protein interaction networks (PPI) analyses with a focus on ageing and longevity associated pathways. Specifically, the topology of PPI of a few extant species was analysed to track the interactions between longevity-associated proteins (LAPs) (e.g. proteins encoded by LAGs) in order to determine the pathways to which these LAPs connected, and whether the patterns of connection of these LAPs presented distinctive topological features that could be exploited to predict additional components of longevity/ageing associated pathways using PPI. Owing to the paucity of the data,

these pioneering studies were generally conducted on one or two species, with a limited number of network metrics (Promislow 2004; Ferrarini et al. 2005; Budovsky et al. 2007; Bell et al. 2009; Wang et al. 2009; Zhang et al. 2016). Nonetheless, they made for stimulating findings. LAPs from model organisms (*Saccharomyces cerevisiae*, *Sc* and *Drosophila melanogaster*, *Dm*) were shown to be central, connected nodes in PPI networks. In particular, LAPs displayed higher node degree (the number of connections per node in the network) than other proteins not proposed to be associated with ageing or longevity (non-LAPs). Such a high connectivity was interpreted as a proxy for the functional pleiotropy of LAPs, in support of the AP theory (Promislow 2004), considering that, as more highly connected proteins tend to be more pleiotropic than expected by chance, these proteins will also be most likely to evolve an association with senescence. Indeed, by chance alone, more pleiotropic proteins are more likely to have some of their effects found at different ages, and that some of these hold opposite consequences on fitness. This idea that AP is a general principle of ageing was also brought forward in (Yanai et al. 2017). Moreover, the high centrality of LAPs in PPI was proposed as evidence that LAPs regulate fundamental biological processes (Fernandes et al. 2016; Tacutu et al. 2018). In addition, pro- and anti-longevity proteins were shown to be intertwined in the interactome of the worm *Caenorhabditis elegans* (*Ce*), with only few significant topological differences between their subnetworks, which represented two sets of interactions with opposing effects on longevity (Fernandes et al. 2016). The interactions between LAPs and non-LAPs in PPI were also a source of important findings. Interactions between LAPs and proteins encoded by age-related diseases (ARD) genes (Tacutu et al. 2011) and cancer genes (Budovsky et al. 2007; Bell et al. 2009; Budovsky et al. 2009; Wang et al. 2009; Zhang et al. 2016) unraveled connections between their respective pathways, hinting at mechanistical connections between some aspects of ageing and some diseases. Furthermore, using LAPs as reference nodes and mining PPI of a few extant species for non-LAP nodes with comparable topological properties than LAPs, allowed some authors to propose subsets of noteworthy non-LAP proteins that may contribute to presently unidentified ageing- or longevity-associated pathways in *Hs*, *Sc*, *Ce* and *Dm* (de Magalhães and Toussaint 2004; Managbanag et al. 2008; Tacutu et al. 2012; Wuttke et al. 2012; Avelar et al. 2020).

While powerful, the predictive approaches mentioned above did not systematically determine how critical for ageing/longevity their predicted candidate LAPs are, and did not fully exploit their comparative potential. Here, we developed evosystemics analyses of PPI (Watson et al. 2020) to uncover important, evolutionary conserved ageing associated pathways, i.e. pathways made of proteins with significant possible effects on ageing/longevity. We relied upon two non-

mutually exclusive criteria to rank proteins and protein interactions as critical to understanding ageing/longevity: their high evolutionary conservation across Opisthokonta, a one-billion-year-old clade, encompassing fungi and animals, and their high centrality in extant and/or ancestral protein interaction networks. Through systematic analyses of the topological properties of LAPs within such neworks and through guilt-by-association analyses, we characterised central evolutionarily conserved pathways associated with ageing/longevity and predicted novel central, evolutionarily conserved LAPs in five Opisthokonta species (*Dm*, *Ce*, *Sc*, with *Mus musculus*, *Mm*, and *Homo sapiens*, *Hs*), some of these non-LAPs that we here proposed as new LAPs were supported by independent bibliographical validation. Promisingly, 265 of these 487 predicted additional LAPs are more central than mTOR in the human interactome and dominated by ribosomal proteins and ubiquitination pathways. Moreover, 28.3 % of the proteins predicted to hold important roles in longevity or ageing-associated pathways in humans are druggable, defining targets for potential novel anti-ageing treatments in humans in the short-term.

Results and Discussion

Theoretical pay-offs of evosystemic PPI analyses

Evosystemics jointly analyses evolutionary and topological signals (Watson et al. 2020). High evolutionary conservation across five species of Opisthokonta and high centrality in PPI (as defined in Figure S1A-D) provide two non-mutually exclusive criteria to rank proteins and protein interactions as critical to understanding ageing/longevity. On the one hand, highly conserved proteins and proteins interactions indicate homologous mechanisms, deeply rooted in the biology of Opisthokonta, which can therefore be experimentally studied in non-human species with potential translational payoffs. Likewise, highly central proteins contribute to interactions across many pathways and/or within large molecular machineries. Thus, changes in the genes coding such central proteins (or changes in their regulations) are likely to have strong impacts on many interconnected processes. Because evolutionarily conserved proteins are encoded by gene families with long time of residency within lineages, evolutionarily conserved proteins have had more opportunities to get involved into diverse functional partnerships, and are often expected to be more central in PPI than proteins from more recently evolved gene families (Bapteste and Huneman 2018). Consequently, uncovering i) highly central proteins and ii) evolutionarily conserved proteins

and interactions associated with ageing/longevity in PPI could identify critical pathways associated with longevity or ageing and suggest important targets to medically interfere with the ageing/longevity process, which could be validated across a broad range of species.

LAPs are highly central across PPI of five extant species of Opisthokonta

Our study used multiple stringency thresholds for PPI networks based on interaction confidence scores, a broader selection of Opisthokonta (*Sc*, *Ce*, *Dm*; *Mm* and *Hs*) and more network metrics (e.g. betwenness, closeness, degree, PageRank, Fig. S1A-D) than former PPI analysis on ageing/longevity (Promislow 2004; Ferrarini et al. 2005; Budovsky et al. 2007; Bell et al. 2009; Wang et al. 2009; Zhang et al. 2016). We used these different metrics, as, although often correlated in real networks, they could have captured slightly different aspects of network centrality. In our study, it turned out that irrespective of what specific network centrality was measured, the general conclusion regarding the centrality of LAPs is the same and generalises two previous findings derived from single species longevity networks. First, across the five tested species of Opisthokonta, LAPs are significantly more central in PPI than non-LAPs. This higher centrality was observed at various stringency thresholds, but limited by network size and the number of identified LAPs at high stringency for *Dm*, *Mm* and *Ce* (Fig. 1). This result, compatible with the AP theory (Promislow 2004; Ferrarini et al. 2005), is true for both pro-LAPs and for anti-LAPs (Fig. S2), with the same dependence on stringency, network size and number of identified LAPs; however, the imbalance between pro- and anti-longevity annotations in *Sc* (13% and 87% of the 400 *Sc* annotated ageing-associated proteins, respectively) may lead to a less robust signal of centrality for pro-longevity proteins. Accordingly, pro- and anti-longevity proteins appeared equally central in longevity networks across these five species of Opisthokonta (Fig S2). A few notable exceptions were found for experimental networks of *Sc*, possibly due to the imbalance mentioned above, and for *Ce*, where pro-longevity proteins displayed significantly higher centrality than anti-longevity proteins. The *Ce* observation is consistent with previously described higher clustering coefficient of pro-longevity proteins in the BioGrid PPI network (Fernandes et al. 2016).

Interestingly, pro-LAPs tend to interact significantly more with pro-LAPs whereas anti-LAPs tend to interact significantly more with anti-LAPs, both in entire interactomes (featuring both LAP and non-LAP nodes) and in longevity networks (featuring only LAPs as nodes) (Fig. 2, S3A), as determined by assortativity analyses and network permutation tests (Fig. S4). But this observation does not mean that there is a neat partition between pro-LAPs and anti-LAPs in the

PPI, since overall, the assortativity (Fig. S1E) values are only slightly positive (Fig. 2). In other words, interacting LAPs with antagonistic effects are widespread in PPI, suggesting that ageing and longevity associated pathways are commonly regulated by a diversity of checks and balances with opposite effects. However, remarkably, some pro-longevity and anti-longevity proteins entertain, in all analysed species, significantly more interactions with one another than expected by chance. It is interesting that our results identified differential correlations between pro-LAP and anti-LAP proteins, because this suggests that these two classes might indeed be biologically distinct, which was not necessarily obvious. Indeed, many of these pro-LAP and anti-LAP were identified by experiments that knock out genes and observe the effect on aging, whereas in nature more subtle variations in expression than a complete turn-off are likely to affect these genes, with effects that can both increase and decrease lifespan, depending on the specific expression changes for a given gene. Bearing this note of caution in mind, we propose that such LAPs, significantly strongly involved in interactions with proteins with opposite effects on longevity, correspond to key regulators in antagonistic regulatory mechanisms of longevity (ARMLs).

Three species harbor key antagonistic regulators of ageing/longevity

Using network permutation tests (Fig. S4), we found that three species displayed significantly stronger connections between pro-LAP and anti-LAP than what would be expected by chance, suggesting that such LAPs may be critically involved in the regulation of ageing/longevity (Fig. 3). Namely, we identified 13 LAPs involved in ARMLs in *Dm*; 38 in *Ce* and 40 in *Sc*. Several of these LAPs are homologs found in all three species and contribute to the mTOR signalling network, including mTOR itself (*Dm* Tor/*Ce* LET-363/*Sc* TOR1), but also the AGC kinases Akt (mTORC1 upstream activator and mTORC2 target: *Dm* Akt1, *Ce* AKT-1) and S6k (mTOR substrate: *Dm* S6k, *Sc* SCH9). As these LAPs are well-characterised for their key role in regulating ageing (Kenyon 2010; Templeman and Murphy 2018; Papadopoli et al. 2019), this observation provides proofs of concept that our approach can identify key antagonistic regulators. *Dm* and *Ce* also share the insulin/mTOR signalling network members PTEN phosphatase (*Dm* Pten/*Ce* DAF-18), Insulin receptor (*Dm* InR/*Ce* DAF-2), FOXO transcriptional regulator (*Dm* foxo/*Ce* DAF-16) and the NAD+-dependent protein acetylase sirtuin Sir2 (*Dm* Sir2/*Ce* SIR-2.1), whereas *Ce* and *Sc* share NAD+-reducing enzymes of the TCA cycle malate dehydrogenase and isocitrate dehydrogenase (*Ce* MDH-2/*Sc* MDH1/MDH2; *Ce* IDH-1/*Sc* IDH1). The existence of homologous key antagonistic regulators across Opisthokonta species supports the idea that

modulating lifespan has been evolutionarily important for at least a billion year and has occasionally relied on the same players, from fungi to animals.

In addition, we identified some LAPs (*Dm*: 3/13; *Ce*: 20/38; *Sc*: 23/40) involved in species-specific ARMLs with a comparable number of antagonistic interactions as emblematic mTOR network members, including, for example, the oxidative stress response protein Keap1, the cardiac-restricted actin-binding protein Vinc and the JNK phosphatase puc in *Dm* (Fig. 3A), which suggests that regulation by these LAPs may deserve careful investigations.

Overall, functions enriched in ARMLs in *Ce* and *Dm* correspond to functions described for proteins in the mTOR/Insulin network, such as stress response, regulation of translation, of regulated cell death and of growth and development (Fig. S5). Functions related to respiration were also enriched among *Ce* and *Sc* ARMLs: TCA cycle in *Ce* and Sc, ATP synthesis and mitochondrial electron transport chain in *Sc*. Finally, *Sc* ARMLs also displayed enrichment for chromatin regulation and DNA integrity checkpoint functions.

Strikingly, 52 ARML nodes and their associated interactions appear evolutionarily conserved at the taxonomic scale of Opisthokonta and can be found in humans, corresponding to 58% of these antagonistic regulators found either in *Ce*, *Dm* and *Sc*. These candidate antagonistic regulators of ageing/longevity in humans are associated with 5-14% of evolutionarily conserved interactions (depending on PPI stringency). Although genes are only seldom annotated as pro- or anti-longevity in humans, association with longevity can be inferred by genome-wide association studies (GWAS) as recorded in the LongevityMap database. Thus, among the 52 human homologs of ARMLs identified in *Dm*, *Ce* and Sc, we found 4 proteins (3 mTOR network members: AKT3, MTOR, RPS6KB1, and SOD2) that are significantly associated with long life in our species. Therefore, 48 other human genes may act as critical, evolutionarily conserved regulators of longevity/ageing in our species. Interestingly, 3 proteins (SOD2, ALDH2, PRKAA2) are also associated with ageing-related diseases (ARD) and can be targeted by drugs (Table 1).

Functional analyses of highly central LAPs

Unveiling highly central LAPs in 'longevity PPI', exclusively composed of LAPs, can point to especially critical components of ageing/longevity pathways. Indeed, by knowing these most central LAPs amongst the LAPs, one can focus on some ageing phenotypes that point to (the

expression of) important (central) proteins, at high risk of negatively affecting organismal or cellular homeostasy, or point to adaptations to longevity involving extremely deep structural components, i.e., the most highly central proteins of the interactome.

We analysed the functions of those LAPS by ranking LAPs by their centrality and by identifying high centrality outliers amongst LAPs in each extant longevity network, using network permutation tests (Fig. S4). Such high centrality outliers were found at all stringency thresholds, including in experimental networks, and their numbers unsurprisingly decreased with stringency (Fig. 4). As expected, many functions enriched among most central LAPs correspond to mTOR/Insulin signalling network-associated functions (Fig. S6), including maintenance/repair mechanisms, oxidative stress response, cell growth or autophagy (although Tor itself did not contribute to the top 20 most enriched functions among *Dm* centrality outliers).

In Bilateria, other signalling pathways involved in development and homeostasis, crosstalking with the mTOR network, were also found within centrality ouliers, including MAPK (*Ce*: LET-23, LET-60, SEM-5, MPK-1, JNK-1; *Dm*: p38b, bsk; *Hs*: ERBB2, EGFR, GRB2, HRAS, MAPK3, MAPK14 and various growth factors), TGFbeta (*Dm*: dpp), Wnt (*Ce*: BAR-1, *Hs*: GSK3B, CTNNB1), Notch (*Ce*: GLP-1), JAK/STAT (*Hs*: JAK2, STAT5B, STAT3, NFkB (*Hs*: RELA, NFKB1), AR (*Hs*: AR) and TP53 (*Hs*: TP53, MDM2, TP53BP1; *Mm*: Trp53, Trp53bp1) signalling pathways. Highly central proteins from these signalling pathways contributed to the enrichment in the same functions as the mTOR network, e.g. MAPK signalling through p38 and JNK was associated with response to stress functions. The above results are compatible with the idea that aspects of ageing and longevity are connected to developmental programs, as well as with claims that some developmental processes can provoke ageing when they are active late in life, executing detrimental quasi-programs due to selection shadow (Blagosklonny 2006; Gems 2022). Besides signalling-associated functions, most central LAPs also displayed enrichment for ribosome biogenesis/protein translation, cellular respiration (ATP synthesis/ mitochondrial electron transport chain/TCA cycle functions) in *Ce* and *Sc*, telomere regulation in *Hs* and *Sc*, and regulated cell death in *Mm* and *Hs* (Fig. S6).

Interestingly, some highly central LAPs belonged to the same orthology family and were consistently recovered as highly central across 3 or 4 different Opisthokonta species (Fig. 4). These conserved centrality outliers were less frequently found in experimental networks, which is likely explained by their small size compared to the thresholded networks (with the exception of *Sc*).

These highly central, evolutionarily conserved LAPs were mTOR, AKT/S6K AGC kinases and PTEN homologs, all acting in the mTOR/Insulin signalling network, as well as the homologs for the oxidative stress regulators superoxide dismutase 2 and catalase, and for the protein acetylase sirtuin2.

Progressive changes in enriched ageing/longevity associated functions during Opisthonkota history

We next turn towards a more systematic analysis of the evolutionary conservation of LAPs and their pathways by analysing ancestral PPI of five species of Opisthokonta. We inferred ancestral PPI networks throughout the phylogeny of these Opisthokonta (Fig. S7) to identify which pathways, implementing which functions, had emerged in which lineages. These ancestral longevity networks are comprised only of nodes corresponding to orthogroups (Fig. S3B) and edges associated with ageing or longevity in at least two extant species. Such edges are important, either because they represent convergences in longevity networks (hinting at their possible functional importance) or because they were inherited from a common ancestor. Considering that possibility, we could infer the ancestral longevity networks composed by such edges by comparing extant longevity networks featuring only orthoproteins as nodes (obtained for increasing levels of stringencies, from PPI edge score >= 500 to the use of experimental edges only) (M&M). Given the small number of species, and the very large number of potential protein-protein interactions, one might worry that the likelihood of both false-positive and false-negative claims for deep evolutionary conservation of PPIs (i.e., both presence of and absence of conserved interactions) could be elevated. We verify this was not the case: using resampling of input PPI networks with networks from sister species of *Ce*, *Dm* or *Sc*, we found that this approach had a false positive rate of 0 for all resampled species, and a false negative rate, depending on PPI score thresholds, comprised between 0 and 3.7 % for *Ce* or *Dm* replacement, and between 8 and 16% for *Sc* replacement, indicating that our inferences of ancestral edges are conservative and that *Sc* networks have the most weight on the inference of the common ancestral network (M&M).

Consequently, we first used these ancestral networks to estimate the proportion of LAPs and their interactions from extant longevity networks that had already evolved in the past. These numbers reflect the proportion of LAPs and their interactions inherited in extant interactomes. Thus, a third of human LAPs and 7 % of their interactions date from ancestral interactomes of

Opisthokonta (Fig. 5). Moreover, extant ARMLs, e. g. 8 to 43% of the human ARML orthologs (Table 1) and 1 to 10 % of their extant interactions, depending on PPI stringency thresholds, can also be found in ancestral networks. Therefore, a phylogenetically broad range of organisms could still be used to experimentally highlight numerous mechanistic aspects associated with human ageing and longevity.

Second, we assigned a GO-term to each node in these ancestral networks by using the most GO-annoted species for each lineage for ancestral networks (i.e. human proteins for the common, bilaterian and euarchontoglire ancestors, and *Ce* proteins for the ecdisozoan ancestor). We identified functionally enriched GO-terms (top 20) for each network with Metascape (M&M) (Fig. 6). To assess whether different GO-terms (and below different functions) had been associated with ageing or longevity as Opisthokonta diverged from their last common ancestor, we compared these top 20 GO functional annotations for ancestral longevity networks. 40 % of the enriched GO-terms were shared between the common and the bilaterian ancestral networks, but only 5% were shared between the bilaterian and the ecdisozoan ancestral networks and 5% were shared between the bilaterian and the euarchontoglire ancestral networks. Thus, functionally enriched GO-terms associated with ageing/longevity shifted over time, with some evolutionary conservation outside bilaterians. Next, we compared which gene families contributed to GO-terms enrichment between ancestral networks (Table S8): for each of the evolutionarily conserved GO-terms, we further checked whether they involved similar or different gene families in the successive ancestral networks, using a Jaccard index between pairs of sequential ancestral networks (M&M). We concluded that a significant proportion of both genes and pathways had been conserved between the common and the bilaterian ancestral networks (Jaccard indices ranging from 0.53 to 0.89), whereas there were less shared gene families between the bilaterian and the ecdisozoan ancestral networks (Jaccard index = 0.21 for their unique shared GO-term) and between the bilaterian and the euarchontoglire ancestral networks (Jaccard index = 0.29 for their unique shared GO-term). These results show a limited overlap between gene families from functionally enriched GO-terms associated with ageing/longevity, reinforcing the notion that important LAPs differ within lineages of Opisthokonta, especially since the last common ancestor of bilaterians, i.e., there are many lineage specific evolutionary roads to ageing and longevity.

Although gene families and functionally enriched GO-terms associated with ageing and longevity showed limited overlap between Opisthokonta, we still wanted to verify whether some convergence in their even more general functions could not be detected for these enriched GO-

terms. For this, we grouped functionally enriched GO-terms into common functions, e.g. autophagy, stress response, or protein translation, etc. Functions enriched in the common ancestral network are linked to protein translation, stress response, energy production, autophagy and apoptosis. Consistent with the above results, the bilaterian ancestral network shared most of these enriched functions found in the common ancestral network, to the exception of apoptosis and with the addition of response to nutrient levels, a function linked to the mTOR signalling network. Interestingly however, ecdisozoan and euarchontoglire ancestral networks that displayed different enrichment of GO terms were also functionally divergent. The ecdisozoan network was enriched in autophagy and cell death, whereas the euarchontoglire network was enriched in DNA repair, telomere, response to nutrient levels, glucose homeostasis, apoptosis, cell cycle regulation and cell senescence-related functions. This distinction may reflect genuine differences in biological processes, i.e. lineage-specific evolution of longevity/ageing processes, or reflect an experimental bias in the functions investigated by researchers for these different clades. Consistently, a Pubmed search for "cellular senescence" in combination with species names and ageing/longevity/lifespan as keywords returns 28 times more abstracts for euarchontoglire species (*Hs*: 1302; *Mm*: 346) than for ecdisozoan species (*Ce*: 41, *Dm*: 18), even though cellular senescence can occur in ecdisozoan at least in *Dm* (Ito and Igaki 2016), but a similar search for "autophagy/mitophagy" returns only 2.5 times more abstracts for euarchontoglire species (*Hs*: 899; *Mm*: 440) than ecdisozoan species (*Ce*: 313, *Dm*: 229). These patterns are indeed in accordance with the imbalance in numbers of studies on cellular senescence performed in humans and mice versus flies and nematodes (~40 times more studies in humans and mice), rather than reflecting a preferential link with ageing and longevity.

Overall, these results suggest a progressive transition in enriched functions associated with ageing/longevity along the Opisthokonta phylogeny, although this interpretation could still be dependent on experimental biases, and the limited species sampling that was available for our study. Indeed, this sampling included four highly lab-adapted species (for which labels relative to ageing/longevity had previously been gathered from experiments) and humans, which have an unusual longevity; and therefore future studies with a broader taxonomic sampling covering even more of the diversity of Opisthokonta will be useful to assess the generality of our conclusions across animals and fungi. Still, resampling-based estimations of false negative and positive rates suggest low rates of type I and moderate rates of type II errors and thus a good representativity of the results even with a limited number of input species.

Inferring new evolutionarily conserved LAPs

Finally, we expanded our analysis of ageing and longevity associated pathways beyond the borders of extant and ancestral longevity networks (composed only of LAPs) by connecting these networks to the rest of the PPI networks from which they constitute a subset (the global interactomes, also featuring non-LAPs). We mined the global PPI networks (comprised of all orthologous proteins from a given organism, or all the conserved orthologous protein families for a clade) and all significantly supported edges (for various stringency thresholds), both for extant interactomes and for inferred ancestral interactomes (Fig. S9), to identify non-LAPs with significantly similar sets of neighbours to LAPs (Fig. S10). We reasoned that when a non-LAP (or a non-LAP family) significantly interacts with the same sets of proteins than a LAP (or a LAP family), this non-LAP may perform biological functions closely related to that of the LAP with which it plays the same structural role in the PPI network.

In extant networks, depending on which species was investigated, hundreds to thousands of non-LAPs shared significantly similar sets of neighbours than LAPs. Achieving phenotypic assays for so many candidate components of longevity or ageing-associated pathways would be overwhelming. Fortunately, analyses of ancestral PPI networks returned a much more manageable number of candidates, which in addition are evolutionarily conserved. Predicted proteins from ancestral networks were enriched for functions such as translation/ribosomal biogenesis in all 5 species, ubiquitination/proteasomal degradation in bilaterians, neddylation, cell cycle progression and DNA repair in euarchontoglires.

Our strategy makes an asymmetric use of LAPs, as these proteins have been known for a long time to have some direct or indirect connections with ageing, and of non-LAPs, which are proteins that were not reported to have direct or indirect connections with ageing in GenAge. Therefore, an analysis of the scientific literature to validate our predicted for novel LAPs from non-LAPs should not capture information that was used, in the first place, to define longevity-associated proteins. Consistently, we validated a subset of these non-LAPs that we predicted to be associated with ageing or longevity by querying either publication records in PubMed database or phenotypic annotations in species-specific databases (M&M). Predictions with such external support amounted to 24% in *Ce*, 9% in *Dm*, 10% in *Hs*, 5% in *Mm* and 8% in *Sc* (Table S11). Although selecting *Dm* genes at random (1321 genes with ageing-related annotations among 13986 protein-coding genes:

9.4%) would lead to a similar number of ageing-related annotations as evosystemic predictions (9 out of 119 predictions: 7.5%, $P > 0.05$), we saw an enrichment for ageing-annotated *Ce* genes (17 out of 74 predictions: 23%) compared to random sampling (1171 genes with ageing-related annotations in Wormbase among 19886 protein-coding genes: 5.9%, $P < 0.05$), suggesting that evosystemic analysis can be used to predict new ageing-associated genes.

Remarkably, 265 non-LAPs that we predicted to be associated with ageing/longevity are more central than MTOR in the human interactome (Table S12), forming a list of novel evolutionarily conserved super-central candidate proteins associated with ageing or longevity, dominated by ribosomal proteins and ubiquitination pathways. This list also includes KEAP1, a candidate regulator of ageing or longevity, since KEAP1 is also homologous to a key antagonistic regulator that we identified in *Dm*. Consistently with our prediction, KEAP1 has been suggested to regulate the ageing of human aortic endothelial cells (EC) in culture, as a repressor of Nrf2 transcription factor, the critical modulator of cellular stress-response (Kopacz et al. 2020). In addition, 138 out of the 487 new LAPs we predicted are potentially druggable, based on documented drug-protein interactions (M&M), and KEAP1 is one of those (Fig. 7, Table S11). Most interestingly for translational purposes, 28/138 of these druggable proteins are more central than MTOR (Table S12) and 1 amongst those is associated with ageing-related diseases (the proto-oncogene small GTPase superfamily member KRAS). Consequently, these candidate LAPs figure as possible targets for potential novel anti-ageing treatments in humans.

Conclusion

We presented a network-based approach to make some progresses in the analysis of ageing and longevity genes. This approach is surely not the only strategy to reach this goal, given that protein interaction networks lack direct information on mutations associated with longevity located in non-coding/regulatory regions of the genomes, however, we showed that evosystemics has some potential for ageing studies and for proposing novel candidate ageing or longevity related genes. Namely, we tracked the evolutionary history of protein interactions associated with ageing or longevity throughout the phylogeny of five species of Opisthokonta, to identify which pathways known to be associated with ageing or longevity had emerged in which lineages, were conserved and central. To do this, we conjugated two non-mutually exclusive criteria to rank proteins and protein interactions by their high evolutionary conservation across these Opisthokonta and their high centrality in extant and in inferred ancestral PPI. We applied our approach to five species of Opisthokonta, a broader taxonomic selection than used thus far in any previous PPI analyses on

ageing and longevity, mapped extant and ancestral networks with LAP, pro- and anti-longevity labels, and analysed their connections with a large range of network metrics. We confirmed that LAPs, be they pro- or anti-longevity, are highly central in extant PPI, and identified key antagonistic regulators of ageing/longevity. While some highly central proteins are evolutionarily conserved, we observed a transition in functionally important components of ageing or longevity along these different Opisthokonta lineages. Still, a third of the human LAPs and 7 % of their interactions date from ancestral interactomes of Opisthokonta, indicating that a phylogenetically broad range of model organisms could be investigated to understand central mechanistic aspects associated with human ageing and longevity. We also predicted new central, evolutionarily conserved LAPs, of which some could be validated by published independent experimental support. Importantly, we propose that a set of 487 LAPs should be included in the human longevity network. About half of them, largely associated with ribosomal proteins and ubiquitination pathways, are more central than mTOR in the human PPI. In addition, 28.3% of the proteins we predict to hold important roles in longevity or ageing-associated pathways in humans are druggable, defining potential targets for novel anti-ageing treatments in humans. While we feel this approach is promising, it is worth keeping in mind that our analysis could at the time being only rely upon five species for which *a priori* knowledge on ageing- and longevity-associated proteins were already available. Although this was the most phylogenetically diverse set of species we could currently analyze by this approach, two of the five species (mice and humans) have diverged less than a hundred million years ago, and as such represent a fraction of the genetic diversity of animals. Consequently, we hope that future evosystemic studies, benefiting from an enlarged taxonomic dataset from fungi to animals, will determine to what extent our conclusions generalize to all Opisthokonta species, beyond the five species carefully investigated here.

Materials and Methods

Protein-protein interaction stringency

Protein-protein interaction (PPI) networks were built from the STRING database (https://string-db.org/)(Szklarczyk et al. 2019) for five species with longevity-related annotations in the GenAge database (http://genomics.senescence.info/genes/, Build 20)(Tacutu et al. 2018): *S. cerevisiae* (*Sc*, txid4932), *C. elegans* (*Ce*, txid6239), *D. melanogaster* (*Dm*, txid7227), *M. musculus* (*Mm*, txid10090) and *H. sapiens* (*Hs*, txid9606). STRING-recorded interactions between pairs of

proteins are weighted by confidence scores ranked from 0 to 1000. STRING PPI networks were filtered at different PPI stringencies either based on interaction score thresholds (scores above 500, 600, 700, 800 or 900), or solely based on interactions experimentally supported (hereafter referred to as experimental networks).

Label-based subnetwork induction

Nodes in PPI networks were labelled as longevity/ageing-associated proteins (LAPs) in accordance with the annotations in the GenAge database. Pro- (genes whose decreased expression by knockout, mutations or RNA interference reduces lifespan and/or whose overexpression extends lifespan) or anti-longevity (genes whose decreased expression extends lifespan and/or whose overexpression decreases it) labelling was also used for *Ce*, *Dm*, *Mm* and *Sc* proteins; genes associated with 'unclear' or 'unannotated' effects on longevity were labelled as 'unclear' in our dataset. LAPs, subdivided into pro-longevity, anti-longevity and 'unclear' labelled nodes and the edges connecting them (at the indicated PPI network threshold) defined the species-specific longevity networks used in this study (Fig S3A).

Orthology relationships

Orthology criteria were those of the Alliance of Genome Resources Portal (Alliance Database Version: 4.1.0, http://www.alliancegenome.org), which focuses on aggregating and curating orthology relationships between model organisms from a diversity of databases (The Alliance of Genome Resources Consortium et al. 2020) to annotate homologs among ARML and centrality outliers (using a '--HH + number' arbitrary code (Table S13). For ancestral PPI network inference, orthology relationships were based on the more stringent OMA orthogroups from the OMA database (Orthologous MAtrix, https://omabrowser.org/oma/home/, OMA All.Jan2020 release)(Altenhoff et al. 2018). Orthology-labelled nodes were used to derive networks of orthologs, sharing the same OMA orthogroup identifiers (Fig. S3B), for each species and at each PPI stringency threshold.

Centrality analysis and outlier detection

Four metrics distributions were computed to determine the centrality of LAPs in PPI networks (Figure S2A-D). Three metrics (betweenness, closeness, and degree) were calculated using the NetworkAnalyser plugin in Cytoscape (Doncheva et al. 2012) and the PageRank (Page

et al. 1999) of each node was calculated using the algorithm implemented in the networkx Python package (https://networkx.org) with default parameters. Metrics distribution for pro-, anti-longevity proteins (model organisms) or only LAPs (for all five species), were compared to proteins not associated with longevity (non-LAPs) using the Mann-Whitney U-test (unilateral or bilateral, as indicated). P-values were adjusted for multiple testing using the Bonferroni method. To detect centrality outliers with statistically significant high values for centrality metrics in longevity networks (Figure S2A-D), normalized betweenness, degree, PageRank and closeness were computed using the networkx Python package at all PPI stringency thresholds. Statistically significant high values were determined by node rewiring permutation tests (see Network permutation tests Methods section). Because network permutation tests scale poorly with increasing network size, we compared node centrality in entire PPI networks by their average degree rank across all PPI stringency threshold.

Homophily analysis and candidate ARML detection

Homophily between labelled nodes in networks, i.e. the preferential connection with the same labels, was measured by computing assortativity coefficients (Figure S2E) as defined in equation II from Newman, 2003 (Newman 2003), in order to quantify the extent to which nodes with the same label connect with each other rather than with differently labelled nodes. Assortativity coefficients were calculated using the attribute_assortativity_coefficient function from the networkx Python package either for LAPs in entire networks or for pro- and anti-longevity labelled nodes in entire networks and longevity networks. Statistically significant assortativity coefficient values were determined by label permutation tests (see Network permutation tests Methods section). To detect candidate key regulators of ARMLs among pro- or anti-longevity labelled nodes in longevity networks, statistically significant high numbers of neighbors with the opposite label were determined by node rewiring permutation tests (see Network permutation tests Methods section).

Inference of ancestral PPI networks

To infer ancestral PPI networks, species-specific networks of orthologs (Fig. S3B) derived from longevity networks (Fig. S3A) at all PPI stringency thresholds and the reference phylogenetic tree associated with these taxa (in the bracketed format: (*Sc*, (*Ce*, *Dm*), (*Mm*, *Hs*))) were used as input for an in-house script (available on GitHub:

https://github.com/TeamAIRE/ancestral_interactome_inference), to detect conserved protein-protein interaction (edges between the same pair of orthologous proteins, present in different species) and map these edges on the phylogeny of five species of Opisthokonta. For any given edge, all mapped extant taxa in which the protein-protein interaction is observed were given as input to the 'get_common_ancestor' function of the ete3 Python package version 3.1.1 (Huerta-Cepas et al. 2016) to conduct a parsimony analysis and identify the last common ancestor (returned as an intermediate node of the phylogenetic tree) in which the protein-protein interaction was likely present (Fig. S7). Next, this last common ancestor was used to define the root of a subtree, subsequently explored to define which of its children intermediate nodes have likely conserved the edge (at least one descendant extant taxon possessing the edge) or lost the edge (none of its descendant extant taxa possessing the edge). For each intermediate node of the phylogeny, all the edges inferred to be present were then used to reconstruct the corresponding ancestral PPI network. To estimate the false negative/positive rates associated to ancestral edge inferences, we used a resampling approach to construct alternative ancestral networks from thresholded entire networks, by replacing the input of either *Sc*, *Ce* and *Dm* networks by the PPI network of a species with the same taxonomic rank (family) in the NCBI reference phylogeny, with more than 85% of protein sequences being 100% identical between the OMA and STRING databases. Alternative species were, for *Ce* : *C. briggsae* (txid6238), *C. remanei* (txid31234); for *Dm*: *D. ananassae* (txid7217), *D. erecta* (txid7220), *D. grimshawi* (txid7222), *D. persimilis* (txid7234), *D. sechellia* (txid7238), *D. simulans* (txid7240), *D. virilis* (txid7244), *D. yakuba* (txid7245), *D. willistoni* (txid7260); for *Sc*: *K. lactis* (txid284590), *C. glabrata* (txid284593), *E. gossypii* (txid284811), *V. polyspora* (txid436907), *L. thermotolerans* (txid559295), *K. naganishii* (txid1071383). False negatives were defined as edges present in all alternative but absent from reference ancestral networks, and false positives as edges present in reference and absent in all alternative ancestral networks. False positive rates were 0 for all three resampled species, and false negative rates were comprised between *Sc*: 12 and 20%; *Ce*: 0.5 and 4%; *Dm*: 0 and 1.5%.

LAP prediction based on ancestral networks

To predict ancestral proteins with similar topological properties as inferred ancestral LAPs, inferred ancestral PPI networks were mined for orthogroups with similar roles. This prediction is of course a first step. We do not consider that when a non-LAP shares the centrality and conservation properties of one or several ageing- or longevity- associated proteins, this topological proximity is in itself a sufficient evidence that the non-LAP is also an ageing- or longevity-

associated protein, e.g. it may not be sufficient to share topological properties with an ageing-associated protein to be another, undetected, ageing-associated protein. Further validation of the prediction is also necessary. However, it is worth noting here that our predictions were very stringent.

Precisely, node label permutation tests were used to identify significantly high Jaccard indices combined with significantly high numbers of common direct neighbors, with a Jaccard index minimal threshold of 0.5 and at least 1 common neighbor. Species-specific LAP predictions were obtained from the non-LAPs with significant LAP neighborhood in at least one of the ancestral networks from the lineage of the focal species. As expected, this approach identified non-LAPs in a species that are homologous to LAPs in another species and figured by construction as non-LAPs in the ancestral networks, which reassuringly supported our guilt-by-association approach. These already documented LAPs, representing from 0 to 28 % of all predictions, depending on the species, were filtered out.

To further validate our approach of functional prediction by guilt-by-association within a PPI network, independently of the ageing-associated labels, we verified that the functional distributions of these protein families and that of the protein families to which they were structurally equivalent matched with one another. To compute the functional similarity between predicting and predicted proteins, each predicting and associated predicted orthogroups were translated to species-specific representative Ensembl identifiers, and the biomaRt R package was used to retrieve species-specific associated GO-terms from the Ensembl database. Semantic similarity analysis was performed using GOGO on pairs of proteins (predictor-predicted) and semantic similarity scores for each GO category were computed as described (Zhao and Wang 2018). Median semantic similarity for molecular function was found superior to 0.5, indicating good functional correspondence between predictors and predicted proteins and supporting the potential involvement of predicted proteins in regulating ageing and longevity (Figs. S14, S15).

Supporting information for a role as a novel candidate LAP in extant species was gathered using systematic queries to the Pubmed database, following the template: {*symbol of the predicted LAG*} AND {*species-specific keywords*} AND (ageing OR aging OR longevity OR lifespan OR "life span" OR senescence). Species-specific keywords were ‘elegans’ for *Ce*, ‘drosophila’ for *Dm*, ‘human OR sapiens’ for *Hs*, ‘mouse OR musculus’ for *Mm* and ‘yeast OR cerevisiae’ for *Sc*. Curated abstracts with mention of a potential link between the predicted LAP and longevity were

retained as supporting data. Further, predicted LAPs for the three species *Sc*, *Dm* and *Ce* were compared with the list of genes associated to lifespan and ageing alterations in genetic experiments recorded in the corresponding species-specific databases *Saccharomyces* Genome Database (yeastgenome.org), Flybase (flybase.org) and Wormbase (wormbase.org). *Sc* phenotypes queried were 'aging', 'lifespan decreased' and 'lifespan increased'; *Dm* phenotypes queried were 'aging', 'lifespan', 'abnormal aging', 'delayed aging', 'premature aging', 'short lived' and 'long lived'; *Ce* phenotypes queried were 'dauer lifespan variant' (WBPhenotype:0001540), 'extended life span' (WBPhenotype:0000061), 'shortened life span' (WBPhenotype:0001171) and 'aging variant' (WBPhenotype:0001739). To calculate enrichments in ageing-related annotations in our predictions relative to random sampling, the number of all known protein-coding genes was derived from the number of genes associated with and Uniprot reference identifier in Wormbase for *Ce*, and from Flybase statistics for *Dm*, and a chi-square test was used. *Hs* predicted LAPs were additionally probed for genes associated with human cell senescence in the CellAge database (https://genomics.senescence.info/cells/, (Avelar et al. 2020)), genes with alleles associated with exceptional human longevity in the LongevityMap database (https://genomics.senescence.info/longevity/, (Budovsky et al. 2013)), Aging-Related Disease (ARD) genes (Fernandes et al. 2016) and druggable proteins recorded in the DGIdb database (Griffith et al. 2013). We also determined from DGIdb the number of drugs, the number of US Food and Drug Administration (FDA)-approved drugs, and the maximum DGIdb interaction score associated with each predicted LAP in human.

Network permutation tests

To detect centrality outlier nodes or candidate key antagonistic regulators, node rewiring permutation tests (Fig. S4) were performed by 1000 random network permutations rewiring the nodes but preserving the total number of edges, without preserving the degree distribution. To detect statistically significant high values of assortativity, and significantly high values of Jaccard index and numbers of common direct neighbors, node label permutation tests (Fig. S4) were performed by randomly shuffling node labels 1000 times. For each node and each metric, a counter was incremented each time the random value was greater than the reference value. P-values were then calculated by the ratio counter/number of permutations, and adjusted for multiple testing using the Bonferroni method.

Functional enrichment analysis

Functional enrichment analysis was performed using the Metascape online tool (https://metascape.org/gp/index.html)(Zhou et al. 2019) with customized Enrichment tab settings to retrieve enriched Biological Processes GO terms only. For inferred ancestral networks, orthogroups were translated to their extant protein representative in the most annoted species for each lineage, according to the Gene Ontology statistics (http://current.geneontology.org/products/pages/downloads.html): *Hs* proteins for the common, bilaterian and euarchontoglire ancestors, and *Ce* proteins for the excdisozoan ancestor. Metascape analysis files were parsed to retrieve the genes annotated with the top 20 enriched GO terms and a Jaccard index was computed to compare gene sets for shared GO terms between networks.

Acknowledgments

We thank Duncan Sussfeld, Cameron Osborne, and three anonymous reviewers, for critical reading of the manuscript. This work was supported by an Emergence grant from Sorbonne Université (S21JR31001 - IP/S/V2 EMERG-ESPA) to EB and JM and by a grant from the Ministère de la Recherche to CB.

Data Availability Statement

The data underlying this article are available in the article and in its online supplementary material.

References

Altenhoff AM, Glover NM, Train C-M, Kaleb K, Warwick Vesztrocy A, Dylus D, de Farias TM, Zile K, Stevenson C, Long J, et al. 2018. The OMA orthology database in 2018: retrieving evolutionary relationships among all domains of life through richer web and programmatic interfaces. *Nucleic Acids Res.* 46:D477–D485.

Avelar RA, Ortega JG, Tacutu R, Tyler EJ, Bennett D, Binetti P, Budovsky A, Chatsirisupachai K, Johnson E, Murray A, et al. 2020. A multidimensional systems biology analysis of cellular senescence in aging and disease. *Genome Biol.* 21:91.

Bapteste E, Huneman P. 2018. Towards a Dynamic Interaction Network of Life to unify and expand the evolutionary theory. *BMC Biol.* 16:56.

Baudisch A, Vaupel JW. 2012. Getting to the Root of Aging. *Science* 338:618–619.

Bell R, Hubbard A, Chettier R, Chen D, Miller JP, Kapahi P, Tarnopolsky M, Sahasrabuhde S, Melov S, Hughes RE. 2009. A Human Protein Interaction Network Shows Conservation of Aging Processes between Human and Invertebrate Species.Kim SK, editor. *PLoS Genet.* 5:e1000414.

Blagosklonny MV. 2006. Aging and Immortality: Quasi-Programmed Senescence and Its Pharmacologic Inhibition. *Cell Cycle* 5:2087–2102.

Budovsky A, Abramovich A, Cohen R, Chalifa-Caspi V, Fraifeld V. 2007. Longevity network: Construction and implications. *Mech. Ageing Dev.* 128:117–124.

Budovsky A, Craig T, Wang J, Tacutu R, Csordas A, Lourenço J, Fraifeld VE, de Magalhães JP. 2013. LongevityMap: a database of human genetic variants associated with longevity. *Trends Genet.* 29:559–560.

Budovsky A, Tacutu R, Yanai H, Abramovich A, Wolfson M, Fraifeld V. 2009. Common gene signature of cancer and longevity. *Mech. Ageing Dev.* 130:33–39.

Doherty A, de Magalhães JP. 2016. Has gene duplication impacted the evolution of Eutherian longevity? *Aging Cell* 15:978–980.

Doncheva NT, Assenov Y, Domingues FS, Albrecht M. 2012. Topological analysis and interactive visualization of biological networks and protein structures. *Nat. Protoc.* 7:670–685.

Farré X, Molina R, Barteri F, Timmers PRHJ, Joshi PK, Oliva B, Acosta S, Esteve-Altava B, Navarro A, Muntané G. 2021. Comparative Analysis of Mammal Genomes Unveils Key Genomic Variability for Human Life Span. *Mol. Biol. Evol.* 38:4948–4961.

Fernandes M, Wan C, Tacutu R, Barardo D, Rajput A, Wang J, Thoppil H, Thornton D, Yang C, Freitas A, et al. 2016. Systematic analysis of the gerontome reveals links between aging and age-related diseases. *Hum. Mol. Genet.* 25:4804–4818.

Ferrarini L, Bertelli L, Feala J, McCulloch AD, Paternostro G. 2005. A more efficient search strategy for aging genes based on connectivity. *Bioinforma. Oxf. Engl.* 21:338–348.

Foley NM, Hughes GM, Huang Z, Clarke M, Jebb D, Whelan CV, Petit EJ, Touzalin F, Farcy O, Jones G, et al. 2018. Growing old, yet staying young: The role of telomeres in bats' exceptional longevity. *Sci. Adv.* 4:eaao0926.

Fortney K, Kotlyar M, Jurisica I. 2010. Inferring the functions of longevity genes with modular subnetwork biomarkers of Caenorhabditis elegans aging. *Genome Biol.* 11:R13.

Gems D. 2022. The hyperfunction theory: An emerging paradigm for the biology of aging. *Ageing Res. Rev.* 74:101557.

Gorbunova V, Seluanov A, Zhang Z, Gladyshev VN, Vijg J. 2014. Comparative genetics of longevity and cancer: insights from long-lived rodents. *Nat. Rev. Genet.* 15:531–540.

Griffith M, Griffith OL, Coffman AC, Weible JV, McMichael JF, Spies NC, Koval J, Das I, Callaway MB, Eldred JM, et al. 2013. DGIdb: mining the druggable genome. *Nat. Methods* 10:1209–1210.

Huang Z, Whelan CV, Foley NM, Jebb D, Touzalin F, Petit EJ, Puechmaille SJ, Teeling EC. 2019. Longitudinal comparative transcriptomics reveals unique mechanisms underlying extended healthspan in bats. *Nat. Ecol. Evol.* 3:1110–1120.

Huerta-Cepas J, Serra F, Bork P. 2016. ETE 3: Reconstruction, Analysis, and Visualization of Phylogenomic Data. *Mol. Biol. Evol.* 33:1635–1638.

Irving AT, Ahn M, Goh G, Anderson DE, Wang L-F. 2021. Lessons from the host defences of bats, a unique viral reservoir. *Nature* 589:363–370.

Ito T, Igaki T. 2016. Dissecting cellular senescence and SASP in Drosophila. *Inflamm. Regen.* 36:25.

Johnson AA, Shokhirev MN, Shoshitaishvili B. 2019. Revamping the evolutionary theories of aging. *Ageing Res. Rev.* 55:100947.

Jones OR, Scheuerlein A, Salguero-Gómez R, Camarda CG, Schaible R, Casper BB, Dahlgren JP, Ehrlén J, García MB, Menges ES, et al. 2014. Diversity of ageing across the tree of life. *Nature* 505:169–173.

Kacprzyk J, Locatelli AG, Hughes GM, Huang Z, Clarke M, Gorbunova V, Sacchi C, Stewart GS, Teeling EC. 2021. Evolution of mammalian longevity: age-related increase in autophagy in bats compared to other mammals. *Aging* 13:7998–8025.

Keane M, Semeiks J, Webb AE, Li YI, Quesada V, Craig T, Madsen LB, van Dam S, Brawand D, Marques PI, et al. 2015. Insights into the evolution of longevity from the bowhead whale genome. *Cell Rep.* 10:112–122.

Keller L, Genoud M. 1997. Extraordinary lifespans in ants: a test of evolutionary theories of ageing. *Nature* 389:958–960.

Kenyon CJ. 2010. The genetics of ageing. *Nature* 464:504–512.

Kirkwood T, Holliday R. 1979. The evolution of ageing and longevity. *Proc. R. Soc. Lond. B Biol. Sci.* 205:531–546.

Kirkwood TBL. 1997. The origins of human ageing.Evans JG, Holliday R, Kirkwood TBL, Laslett P, Tyler L, editors. *Philos. Trans. R. Soc. Lond. B. Biol. Sci.* 352:1765–1772.

Kolora SRR, Owens GL, Vazquez JM, Stubbs A, Chatla K, Jainese C, Seeto K, McCrea M, Sandel MW, Vianna JA, et al. 2021. Origins and evolution of extreme life span in Pacific Ocean rockfishes. *Science* 374:842–847.

Kopacz A, Kloska D, Targosz-Korecka M, Zapotoczny B, Cysewski D, Personnic N, Werner E, Hajduk K, Jozkowicz A, Grochot-Przeczek A. 2020. Keap1 governs ageing-induced protein aggregation in endothelial cells. *Redox Biol.* 34:101572.

Li Y, de Magalhães JP. 2013. Accelerated protein evolution analysis reveals genes and pathways associated with the evolution of mammalian longevity. *Age Dordr. Neth.* 35:301–314.

Lu JY, Simon M, Zhao Y, Ablaeva J, Corson N, Choi Y, Yamada KYH, Schork NJ, Hood WR, Hill GE, et al. 2022. Comparative transcriptomics reveals circadian and pluripotency networks as two pillars of longevity regulation. *Cell Metab.* 34:836-856.e5.

Lunghi E, Bilandžija H. 2022. Longevity in Cave Animals. *Front. Ecol. Evol.* 10:874123.

de Magalhães JP, Toussaint O. 2004. GenAge: a genomic and proteomic network map of human ageing. *FEBS Lett.* 571:243–247.

Managbanag JR, Witten TM, Bonchev D, Fox LA, Tsuchiya M, Kennedy BK, Kaeberlein M. 2008. Shortest-path network analysis is a useful approach toward identifying genetic determinants of longevity. *PloS One* 3:e3802.

Medawar PB. 1952. An unsolved problem of biology. College

Muntané G, Farré X, Rodríguez JA, Pegueroles C, Hughes DA, de Magalhães JP, Gabaldón T, Navarro A. 2018. Biological Processes Modulating Longevity across Primates: A Phylogenetic Genome-Phenome Analysis.Wray G, editor. *Mol. Biol. Evol.* 35:1990–2004.

Newman MEJ. 2003. Mixing patterns in networks. *Phys. Rev. E* 67:026126.

Orkin JD, Montague MJ, Tejada-Martinez D, de Manuel M, Del Campo J, Cheves Hernandez S, Di Fiore A, Fontsere C, Hodgson JA, Janiak MC, et al. 2021. The genomics of ecological flexibility, large brains, and long lives in capuchin monkeys revealed with fecalFACS. *Proc. Natl. Acad. Sci. U. S. A.* 118:e2010632118.

Page L, Brin S, Motwani R, Winograd T. 1999. The PageRank Citation Ranking: Bringing Order to the Web. Stanford InfoLab Available from: http://ilpubs.stanford.edu:8090/422/

Papadopoli D, Boulay K, Kazak L, Pollak M, Mallette F, Topisirovic I, Hulea L. 2019. mTOR as a central regulator of lifespan and aging. *F1000Research* 8:998.

Promislow DEL. 2004. Protein networks, pleiotropy and the evolution of senescence. *Proc. Biol. Sci.* 271:1225–1234.

Rando TA, Chang HY. 2012. Aging, Rejuvenation, and Epigenetic Reprogramming: Resetting the Aging Clock. *Cell* 148:46–57.

Sahm A, Bens M, Szafranski K, Holtze S, Groth M, Görlach M, Calkhoven C, Müller C, Schwab M, Kraus J, et al. 2018. Long-lived rodents reveal signatures of positive selection in genes associated with lifespan.Barsh GS, editor. *PLOS Genet.* 14:e1007272.

da Silva R, Conde DA, Baudisch A, Colchero F. 2022. Slow and negligible senescence among testudines challenges evolutionary theories of senescence. *Science* 376:1466–1470.

Singh PP, Demmitt BA, Nath RD, Brunet A. 2019. The Genetics of Aging: A Vertebrate Perspective. *Cell* 177:200–220.

Szklarczyk D, Gable AL, Lyon D, Junge A, Wyder S, Huerta-Cepas J, Simonovic M, Doncheva NT, Morris JH, Bork P, et al. 2019. STRING v11: protein–protein association networks with increased coverage, supporting functional discovery in genome-wide experimental datasets. *Nucleic Acids Res.* 47:D607–D613.

Tacutu R, Budovsky A, Yanai H, Fraifeld VE. 2011. Molecular links between cellular senescence, longevity and age-related diseases – a systems biology perspective. *Aging* 3:1178–1191.

Tacutu R, Shore DE, Budovsky A, de Magalhães JP, Ruvkun G, Fraifeld VE, Curran SP. 2012. Prediction of C. elegans Longevity Genes by Human and Worm Longevity Networks.Suh Y, editor. *PLoS ONE* 7:e48282.

Tacutu R, Thornton D, Johnson E, Budovsky A, Barardo D, Craig T, Diana E, Lehmann G, Toren D, Wang J, et al. 2018. Human Ageing Genomic Resources: new and updated databases. *Nucleic Acids Res.* 46:D1083–D1090.

Tejada-Martinez D, Avelar RA, Lopes I, Zhang B, Novoa G, de Magalhães JP, Trizzino M. 2022. Positive Selection and Enhancer Evolution Shaped Lifespan and Body Mass in Great Apes. *Mol. Biol. Evol.* 39:msab369.

Templeman NM, Murphy CT. 2018. Regulation of reproduction and longevity by nutrient-sensing pathways. *J. Cell Biol.* 217:93–106.

The Alliance of Genome Resources Consortium, Agapite J, Albou L-P, Aleksander S, Argasinska J, Arnaboldi V, Attrill H, Bello SM, Blake JA, Blodgett O, et al. 2020. Alliance of Genome Resources Portal: unified model organism research platform. *Nucleic Acids Res.* 48:D650–D658.

Toren D, Kulaga A, Jethva M, Rubin E, Snezhkina AV, Kudryavtseva AV, Nowicki D, Tacutu R, Moskalev AA, Fraifeld VE. 2020. Gray whale transcriptome reveals longevity adaptations associated with DNA repair and ubiquitination. *Aging Cell* 19:e13158.

Treaster S, Karasik D, Harris MP. 2021. Footprints in the Sand: Deep Taxonomic Comparisons in Vertebrate Genomics to Unveil the Genetic Programs of Human Longevity. *Front. Genet.* 12:678073.

Wang J, Zhang S, Wang Y, Chen L, Zhang X-S. 2009. Disease-Aging Network Reveals Significant Roles of Aging Genes in Connecting Genetic Diseases.Searls DB, editor. *PLoS Comput. Biol.* 5:e1000521.

Watson AK, Habib M, Bapteste E. 2020. Phylosystemics: Merging Phylogenomics, Systems Biology, and Ecology to Study Evolution. *Trends Microbiol.* 28:176–190.

Williams GC. 1957. Pleiotropy, natural selection, and the evolution of senescence. *Evolution* 11:398–411.

Witten TM, Bonchev D. 2007. Predicting aging/longevity-related genes in the nematode Caenorhabditis elegans. *Chem. Biodivers.* 4:2639–2655.

Wuttke D, Connor R, Vora C, Craig T, Li Y, Wood S, Vasieva O, Shmookler Reis R, Tang F, de Magalhães JP. 2012. Dissecting the Gene Network of Dietary Restriction to Identify Evolutionarily Conserved Pathways and New Functional Genes.Kim SK, editor. *PLoS Genet.* 8:e1002834.

Yanai H, Budovsky A, Barzilay T, Tacutu R, Fraifeld VE. 2017. Wide-scale comparative analysis of longevity genes and interventions. *Aging Cell* 16:1267–1275.

Zhang Q, Nogales-Cadenas R, Lin J-R, Zhang W, Cai Y, Vijg J, Zhang ZD. 2016. Systems-level analysis of human aging genes shed new light on mechanisms of aging. *Hum. Mol. Genet.*:ddw145.

Zhao C, Wang Z. 2018. GOGO: An improved algorithm to measure the semantic similarity between gene ontology terms. *Sci. Rep.* 8:15107.

Zhou Y, Zhou B, Pache L, Chang M, Khodabakhshi AH, Tanaseichuk O, Benner C, Chanda SK. 2019. Metascape provides a biologist-oriented resource for the analysis of systems-level datasets. *Nat. Commun.* 10:1523.

Figure legends

Figure 1. Analysis of the centrality of LAPs in PPI networks.

Matrix displaying pairwise comparisons (LAPs VS non-LAPs) of node centrality metrics distributions in the PPI networks from five Opisthokonta species (*S. cerevisiae*, *D. melanogaster*, *C. elegans*, *M. musculus* and *H. sapiens*) for six PPI stringency thresholds (from 500: less stringent networks to exp: mores stringent networks). Stars in red cells indicate significantly higher centrality values for LAPs. Significance was determined using the unilateral Mann-Whitney U-test: **: $P < 0.001$; *: $P < 0.05$; NS: not significant (blue cells). P-values were adjusted for multiple testing using the Bonferroni method. This analysis shows that LAPs are more central than non-LAPs in PPI networks.

Figure 2. Homophily of LAPs in entire PPI networks and in longevity networks.

Homophily represents preferential interactions between similar kinds of nodes, and is estimated by assortativity coefficients. The distributions of assortativity coefficients were computed at six PPI stringency thresholds: (A) for LAPs and non-LAPs in the entire PPI networks of *S. cerevisiae*, *D. melanogaster*, *C. elegans*, *M. musculus* and *H. sapiens*; (B) for pro-longevity LAPs (pro-LAPs) and anti-longevity LAPs (anti-LAPs) in the entire PPI networks of *S. cerevisiae*, *D. melanogaster*, *C. elegans* and *M. musculus*; (C) for pro-LAPs and anti-LAPs in the longevity networks of *S. cerevisiae*, *D. melanogaster*, *C. elegans* and *M. musculus*. Assortativity coefficients were all significantly positive in node label permutation tests ($P < 0.05$), except in the *C. elegans* experimental longevity network (NS: not significant), indicating that proteins belonging to the same kind of LAPs (hence with the same effects on longevity) preferentially interact together.

Figure 3. Identification of candidate antagonistic regulatory mechanisms of longevity in longevity networks.

In longevity networks, some LAPs display a significantly high proportion of direct neighbours with an opposite effect on longevity (e.g. a pro-LAP being connected to significantly more anti-LAPs than expected by chance) and are therefore candidate regulators of longevity. Matrices of nodes with such a property for one or more PPI stringencies are indicated for three species: (A) *D. melanogaster*, (B) *C. elegans* and (C) *S. cerevisiae*. For each protein, the proportion of its neighbours with opposite effect on longevity is color-coded in cells, from blue: 0% to red: 100%.

Black cells indicate that the corresponding protein is absent from the network at the corresponding PPI stringency thresholds. The numbers of neighbors with opposite effects are indicated in the relevant cells only when significantly higher than by chance according to a node rewiring permutation test. Homolog outlier LAPs, i.e. LAPs found in multiple species, are indicated by a '--H + number' homology code (as defined in Table S13) to the right of the protein names, highlighted in blue (when shared by two species) or yellow (when shared by three species), whereas species-specific outlier LAPs are indicated in bold. A star labels LAPs which were not found among centrality outliers in Fig. 4, indicating candidate regulators of longevity that are not highly central in the network. The white, light grey and dark grey bars on the left of each matrix further classify proteins depending on their outlier status, respectively, in both thresholded and experimentally-supported (exp) networks, in thresholded networks only, or in exp networks only. This figure shows that several species host evolutionary conserved LAPs highly connected to proteins with opposite effects on longevity/ageing.

Figure 4. Identification of the most central LAPs in longevity networks.

Some LAPs display a significantly high centrality in longevity networks, defined as possessing a significantly high value for at least two centrality metrics among betweenness, closeness, degree and PageRank. Matrices of nodes with such a property for one or more PPI stringencies are indicated for five species: (A) *S. cerevisiae*, (B) *C. elegans*, (C) *D. melanogaster*, (D) *M. musculus* and (E) *H. sapiens*. For each protein, the number of significantly high centrality metrics is color-coded in cells, from blue: 0-1 to red: 4. Homolog outlier LAPs found in multiple species are indicated by a '--H + number' homology code (as defined in Table S13) to the right of the protein names, highlighted in blue (when present in four species) or yellow (when present in five species), whereas species-specific outlier LAPs are indicated in bold. The white, light grey and dark grey bars on the left of each matrix further classify proteins depending on their outlier status, respectively, in both thresholded and experimentally-supported (exp) networks, in thresholded networks only, or in exp networks only. This figure shows that several species host evolutionary conserved highly central LAPs in their longevity networks.

Figure 5. Inference of ancestral interactions based on shared LAP-LAP interactions between longevity networks.

The longevity networks of orthologs from *S. cerevisiae* (*Sc*), *C. elegans* (*Ce*), *D. melanogaster* (*Dm*), *M. musculus* (*Mm*) and *H. sapiens* (*Hs*) were used to infer ancestral networks at inner branches of the species phylogeny (as described in Figure S7) from ortholog-ortholog interactions shared between species. The resulting ancestral networks are shown here for PPI stringency threshold = 500. In these ancestral networks, node and edge colours indicate inferred presence in the last common ancestor of all 5 species (blue, in the last common ancestor of Opisthokonta), of all 4 bilaterian species (pink, in the bilaterian ancestor), of *Hs* and *Mm* (yellow, in the euarchontoglire ancestor) or of *Dm* and *Ce* (green, in the ecdisozoan ancestor). Extant longevity networks and proportions of ancestral nodes and edges in these networks are displayed to the right of the species phylogeny. These extant networks represent the interactions between LAPs belonging to shared orthogroups for each species. Nodes and edges in extant networks are coloured based on their inferred phylogenetic date of appearance, or grey if only present in the corresponding species. This figure shows that each extant longevity network contains evolutionarily conserved interactions, some of which as old as the last common ancestor of Opisthokonta.

Figure 6. Functional enrichment analysis of ancestral longevity networks.

To perform functional enrichment analysis of the proteic interactions inferred to be present in ancestral networks, ancestral orthogroups identified at each PPI stringency were analyzed using Metascape. *H. sapiens* protein identifiers were used as Metascape input to represent the functions of orthogroups found in common, bilaterian and euarchontoglire ancestral networks, and *C. elegans* protein identifiers were used as Metascape input to represent the functions of orthogroups found in ecdisozoan ancestral networks. On the species phylogeny, the top 20 enriched GO-terms identified by Metascape for ancestral proteins are positioned at the inner branches, and the top 20 enriched GO-terms for extant proteins (orthogroups found in extant longevity networks) are positioned at the leaves. Identical enriched GO-terms between ancestors or between ancestor and extant species are highlighted with the color corresponding to the oldest ancestor implementing the function (blue: for the last common ancestor of Opisthokonta; pink: for the bilaterian ancestor; yellow: for the euarchontoglire ancestor; green: for the ecdisozoan ancestor). Colored boxes surround GO-terms absent from ancestral networks but identical between sister species, suggesting that the same functions are used by closely related species to regulate longevity. This figure shows that the main enriched functions associated with longevity/ageing regulation have changed with the history of species.

Figure 7. Druggable human predicted LAPs.

We predicted 138 novel human LAPs, most with known drug interactions recorded in the DGIdb database. Predicted LAPS are ordered from left to right by their inferred age of first appearance (as old as the last common ancestor of Opisthokonta, as old as the Bilaterian ancestor, as old as the euarchontoglire ancestor) and by decreasing average centrality (average degree rank) in the corresponding ancestral longevity networks. A bar plot indicates the number of drugs linked to each of the 138 predicted human LAPs, with the number of FDA-approved drugs, when available, on top of each bar. Below the bar plot, a matrix displays support (purple cells) for a LAP function from (P) the literature in Pubmed abstracts, (C) the cellular senescence database Cellage or (L) GWAS data providing an association with longevity from the LongevityMap database. (A) indicates whether the LAP is associated to an Aging-Related Disease (ARD). This figure reports predicted evolutionary conserved human longevity-associated proteins, currently known to be targeted by drugs.

Figure 1

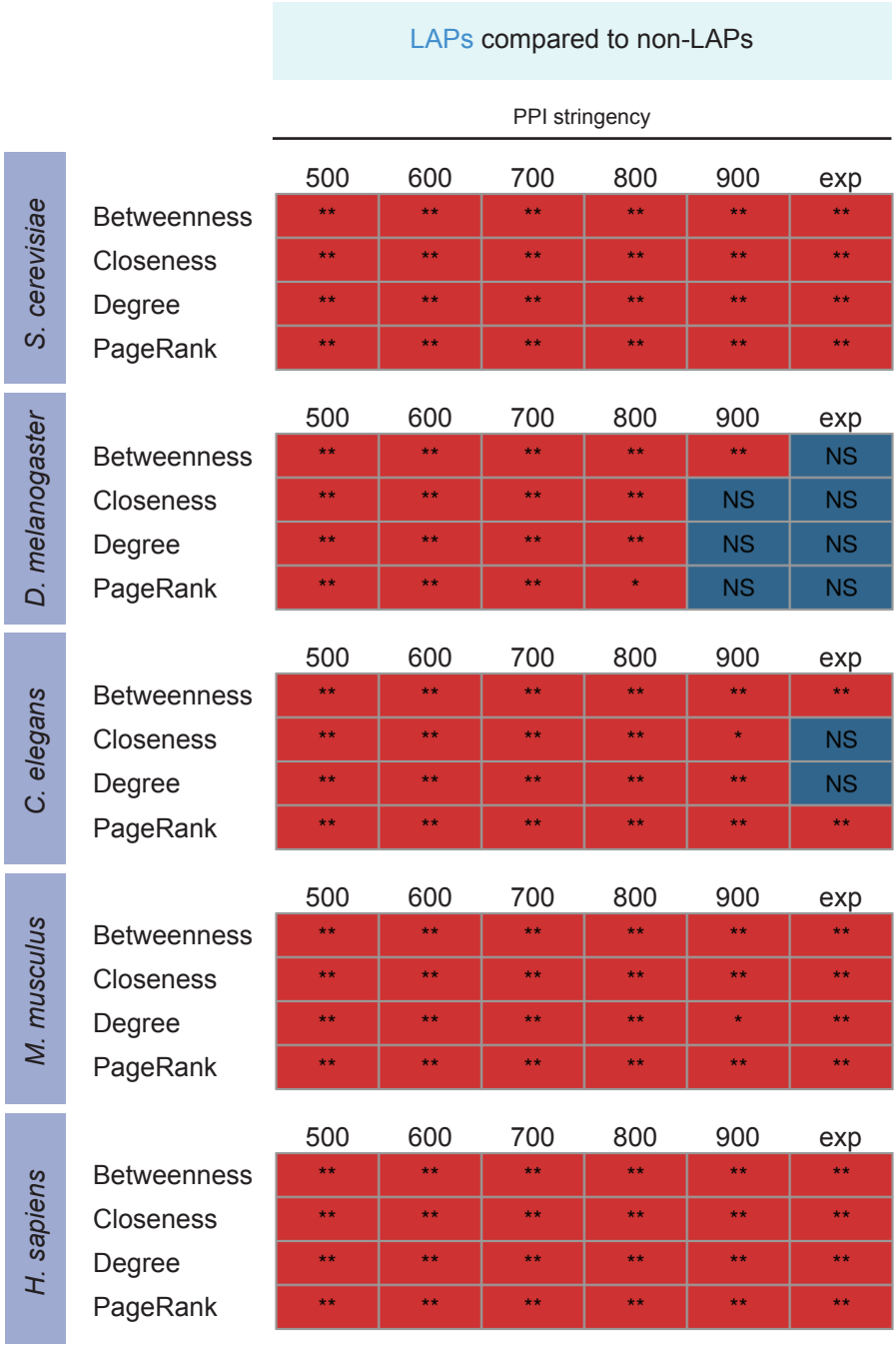
LAPs compared to non-LAPs
PPI stringency
500 600 700 800 900 exp
S. cerevisiae
Betweenness ** ** ** ** ** **
Closeness ** ** ** ** ** **
Degree ** ** ** ** ** **
PageRank ** ** ** ** ** **
D. melanogaster
Betweenness ** ** ** ** ** NS
Closeness ** ** ** ** NS NS
Degree ** ** ** ** NS NS
PageRank ** ** ** * NS NS
C. elegans
Betweenness ** ** ** ** ** **
Closeness ** ** ** ** * NS
Degree ** ** ** ** ** NS
PageRank ** ** ** ** ** **
M. musculus
Betweenness ** ** ** ** ** **
Closeness ** ** ** ** ** **
Degree ** ** ** ** * **
PageRank ** ** ** ** ** **
H. sapiens
Betweenness ** ** ** ** ** **
Closeness ** ** ** ** ** **
Degree ** ** ** ** ** **
PageRank ** ** ** ** ** **

Figure 2

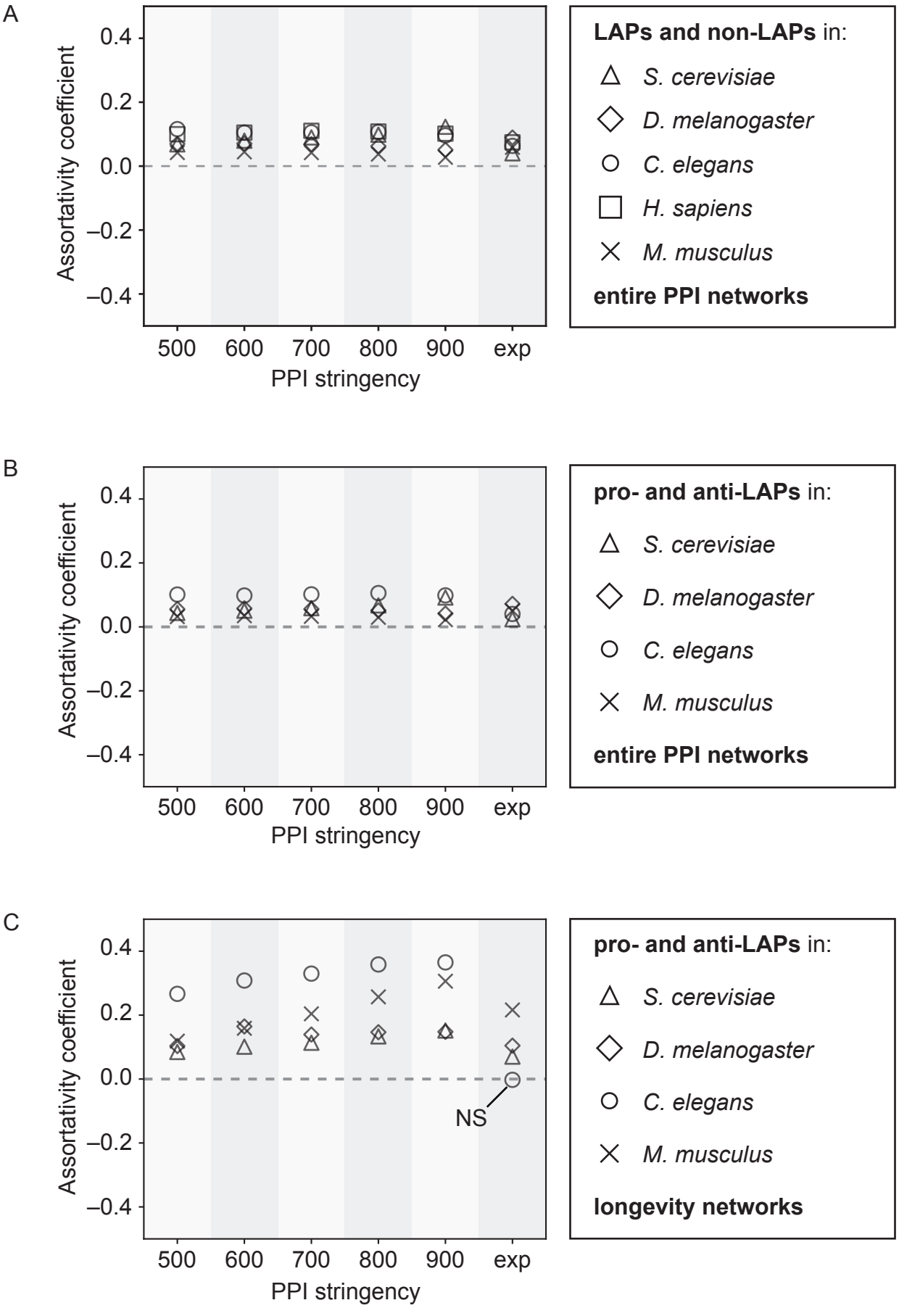
A
Assortativity coefficient
0.4
0.2
0.0
–0.2
–0.4
500
600
700
800
900
exp
PPI stringency
LAPs and non-LAPs in:
S. cerevisiae
D. melanogaster
C. elegans
H. sapiens
M. musculus
entire PPI networks
B
Assortativity coefficient
0.4
0.2
0.0
–0.2
–0.4
500
600
700
800
900
exp
PPI stringency
pro- and anti-LAPs in:
S. cerevisiae
D. melanogaster
C. elegans
M. musculus
entire PPI networks
C
Assortativity coefficient
0.4
0.2
0.0
–0.2
–0.4
NS
500
600
700
800
900
exp
PPI stringency
pro- and anti-LAPs in:
S. cerevisiae
D. melanogaster
C. elegans
M. musculus
longevity networks

Figure 3

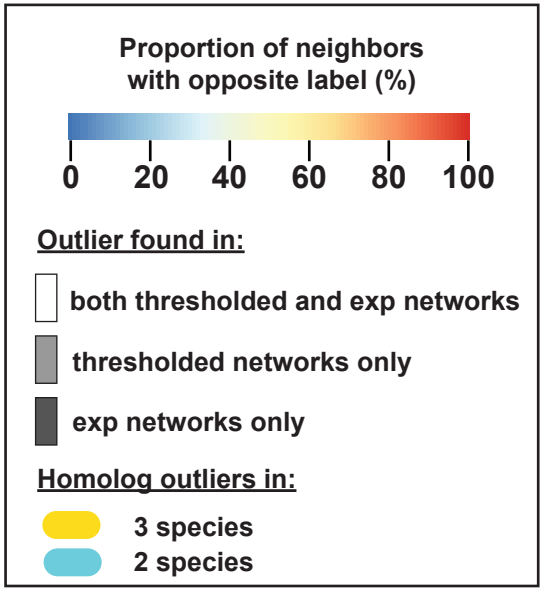
Proportion of neighbors with opposite label (%)
0
20
40
60
80
100
Outlier found in:
both thresholded and exp networks
thresholded networks only
exp networks only
Homolog outliers in:
3 species
2 species

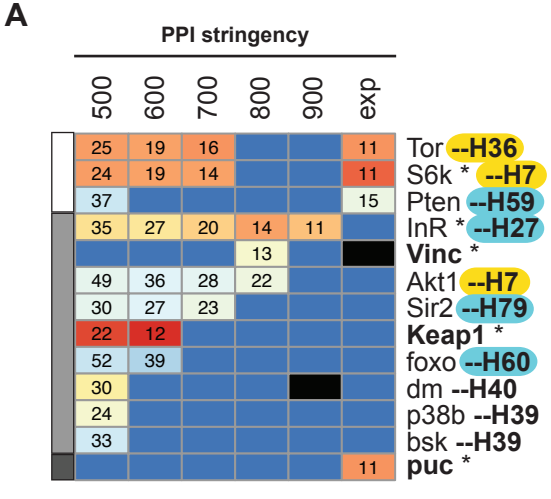
A
PPI stringency
500
600
700
800
900
exp
25 19 16 11 Tor --H36
24 19 14 11 S6k * --H7
37 15 Pten --H59
35 27 20 14 11 InR * --H27
13 Vinc *
49 36 28 22 Akt1 --H7
30 27 23 Sir2 --H79
22 12 Keap1 *
52 39 foxo --H60
30 dm --H40
24 p38b --H39
33 bsk --H39
11 puc *

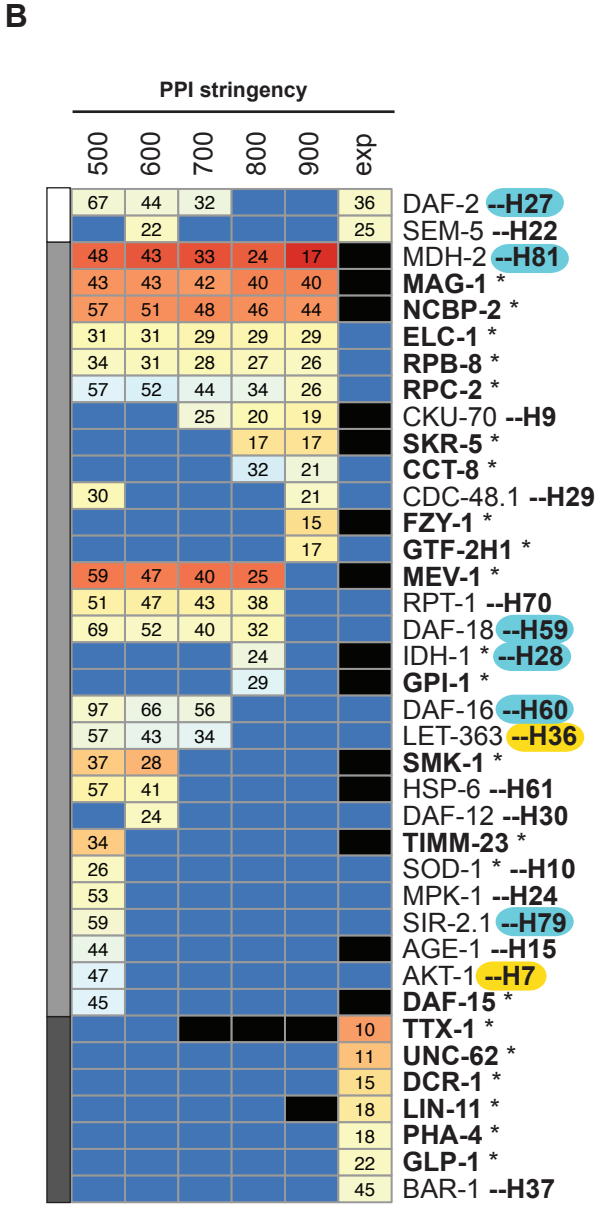
B
PPI stringency
500
600
700
800
900
exp
67 44 32 36 DAF-2 --H27
22 25 SEM-5 --H22
48 43 33 24 17 MDH-2 --H81
43 43 42 40 40 MAG-1 *
57 51 48 46 44 NCBP-2 *
31 31 29 29 29 ELC-1 *
34 31 28 27 26 RPB-8 *
57 52 44 34 26 RPC-2 *
25 20 19 CKU-70 --H9
17 17 SKR-5 *
32 21 CCT-8 *
30 21 CDC-48.1 --H29
15 FZY-1 *
17 GTF-2H1 *
59 47 40 25 MEV-1 *
51 47 43 38 RPT-1 --H70
69 52 40 32 DAF-18 --H59
24 IDH-1 * --H28
29 GPI-1 *
97 66 56 DAF-16 --H60
57 43 34 LET-363 --H36
37 28 SMK-1 *
57 41 HSP-6 --H61
24 DAF-12 --H30
34 TIMM-23 *
26 SOD-1 * --H10
53 MPK-1 --H24
59 SIR-2.1 --H79
44 AGE-1 --H15
47 AKT-1 --H7
45 DAF-15 *
10 TTX-1 *
11 UNC-62 *
15 DCR-1 *
18 LIN-11 *
18 PHA-4 *
22 GLP-1 *
45 BAR-1 --H37

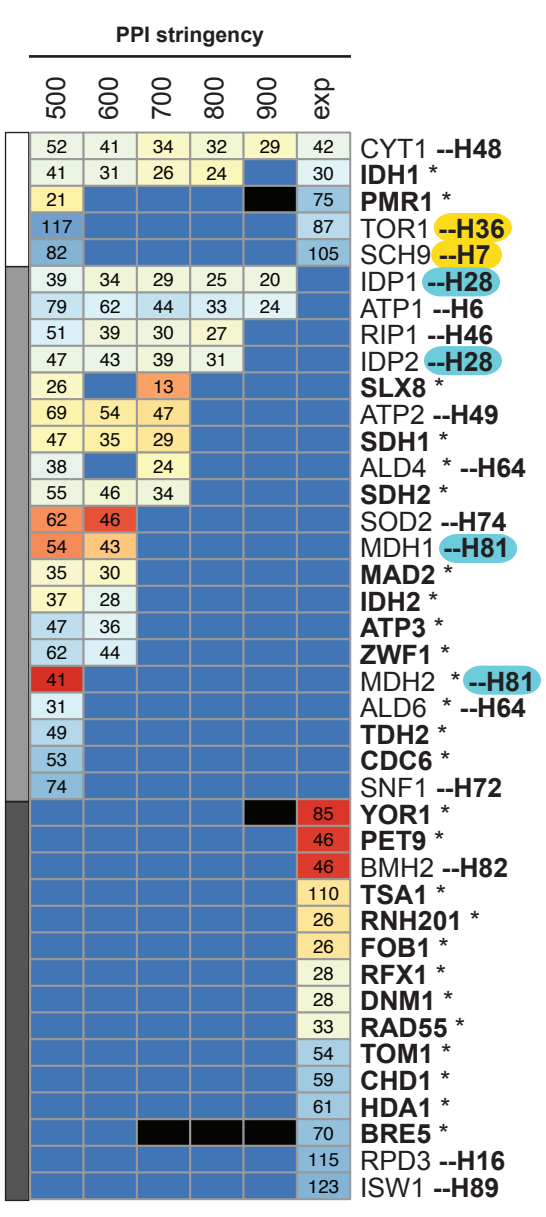
C
PPI stringency
500
600
700
800
900
exp
52 41 34 32 29 42 CYT1 --H48
41 31 26 24 30 IDH1 *
21 75 PMR1 *
117 87 TOR1 --H36
82 105 SCH9 --H7
39 34 29 25 20 IDP1 --H28
79 62 44 33 24 ATP1 --H6
51 39 30 27 RIP1 --H46
47 43 39 31 IDP2 --H28
26 13 SLX8 *
69 54 47 ATP2 --H49
47 35 29 SDH1 *
38 24 ALD4 * --H64
55 46 34 SDH2 *
62 46 SOD2 --H74
54 43 MDH1 --H81
35 30 MAD2 *
37 28 IDH2 *
47 36 ATP3 *
62 44 ZWF1 *
41 MDH2 * --H81
31 ALD6 * --H64
49 TDH2 *
53 CDC6 *
74 SNF1 --H72
85 YOR1 *
46 PET9 *
46 BMH2 --H82
110 TSA1 *
26 RNH201 *
26 FOB1 *
28 RFX1 *
28 DNM1 *
33 RAD55 *
54 TOM1 *
59 CHD1 *
61 HDA1 *
70 BRE5 *
115 RPD3 --H16
123 ISW1 --H89

Figure 4

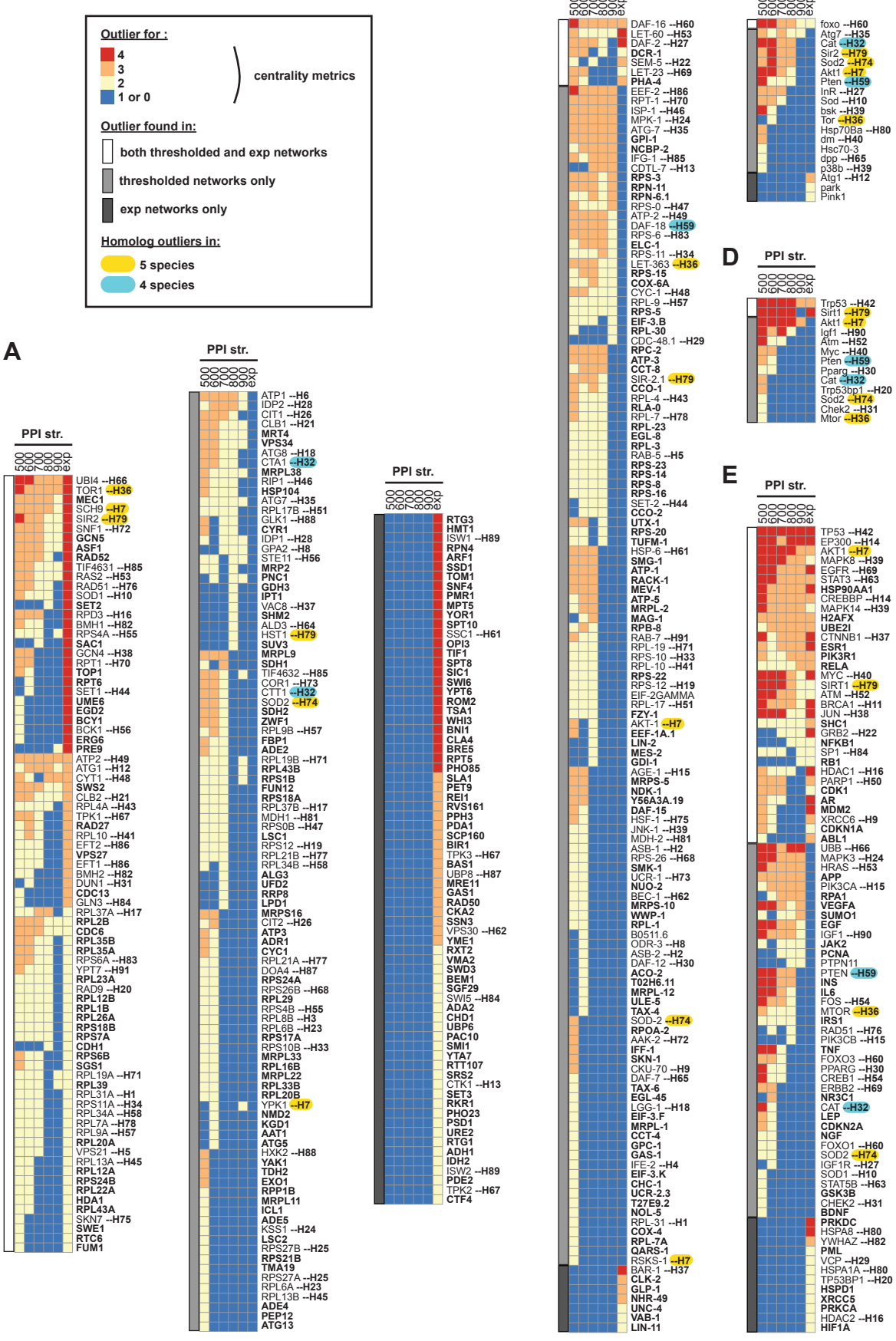
Outlier for :
4
3
2
1 or 0
centrality metrics
Outlier found in:
both thresholded and exp networks
thresholded networks only
exp networks only
Homolog outliers in:
5 species
4 species
A
PPI str.
500
600
700
800
900
exp
UBI4 --H66
TOR1 --H36
MEC1
SCH9 --H7
SIR2 --H79
SNF1 --H72
GCN5
ASF1
RAD52
TIF4631 --H85
RAS2 --H53
RAD51 --H76
SOD1 --H10
SET2
RPD3 --H16
BMH1 --H82
RPS4A --H55
SAC1
GCN4 --H38
RPT1 --H70
TOP1
RPT6
SET1 --H44
UME6
EGD2
BCY1
BCK1 --H56
ERG6
PRE9
ATP2 --H49
ATG1 --H12
CYT1 --H48
SWS2
CLB2 --H21
RPL4A --H43
TPK1 --H67
RAD27
RPL10 --H41
EFT2 --H86
VPS27
EFT1 --H86
BMH2 --H82
DUN1 --H31
CDC13
GLN3 --H84
RPL37A --H17
RPL2B
CDC6
RPL35B
RPL35A
RPS6A --H83
YPT7 --H91
RPL23A
RAD9 --H20
RPL12B
RPL1B
RPL26A
RPS18B
RPS7A
CDH1
RPS6B
SGS1
RPL19A --H71
RPL39
RPL31A --H1
RPS11A --H34
RPL34A --H58
RPL7A --H78
RPL9A --H57
RPL20A
VPS21 --H5
RPL13A --H45
RPL12A
RPS24B
RPL22A
HDA1
RPL43A
SKN7 --H75
SWE1
RTC6
FUM1
PPI str.
500
600
700
800
900
exp
ATP1 --H6
IDP2 --H28
CIT1 --H26
CLB1 --H21
MRT4
VPS34
ATG8 --H18
CTA1 --H32
MRPL38
RIP1 --H46
HSP104
ATG7 --H35
RPL17B --H51
GLK1 --H88
CYR1
IDP1 --H28
GPA2 --H8
STE11 --H56
MRP2
PNC1
GDH3
IPT1
VAC8 --H37
SHM2
ALD3 --H64
HST1 --H79
SUV3
MRPL9
SDH1
TIF4632 --H85
COR1 --H73
CIT1 --H32
SOD2 --H74
SDH2
ZWF1
RPL9B --H57
FBP1
ADE2
RPL19B --H71
RPL43B
RPS1B
FUN12
RPS18A
RPL37B --H17
MDH1 --H81
RPS0B --H47
LSC1
RPS12 --H19
RPL21B --H77
RPL34B --H58
ALG3
UFD2
RRP8
LPD1
MRPS16
CIT2 --H26
ATP3
ADR1
CYC1
RPL21A --H77
DOA4 --H87
RPS24A
RPS26B --H68
RPL29
RPS4B --H55
RPL8B --H3
RPL6B --H23
RPS17A
RPS10B --H33
MRPL33
RPL16B
MRPL22
RPL33B
RPL20B
YPK1 --H7
NMD2
KGD1
AAT1
ATG5
HXK2 --H88
YAK1
TDH2
EXO1
RPP1B
MRPL11
ICL1
ADE5
KSS1 --H24
LSC2
RPS27B --H25
RPS21B
TMA19
RPS27A --H25
RPL6A --H23
RPL13B --H45
ADE4
PEP12
ATG13
PPI str.
500
600
700
800
900
exp
RTG3
HMT1
ISW1 --H89
RPN4
ARF1
SSD1
TOM1
SNF4
PMR1
MPT5
YOR1
SPT10
SSC1 --H61
OPI3
TIF1
SPT8
SIC1
SWI6
YPT6
ROM2
TSA1
WHI3
BNI1
CLA4
BRE5
RPT5
PHO85
SLA1
PET9
REI1
RVS161
PPH3
PDA1
SCP160
BIR1
TPK3 --H67
BAS1
UBP8 --H87
MRE11
GAS1
RAD50
CKA2
SSN3
VPS30 --H62
YME1
RXT2
VMA2
SWD3
BEM1
SGF29
SWI5 --H84
ADA2
CHD1
UBP6
PAC10
SMI1
YTA7
RTT107
SRS2
CTK1 --H13
SET3
RKR1
PHO23
PSD1
URE2
RTG1
ADH1
IDH2
ISW2 --H89
PDE2
TPK2 --H67
CTF4
B
PPI str.
500
600
700
800
900
exp
DAF-16 --H60
LET-60 --H53
DAF-2 --H27
DCR-1
SEM-5 --H22
LET-23 --H69
PHA-4
EEF-2 --H86
RPT-1 --H70
ISP-1 --H46
MPK-1 --H24
ATG-7 --H35
GPI-1
NCBP-2
IFG-1 --H85
CDTL-7 --H13
RPS-3
RPN-11
RPN-6.1
RPS-0 --H47
ATP-2 --H49
DAF-18 --H59
RPS-6 --H83
ELC-1
RPS-11 --H34
LET-363 --H36
RPS-15
COX-6A
CYC-1 --H48
RPL-9 --H57
RPS-5
EIF-3.B
RPL-30
CDC-48.1 --H29
RPC-2
ATP-3
CCT-8
SIR-2.1 --H79
CCO-1
RPL-4 --H43
RLA-0
RPL-7 --H78
RPL-23
EGL-8
RPL-3
RAB-5 --H5
RPS-23
RPS-14
RPS-8
RPS-16
SET-2 --H44
CCO-2
UTX-1
RPS-20
TUFM-1
HSP-6 --H61
SMG-1
ATP-1
RACK-1
MEV-1
ATP-5
MRPL-2
MAG-1
RPB-8
RAB-7 --H91
RPL-19 --H71
RPS-10 --H33
RPL-10 --H41
RPS-22
RPS-12 --H19
EIF-2GAMMA
RPL-17 --H51
FZY-1
AKT-1 --H7
EEF-1A.1
LIN-2
MES-2
GDI-1
AGE-1 --H15
MRPS-5
NDK-1
Y56A3A.19
DAF-15
HSF-1 --H75
JNK-1 --H39
MDH-2 --H81
ASB-1 --H2
RPS-26 --H68
SMK-1
UCR-1 --H73
NUO-2
BEC-1 --H62
MRPS-10
WWP-1
RPL-1
B0511.6
ODR-3 --H8
ASB-2 --H2
DAF-12 --H30
ACO-2
T02H6.11
MRPL-12
ULE-5
TAX-4
SOD-2 --H74
RPOA-2
AAK-2 --H72
IFF-1
SKN-1
CKU-70 --H9
DAF-7 --H65
TAX-6
EGL-45
LGG-1 --H18
EIF-3.F
MRPL-1
CCT-4
GPC-1
GAS-1
IFE-2 --H4
EIF-3.K
CHC-1
UCR-2.3
T27E9.2
NOL-5
RPL-31 --H1
COX-4
RPL-7A
QARS-1
RSKS-1 --H7
BAR-1 --H37
CLK-2
GLP-1
NHR-49
UNC-4
VAB-1
LIN-11
C
PPI str.
500
600
700
800
900
exp
foxo --H60
Atg7 --H35
Cat --H32
Sir2 --H79
Sod2 --H74
Akt1 --H7
Pten --H59
InR --H27
Sod --H10
bsk --H39
Tor --H36
Hsp70Ba --H80
dm --H40
Hsc70-3
dpp --H65
p38b --H39
Atg1 --H12
park
Pink1
D
PPI str.
500
600
700
800
900
exp
Trp53 --H42
Sirt1 --H79
Akt1 --H7
Igf1 --H90
Atm --H52
Myc --H40
Pten --H59
Pparg --H30
Cat --H32
Trp53bp1 --H20
Sod2 --H74
Chek2 --H31
Mtor --H36
E
PPI str.
500
600
700
800
900
exp
TP53 --H42
EP300 --H14
AKT1 --H7
MAPK8 --H39
EGFR --H69
STAT3 --H63
HSP90AA1
CREBBP --H14
MAPK14 --H39
H2AFX
EIF2I
CTNNB1 --H37
ESR1
PIK3R1
RELA
MYC --H40
SIRT1 --H79
ATM --H52
BRCA1 --H11
JUN --H38
SHC1
GRB2 --H22
NFKB1
SP1 --H84
RB1
HDAC1 --H16
PARP1 --H50
CDK1
AR
MDM2
XRCC6 --H9
CDKN1A
ABL1
UBB --H66
MAPK3 --H24
HRAS --H53
APP
PIK3CA --H15
RPA1
VEGFA
SUMO1
EGF
IGF1 --H90
JAK2
PCNA
PTPN11
PTEN --H59
INS
IL6
FOS --H54
MTOR --H36
IRS1
RAD51 --H76
PIK3CB --H15
TNF
FOXO3 --H60
PPARG --H30
CREB1 --H54
ERBB2 --H69
NR3C1
CAT --H32
LEP
CDKN2A
NGF
FOXO1 --H60
SOD2 --H74
IGF1R --H27
SOD1 --H10
STAT5B --H63
GSK3B
CHEK2 --H31
BDNF
PRKDC
HSPA8 --H80
YWHAZ --H82
PML
VCP --H29
HSPA1A --H80
TP53BP1 --H20
HSPD1
XRCC5
PRKCA
HDAC2 --H16
HIF1A

Figure 5

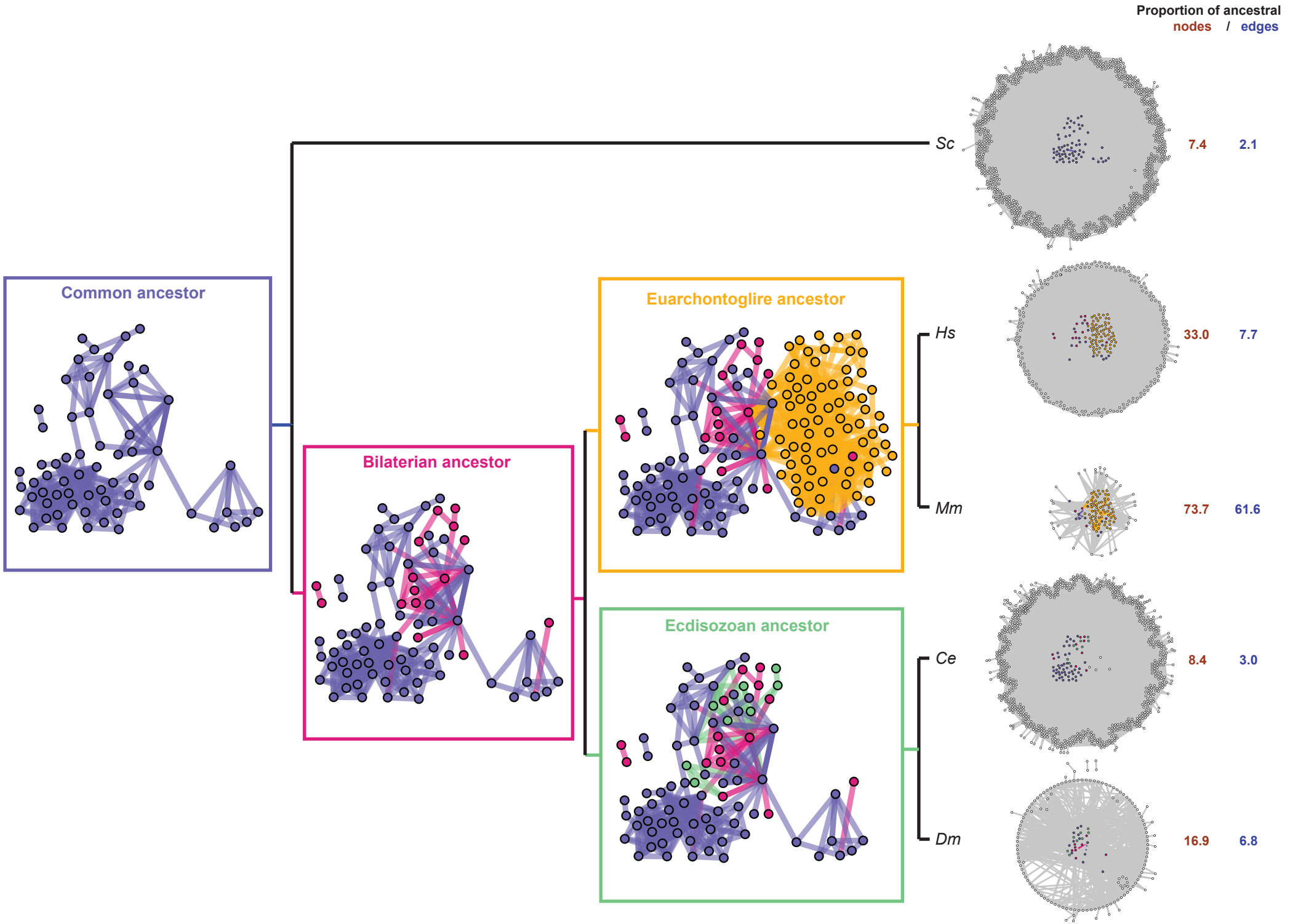
Proportion of ancestral
nodes / edges
Common ancestor
Bilaterian ancestor
Euarchontoglire ancestor
Ecdisozoan ancestor
Sc
Hs
Mm
Ce
Dm
7.4
2.1
33.0
7.7
73.7
61.6
8.4
3.0
16.9
6.8

Figure 6

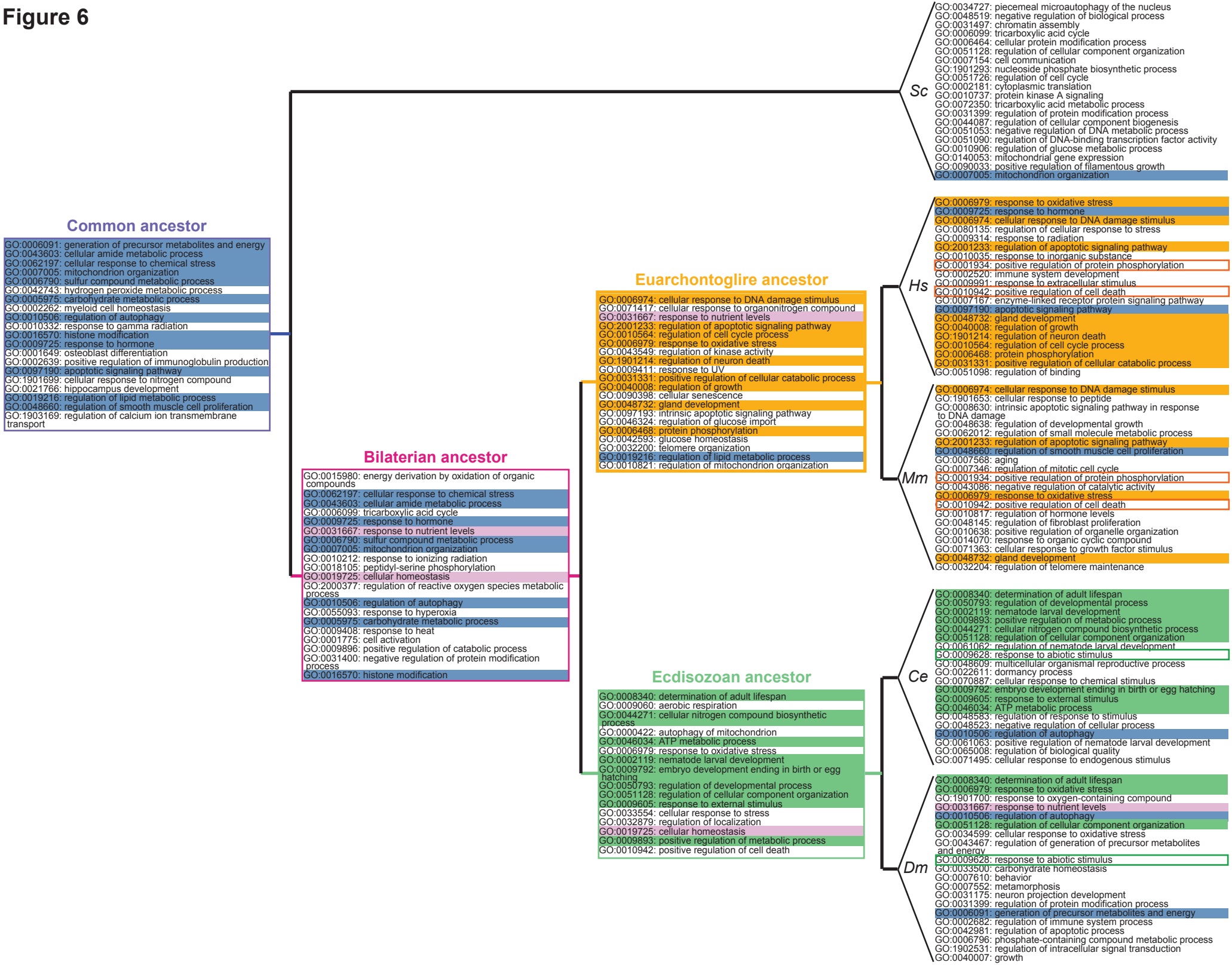
Common ancestor
GO:0006091: generation of precursor metabolites and energy
GO:0043603: cellular amide metabolic process
GO:0062197: cellular response to chemical stress
GO:0007005: mitochondrion organization
GO:0006790: sulfur compound metabolic process
GO:0042743: hydrogen peroxide metabolic process
GO:0005975: carbohydrate metabolic process
GO:0002262: myeloid cell homeostasis
GO:0010506: regulation of autophagy
GO:0010332: response to gamma radiation
GO:0016570: histone modification
GO:0009725: response to hormone
GO:0001649: osteoblast differentiation
GO:0002639: positive regulation of immunoglobulin production
GO:0097190: apoptotic signaling pathway
GO:1901699: cellular response to nitrogen compound
GO:0021766: hippocampus development
GO:0019216: regulation of lipid metabolic process
GO:0048660: regulation of smooth muscle cell proliferation
GO:1903169: regulation of calcium ion transmembrane transport
Bilaterian ancestor
GO:0015980: energy derivation by oxidation of organic compounds
GO:0062197: cellular response to chemical stress
GO:0043603: cellular amide metabolic process
GO:0006099: tricarboxylic acid cycle
GO:0009725: response to hormone
GO:0031667: response to nutrient levels
GO:0006790: sulfur compound metabolic process
GO:0007005: mitochondrion organization
GO:0010212: response to ionizing radiation
GO:0018105: peptidyl-serine phosphorylation
GO:0019725: cellular homeostasis
GO:2000377: regulation of reactive oxygen species metabolic process
GO:0010506: regulation of autophagy
GO:0055093: response to hyperoxia
GO:0005975: carbohydrate metabolic process
GO:0009408: response to heat
GO:0001775: cell activation
GO:0009896: positive regulation of catabolic process
GO:0031400: negative regulation of protein modification process
GO:0016570: histone modification
Euarchontoglire ancestor
GO:0006974: cellular response to DNA damage stimulus
GO:0071417: cellular response to organonitrogen compound
GO:0031667: response to nutrient levels
GO:2001233: regulation of apoptotic signaling pathway
GO:0010564: regulation of cell cycle process
GO:0006979: response to oxidative stress
GO:0043549: regulation of kinase activity
GO:1901214: regulation of neuron death
GO:0009411: response to UV
GO:0031331: positive regulation of cellular catabolic process
GO:0040008: regulation of growth
GO:0090398: cellular senescence
GO:0048732: gland development
GO:0097193: intrinsic apoptotic signaling pathway
GO:0046324: regulation of glucose import
GO:0006468: protein phosphorylation
GO:0042593: glucose homeostasis
GO:0032200: telomere organization
GO:0019216: regulation of lipid metabolic process
GO:0010821: regulation of mitochondrion organization
Ecdisozoan ancestor
GO:0008340: determination of adult lifespan
GO:0009060: aerobic respiration
GO:0044271: cellular nitrogen compound biosynthetic process
GO:0000422: autophagy of mitochondrion
GO:0046034: ATP metabolic process
GO:0006979: response to oxidative stress
GO:0002119: nematode larval development
GO:0009792: embryo development ending in birth or egg hatching
GO:0050793: regulation of developmental process
GO:0051128: regulation of cellular component organization
GO:0009605: response to external stimulus
GO:0033554: cellular response to stress
GO:0032879: regulation of localization
GO:0019725: cellular homeostasis
GO:0009893: positive regulation of metabolic process
GO:0010942: positive regulation of cell death
Sc
GO:0034727: piecemeal microautophagy of the nucleus
GO:0048519: negative regulation of biological process
GO:0031497: chromatin assembly
GO:0006099: tricarboxylic acid cycle
GO:0006464: cellular protein modification process
GO:0051128: regulation of cellular component organization
GO:0007154: cell communication
GO:1901293: nucleoside phosphate biosynthetic process
GO:0051726: regulation of cell cycle
GO:0002181: cytoplasmic translation
GO:0010737: protein kinase A signaling
GO:0072350: tricarboxylic acid metabolic process
GO:0031399: regulation of protein modification process
GO:0044087: regulation of cellular component biogenesis
GO:0051053: negative regulation of DNA metabolic process
GO:0051090: regulation of DNA-binding transcription factor activity
GO:0010906: regulation of glucose metabolic process
GO:0140053: mitochondrial gene expression
GO:0090033: positive regulation of filamentous growth
GO:0007005: mitochondrion organization
Hs
GO:0006979: response to oxidative stress
GO:0009725: response to hormone
GO:0006974: cellular response to DNA damage stimulus
GO:0080135: regulation of cellular response to stress
GO:0009314: response to radiation
GO:2001233: regulation of apoptotic signaling pathway
GO:0010035: response to inorganic substance
GO:0001934: positive regulation of protein phosphorylation
GO:0002520: immune system development
GO:0009991: response to extracellular stimulus
GO:0010942: positive regulation of cell death
GO:0007167: enzyme-linked receptor protein signaling pathway
GO:0097190: apoptotic signaling pathway
GO:0048732: gland development
GO:0040008: regulation of growth
GO:1901214: regulation of neuron death
GO:0010564: regulation of cell cycle process
GO:0006468: protein phosphorylation
GO:0031331: positive regulation of cellular catabolic process
GO:0051098: regulation of binding
Mm
GO:0006974: cellular response to DNA damage stimulus
GO:1901653: cellular response to peptide
GO:0008630: intrinsic apoptotic signaling pathway in response to DNA damage
GO:0048638: regulation of developmental growth
GO:0062012: regulation of small molecule metabolic process
GO:2001233: regulation of apoptotic signaling pathway
GO:0048660: regulation of smooth muscle cell proliferation
GO:0007568: aging
GO:0007346: regulation of mitotic cell cycle
GO:0001934: positive regulation of protein phosphorylation
GO:0043086: negative regulation of catalytic activity
GO:0006979: response to oxidative stress
GO:0010942: positive regulation of cell death
GO:0010817: regulation of hormone levels
GO:0048145: regulation of fibroblast proliferation
GO:0010638: positive regulation of organelle organization
GO:0014070: response to organic cyclic compound
GO:0071363: cellular response to growth factor stimulus
GO:0048732: gland development
GO:0032204: regulation of telomere maintenance
Ce
GO:0008340: determination of adult lifespan
GO:0050793: regulation of developmental process
GO:0002119: nematode larval development
GO:0009893: positive regulation of metabolic process
GO:0044271: cellular nitrogen compound biosynthetic process
GO:0051128: regulation of cellular component organization
GO:0061062: regulation of nematode larval development
GO:0009628: response to abiotic stimulus
GO:0048609: multicellular organismal reproductive process
GO:0022611: dormancy process
GO:0070887: cellular response to chemical stimulus
GO:0009792: embryo development ending in birth or egg hatching
GO:0009605: response to external stimulus
GO:0046034: ATP metabolic process
GO:0048583: regulation of response to stimulus
GO:0048523: negative regulation of cellular process
GO:0010506: regulation of autophagy
GO:0061063: positive regulation of nematode larval development
GO:0065008: regulation of biological quality
GO:0071495: cellular response to endogenous stimulus
Dm
GO:0008340: determination of adult lifespan
GO:0006979: response to oxidative stress
GO:1901700: response to oxygen-containing compound
GO:0031667: response to nutrient levels
GO:0010506: regulation of autophagy
GO:0051128: regulation of cellular component organization
GO:0034599: cellular response to oxidative stress
GO:0043467: regulation of generation of precursor metabolites and energy
GO:0009628: response to abiotic stimulus
GO:0033500: carbohydrate homeostasis
GO:0007610: behavior
GO:0007552: metamorphosis
GO:0031175: neuron projection development
GO:0031399: regulation of protein modification process
GO:0006091: generation of precursor metabolites and energy
GO:0002682: regulation of immune system process
GO:0042981: regulation of apoptotic process
GO:0006796: phosphate-containing compound metabolic process
GO:1902531: regulation of intracellular signal transduction
GO:0040007: growth

Figure 7

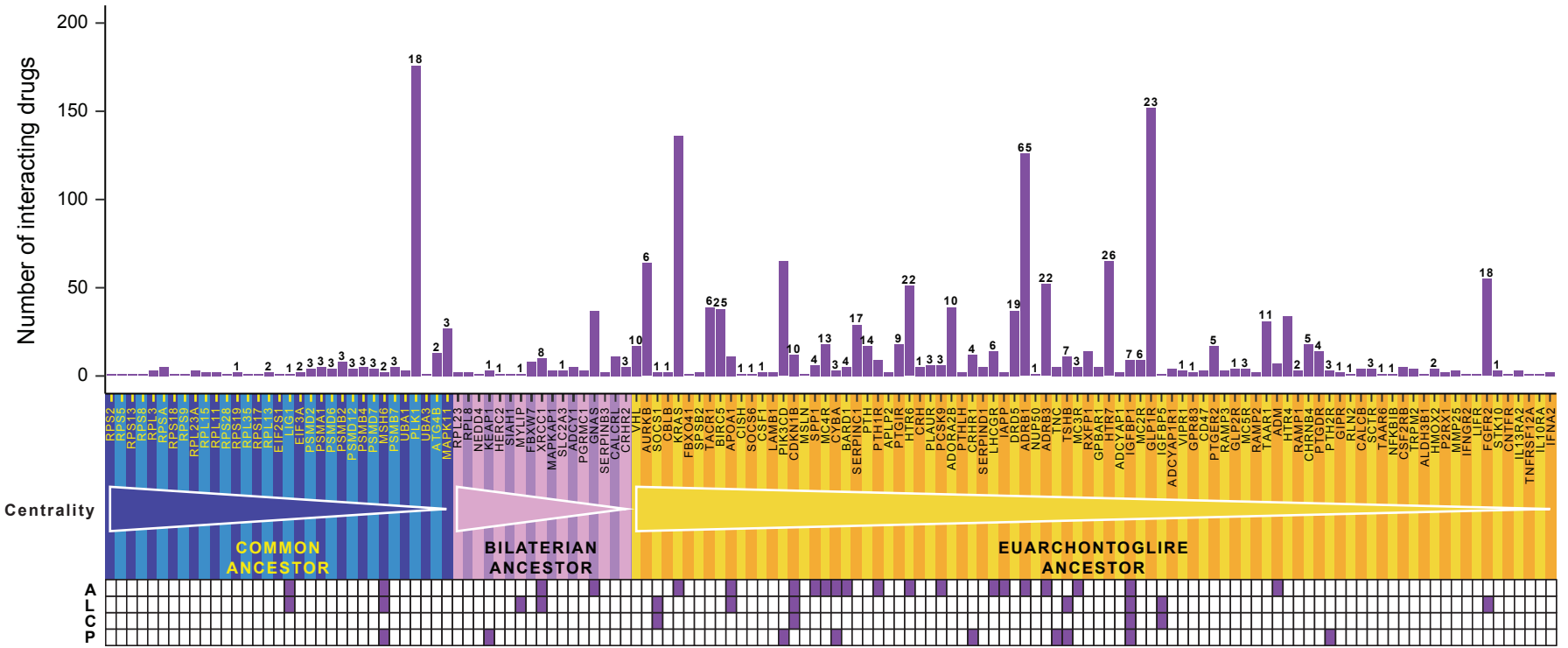
Number of interacting drugs
200
150
100
50
0
Centrality
COMMON ANCESTOR
BILATERIAN ANCESTOR
EUARCHONTOGLIRE ANCESTOR
A
L
C
P

Supplementary figure legends

Supplementary figure 1: Centrality and homophily metrics.

The centrality of nodes in networks was estimated using four centrality metrics: (A) the degree, that is the number of direct connections to this node; (B) the closeness, the reciprocal of the sum of the shortest path distances from a node to all the other nodes, normalised by the sum of all shortest paths, measuring how close a node is from all the others; (C) the betweenness, the sum of the fraction of shortest paths between all pairs of nodes that pass through a node, measuring the 'hubness' of a node; (D) the PageRank, originally designed as an algorithm to rank web pages (Page et al. 1999), that ranks all nodes based on the structure of the incoming links. Homophily between labelled nodes in a network was estimated using (E) the assortativity coefficient of the network, i.e. the Pearson correlation coefficient of degree between pairs of linked nodes (Newman 2003), taking a value between -1 (completely disassortative network) and 1 (completely assortative network).

Supplementary figure 2: Analysis of the centrality of pro-LAPs and anti-LAPs in PPI networks.

Pairwise comparisons of node centrality metrics distributions were performed between (left panel) pro-LAPs and non-LAPs; (centre panel) anti-LAPs and non-LAPs; (right panel) pro-LAPs and anti-LAPs for PPI networks from five Opisthokonta species for each PPI stringency threshold. Stars indicate significantly higher values for LAPs in red cells (left and centre panels), or significant differences between LAPs in yellow cells (right panel). Significance was determined using the unilateral (left and centre panels) or bilateral (right panel) Mann-Whitney U-test: **: $P < 0.001$; *: $P < 0.05$; NS: not significant (blue cells). P-values were adjusted for multiple testing using the Bonferroni method.

Supplementary figure 3: Derivation of subnetworks from node labels.

Nodes in PPI networks were labelled to derive subnetworks: (A) using LAGs annotations in the GenAge database (http://genomics.senescence.info/genes/, Build 20), defining longevity networks constituted by LAP-LAP interactions, either connecting nodes with identical labels (blue edges) or with opposite labels (orange edges); (B) using orthogroup labels from the OMA database (https://omabrowser.org/oma/home/, OMA All.Jan2020 release), defining networks of homologs/orthologs, allowing comparative analysis of interactions between conserved proteins between species (purple edges), or aggregation of subnetworks from different species.

Supplementary figure 4: Network permutation tests.

To detect outlier nodes with statistically significant values of degree, closeness, betweenness and PageRank, as well as nodes with statistically significant numbers of neighbors with opposite label, node rewiring permutation tests were performed by 1000 random network permutations rewiring the nodes but preserving the total number of edges. To detect statistically significant high values of assortativity, and to detect

significantly high values of Jaccard index and numbers of common direct neighbors, node label permutation tests were performed by 1000 random shufflings of the node labels.

Supplementary figure 5: Functional enrichment analysis of candidate ARMLs.
Metascape top 20 enriched GO-terms for (A) *Ce*, (B) *Dm* and (C) *Sc* candidate ARMLs.

Supplementary figure 6: Functional enrichment analysis of the most central LAPs.
Metascape top 20 enriched GO-terms for (A) *Ce*, (B) *Dm*, (C) *Hs*, (D) *Mm* and (E) *Sc* centrality outliers.

Supplementary figure 7: Inference of ancestral networks of orthologs.
Extant species-specific networks of orthologs (node colours indicate orthogroup labels) and a reference phylogenetic tree associated with these species were used to detect conserved protein-protein interaction (edges between the same pair of orthologous proteins, present in different species) and map these edges on the phylogeny (edge colours correspond to their inferred last common ancestor's colour). See M&M for methodological details.

Supplementary figure 8: Inference of ancestral interactions based on conserved LAP-LAP interactions from entire PPI networks.

The entire PPI networks of orthologs from five extant Opisthokonta species were used to infer ancestral networks at inner branches of the phylogeny (Figure S7), shown here for networks at PPI stringency threshold 500. Node and edge colours indicate inferred presence in the common ancestor of all 5 species (blue, common ancestor), of all 4 bilaterian species (pink, bilaterian ancestor), of *Hs* and *Mm* (yellow, euarchontoglire ancestor) or of *Dm* and *Ce* (green, ecdisozoan ancestor). The proportions of ancestral nodes and edges in extant networks of orthologs is indicated at the leaves.

Supplementary figure 9: Guilt-by-association approach for ancestral LAP prediction.

To detect non-LAP ancestral node with similar neighbours than LAP ancestral nodes in inferred ancestral networks, we used the Jaccard index and the absolute number of direct common neighbors (red) between LAP (yellow) and non-LAP (blue) nodes. Significant values of Jaccard index (the ratio between the intersection of the two neighborhoods for a pair of nodes to the union of these two neighborhoods) and of number of common neighbours were determined by network permutation tests (Fig. S4).

Supplementary figure 10: Semantic similarity between GO-terms associated with predicting and predicted proteins

Distribution box plots of GOGO semantic similarity scores (Molecular Function Ontology) using all pairs of GO-term sets associated with predicting and predicted proteins as inputs, for the five species analysed in this study.

Supplementary figure 11: Functional enrichment analysis of predicted LAPs.
Metascape top 20 enriched GO-terms for (A) *Ce*, (B) *Dm*, (C) *Hs*, (D) *Mm* and (E) *Sc* predicted LAPs.

Supplementary table 1: Proteins contributing to the functional enrichment in ancestral networks.
Protein hits for each Metascape top20 enriched GO-terms in ancestral networks.

Supplementary table 2: LAP prediction in five species of Opisthokonta.

For each species, the ancestral network (either common, bilaterian, ecdisozoan or euarchontoglire) where they were predicted is indicated with a number code: non-predicted (0), predicted in thresholded and experimental networks (1), predicted in thresholded networks only (2), predicted in experimental networks only (3). The average degree rank (ADR) in each ancestral network for each predicted LAP is indicated, as well as the number of unique predictors across all ancestral networks (ancestral LAPs with a significant similarity with the predicted ancestral LAP). The Pubmed column contains PMID for abstracts which support a LAP role for the predicted LAP (0 if there is no support). The other columns contain other species-specific sources of support: phenotypic annotations in databases (*Ce*: Wormbase; *Dm*: Flybase; *Sc*: Saccharomyces Genome Database) or presence in aging and longevity-related gene sets (*Hs*: Cellage, ARD, LongevityMap, see M&M). Support is indicated by 1, no support is indicated by 0. Human-specific annotations on druggability comprise the columns Druggable (yes: 1, no: 0), nb_drugs (number of drugs targeting the predicted LAP in DGIdb) , FDA_approved_drugs (number of FDA-approved drugs targeting the predicted LAP in DGIdb, when there is only one its name is indicated), max_interaction_score (highest DGIdb drug-target interaction score).

Supplementary table 3: Super-central predicted human LAPs.

The 265 human predicted LAPs with an average degree rank (ADR) over all PPI stringency thresholds lower than MTOR (232.3). Associations with cellular senescence (from the CellAge gene set), with longevity (from the LongevityMap database), or with Ageing-Related Diseases (ARD gene set from Fernandes et al. 2016) and druggability according to the DGIdb database are indicated.

Supplementary table 4: Homology codes used to annotate outliers in extant longevity networks.

Annotations based on orthology relationships from the Alliance of Genome Resources Portal (Alliance Database Version: 4.1.0, http://www.alliancegenome.org). Arbitrary --H codes have been attributed to ARMLs and centrality outliers to compare extant species. The STRING, Alliance and gene symbol identifiers are indicated for the members of each --H group.

Figure S1

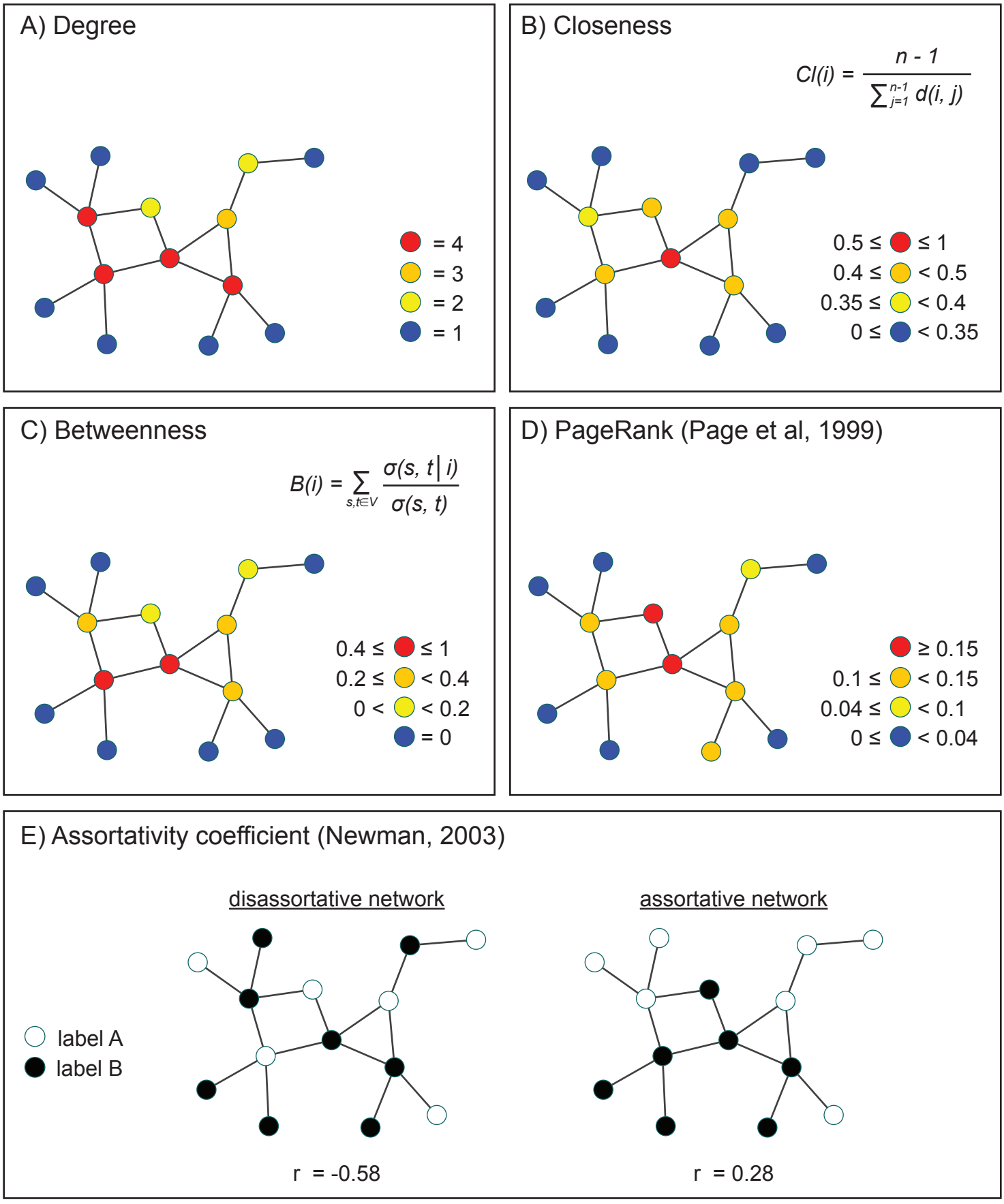
A) Degree
= 4
= 3
= 2
= 1
B) Closeness
$Cl(i) = \frac{n-1}{\sum_{j=1}^{n-1} d(i,j)}$
0.5 ≤ ≤ 1
0.4 ≤ < 0.5
0.35 ≤ < 0.4
0 ≤ < 0.35
C) Betweenness
$B(i) = \sum_{s,t \in V} \frac{\sigma(s,t|i)}{\sigma(s,t)}$
0.4 ≤ ≤ 1
0.2 ≤ < 0.4
0 < < 0.2
= 0
D) PageRank (Page et al, 1999)
≥ 0.15
0.1 ≤ < 0.15
0.04 ≤ < 0.1
0 ≤ < 0.04
E) Assortativity coefficient (Newman, 2003)
label A
label B
disassortative network
r = -0.58
assortative network
r = 0.28

Figure S2


pro-LAPs compared to non-LAPs
anti-LAPs compared to non-LAPs
pro-LAPs compared to anti-LAPs
PPI stringency
500 600 700 800 900 exp
S. cerevisiae
Betweenness ** ** ** ** * **
Closeness ** ** * NS NS **
Degree ** ** * * NS **
PageRank ** ** * * NS **
Betweenness ** ** ** ** ** **
Closeness ** ** ** ** * **
Degree ** ** ** ** ** **
PageRank ** ** ** ** ** **
Betweenness NS NS NS NS NS *
Closeness NS NS NS NS NS NS
Degree NS NS NS NS NS NS
PageRank NS NS NS NS NS NS
D. melanogaster
Betweenness ** ** ** ** ** NS
Closeness ** ** ** ** NS NS
Degree ** ** ** ** NS NS
PageRank ** ** ** * NS NS
Betweenness ** ** ** * NS NS
Closeness ** ** * NS NS NS
Degree ** * * NS NS NS
PageRank ** * NS NS NS NS
Betweenness NS NS NS NS NS NS
Closeness NS NS NS NS NS NS
Degree NS NS NS NS NS NS
PageRank NS NS NS NS NS NS
C. elegans
Betweenness ** ** ** ** ** **
Closeness ** ** ** * NS NS
Degree ** ** ** ** * **
PageRank ** ** ** ** ** **
Betweenness ** ** ** ** ** NS
Closeness ** ** ** ** NS NS
Degree ** ** ** ** ** NS
PageRank ** ** ** ** ** NS
Betweenness NS NS NS NS NS *
Closeness NS NS NS NS NS NS
Degree NS NS NS NS NS *
PageRank NS NS NS NS NS *
M. musculus
Betweenness ** ** ** ** ** **
Closeness ** ** ** ** * NS
Degree ** ** ** ** * **
PageRank ** ** ** ** ** **
Betweenness ** ** ** ** * *
Closeness ** ** ** * NS *
Degree ** ** ** * NS NS
PageRank ** ** ** * NS **
Betweenness NS NS NS NS NS NS
Closeness NS NS NS NS NS NS
Degree NS NS NS NS NS NS
PageRank NS NS NS NS NS NS

Figure S3

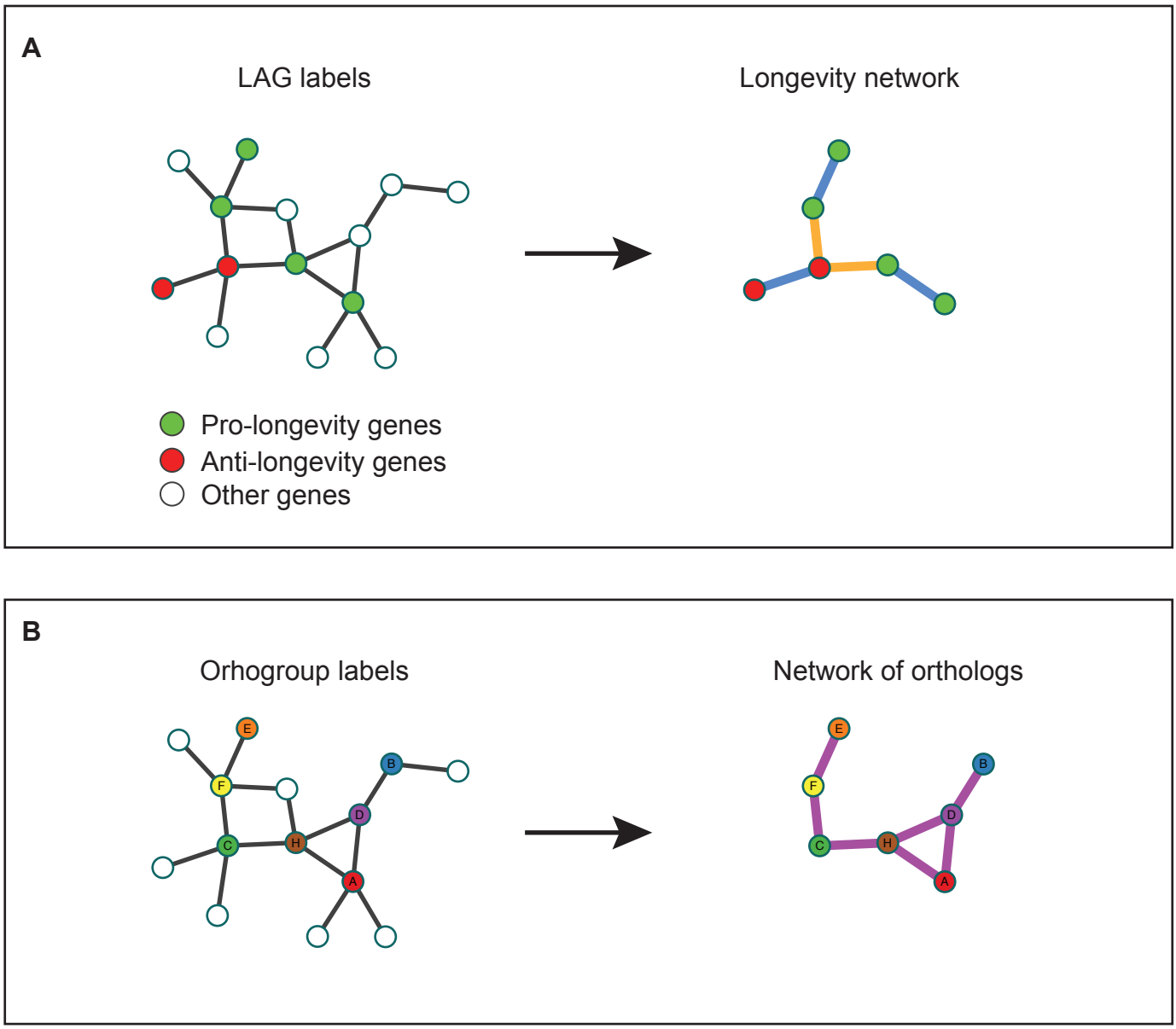
A
LAG labels
Longevity network
Pro-longevity genes
Anti-longevity genes
Other genes
B
Orhogroup labels
Network of orthologs
E
F
B
D
C
H
A

Figure S4

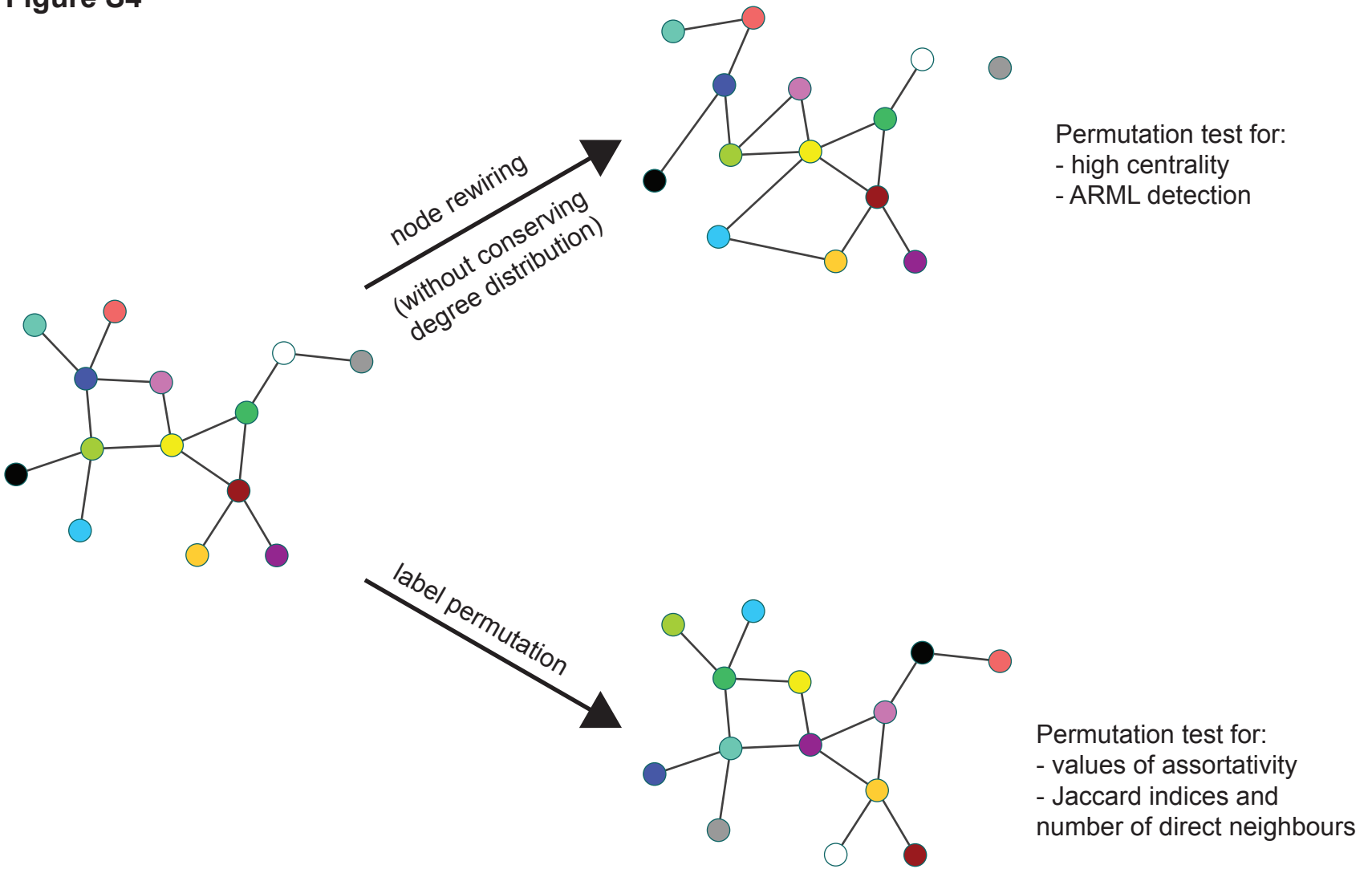
node rewiring
(without conserving
degree distribution)
label permutation
Permutation test for:
- high centrality
- ARML detection
Permutation test for:
- values of assortativity
- Jaccard indices and
number of direct neighbours

Figure S5

A

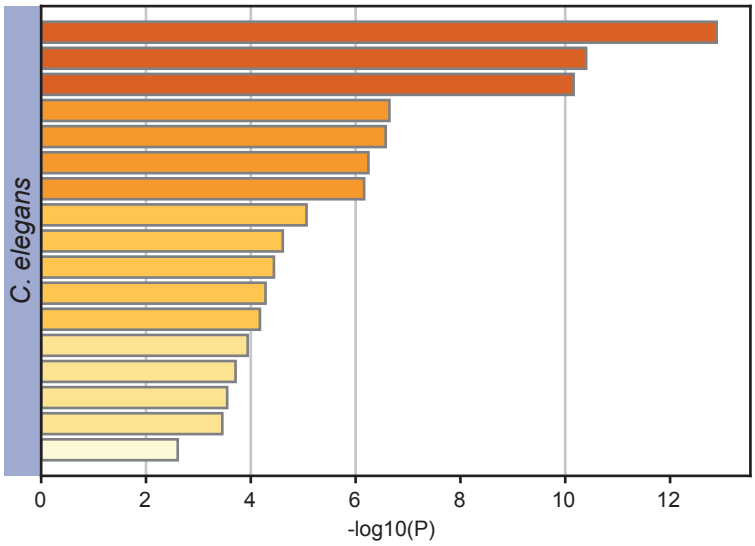

GO:0008340: determination of adult lifespan
GO:1902074: response to salt
GO:0051173: positive regulation of nitrogen compound metabolic process
GO:0008582: regulation of synaptic assembly at neuromuscular junction
GO:0010557: positive regulation of macromolecule biosynthetic process
GO:0006979: response to oxidative stress
GO:0009617: response to bacterium
GO:0022414: reproductive process
GO:0033554: cellular response to stress
GO:0007389: pattern specification process
GO:0045727: positive regulation of translation
GO:0006099: tricarboxylic acid cycle
GO:0040034: regulation of development, heterochronic
GO:1902115: regulation of organelle assembly
GO:0006351: transcription, DNA-templated
GO:0040028: regulation of vulval development
GO:0061061: muscle structure development

B

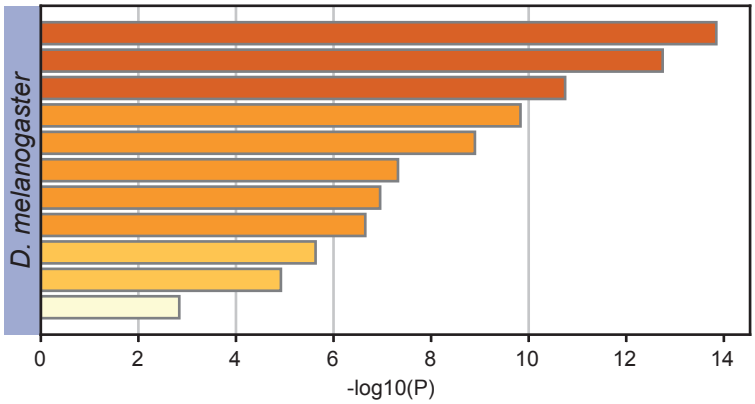

GO:0040014: regulation of multicellular organism growth
GO:0006979: response to oxidative stress
GO:0051239: regulation of multicellular organismal process
GO:0046620: regulation of organ growth
GO:0040012: regulation of locomotion
GO:0034599: cellular response to oxidative stress
GO:0006468: protein phosphorylation
GO:0010941: regulation of cell death
GO:0060259: regulation of feeding behavior
GO:0042325: regulation of phosphorylation
GO:0031399: regulation of protein modification process

C

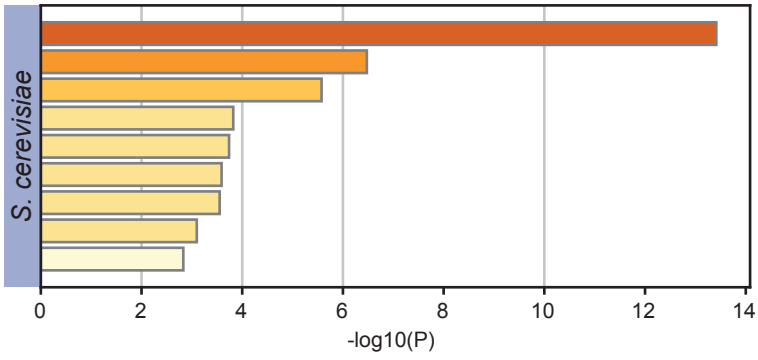

GO:0006091: generation of precursor metabolites and energy
GO:0006739: NADP metabolic process
GO:0046034: ATP metabolic process
GO:1905268: negative regulation of chromatin organization
GO:0022904: respiratory electron transport chain
GO:0072593: reactive oxygen species metabolic process
GO:0031570: DNA integrity checkpoint signaling
GO:0000041: transition metal ion transport
GO:0006006: glucose metabolic process

Figure S6

A

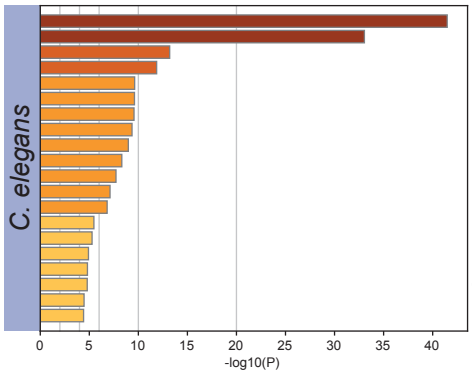

GO:0008340: determination of adult lifespan
GO:0006412: translation
GO:0040024: dauer larval development
GO:0002181: cytoplasmic translation
GO:0046034: ATP metabolic process
GO:0050793: regulation of developmental process
GO:0009894: regulation of catabolic process
GO:0022618: ribonucleoprotein complex assembly
GO:0048609: multicellular organismal reproductive process
GO:0009145: purine nucleoside triphosphate biosynthetic process
GO:0051128: regulation of cellular component organization
GO:1902074: response to salt
GO:0035556: intracellular signal transduction
GO:0040026: positive regulation of vulval development
GO:1901701: cellular response to oxygen-containing compound
GO:0006935: chemotaxis
GO:0042176: regulation of protein catabolic process
GO:0007611: learning or memory
GO:0009416: response to light stimulus
GO:0043620: regulation of DNA-templated transcription in response to stress

B

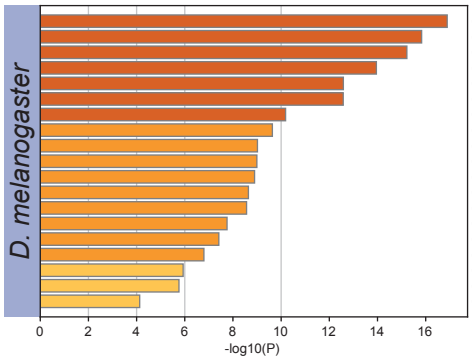

GO:0051239: regulation of multicellular organismal process
GO:0010506: regulation of autophagy
GO:0006979: response to oxidative stress
GO:0070887: cellular response to chemical stimulus
GO:0040014: regulation of multicellular organism growth
GO:0051094: positive regulation of developmental process
GO:0010508: positive regulation of autophagy
GO:0051093: negative regulation of developmental process
GO:0007167: enzyme-linked receptor protein signaling pathway
GO:0002682: regulation of immune system process
GO:0042594: response to starvation
GO:0035206: regulation of hemocyte proliferation
GO:0008340: determination of adult lifespan
GO:1902532: negative regulation of intracellular signal transduction
GO:0006468: protein phosphorylation
GO:0048520: positive regulation of behavior
GO:0007568: aging
GO:0014066: regulation of phosphatidylinositol 3-kinase signaling
GO:0010605: negative regulation of macromolecule metabolic process

C

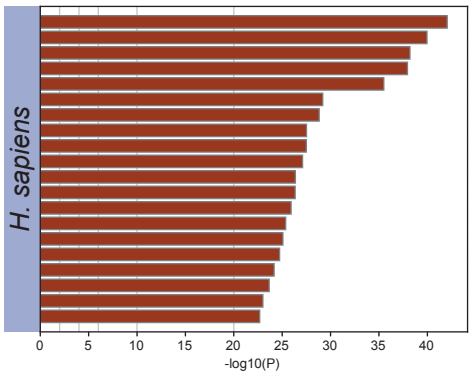

GO:0071417: cellular response to organonitrogen compound
GO:0080135: regulation of cellular response to stress
GO:0009314: response to radiation
GO:0062197: cellular response to chemical stress
GO:0071363: cellular response to growth factor stimulus
GO:0040008: regulation of growth
GO:2001233: regulation of apoptotic signaling pathway
GO:0010942: positive regulation of cell death
GO:0048511: rhythmic process
GO:0002520: immune system development
GO:0001934: positive regulation of protein phosphorylation
GO:0048732: gland development
GO:0043408: regulation of MAPK cascade
GO:0071396: cellular response to lipid
GO:0051090: regulation of DNA-binding transcription factor activity
GO:0051054: positive regulation of DNA metabolic process
GO:0030335: positive regulation of cell migration
GO:0031331: positive regulation of cellular catabolic process
GO:0048660: regulation of smooth muscle cell proliferation
GO:1901214: regulation of neuron death

D

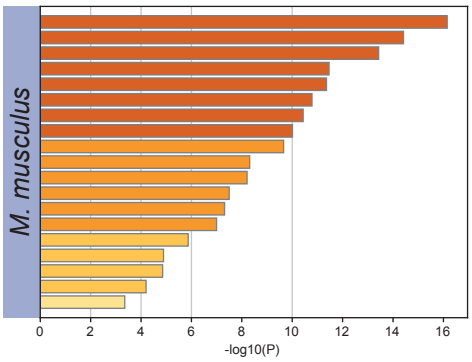

GO:0070482: response to oxygen levels
GO:0009314: response to radiation
GO:0048660: regulation of smooth muscle cell proliferation
GO:1902532: negative regulation of intracellular signal transduction
GO:0008630: intrinsic apoptotic signaling pathway in response to DNA damage
GO:0010660: regulation of muscle cell apoptotic process
GO:0006974: cellular response to DNA damage stimulus
GO:0062197: cellular response to chemical stress
GO:0045598: regulation of fat cell differentiation
GO:0048145: regulation of fibroblast proliferation
GO:0010661: positive regulation of muscle cell apoptotic process
GO:0010823: negative regulation of mitochondrion organization
GO:0031641: regulation of myelination
GO:0045428: regulation of nitric oxide biosynthetic process
GO:0035264: multicellular organism growth
GO:0014068: positive regulation of phosphatidylinositol 3-kinase signaling
GO:2001021: negative regulation of response to DNA damage stimulus
GO:0001655: urogenital system development
GO:0051259: protein complex oligomerization

E

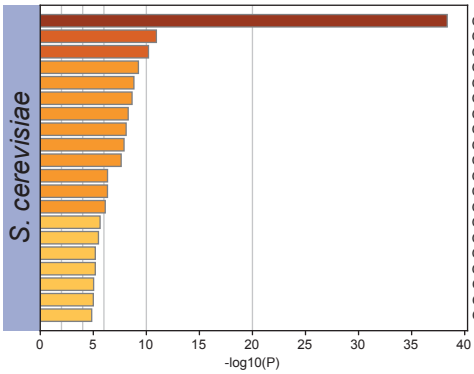

GO:0002181: cytoplasmic translation
GO:0019219: regulation of nucleobase-containing compound metabolic process
GO:0006099: tricarboxylic acid cycle
GO:0070925: organelle assembly
GO:0007154: cell communication
GO:0051128: regulation of cellular component organization
GO:0051726: regulation of cell cycle
GO:0051052: regulation of DNA metabolic process
GO:0042273: ribosomal large subunit biogenesis
GO:0006995: cellular response to nitrogen starvation
GO:0072593: reactive oxygen species metabolic process
GO:0044087: regulation of cellular component biogenesis
GO:0010737: protein kinase A signaling
GO:0010506: regulation of autophagy
GO:0051246: regulation of protein metabolic process
GO:0032200: telomere organization
GO:0072350: tricarboxylic acid metabolic process
GO:0006950: response to stress
GO:0000018: regulation of DNA recombination
GO:0051090: regulation of DNA-binding transcription factor activity

Figure S7

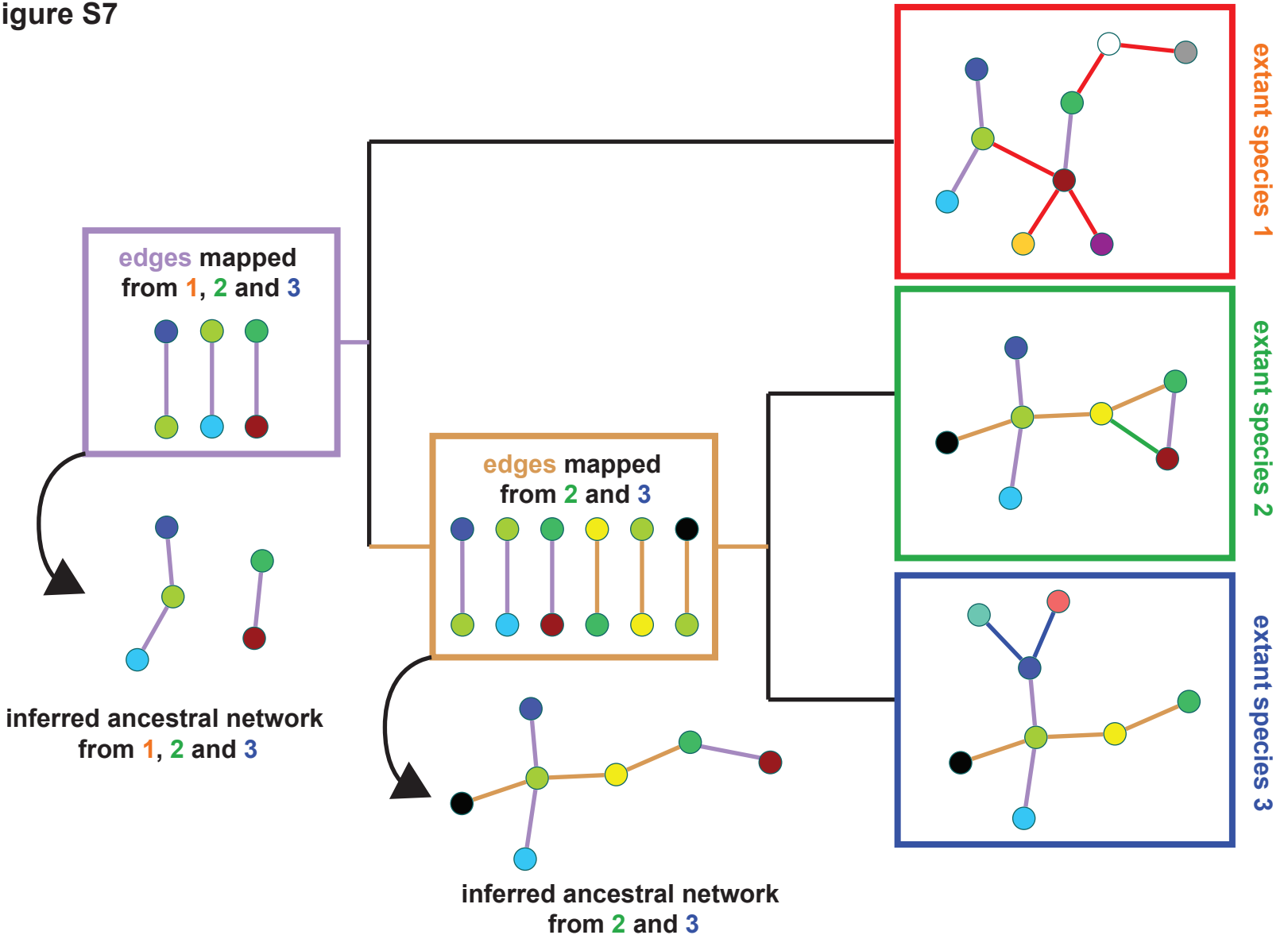
edges mapped
from 1, 2 and 3
inferred ancestral network
from 1, 2 and 3
edges mapped
from 2 and 3
inferred ancestral network
from 2 and 3
extant species 1
extant species 2
extant species 3

Figure S8

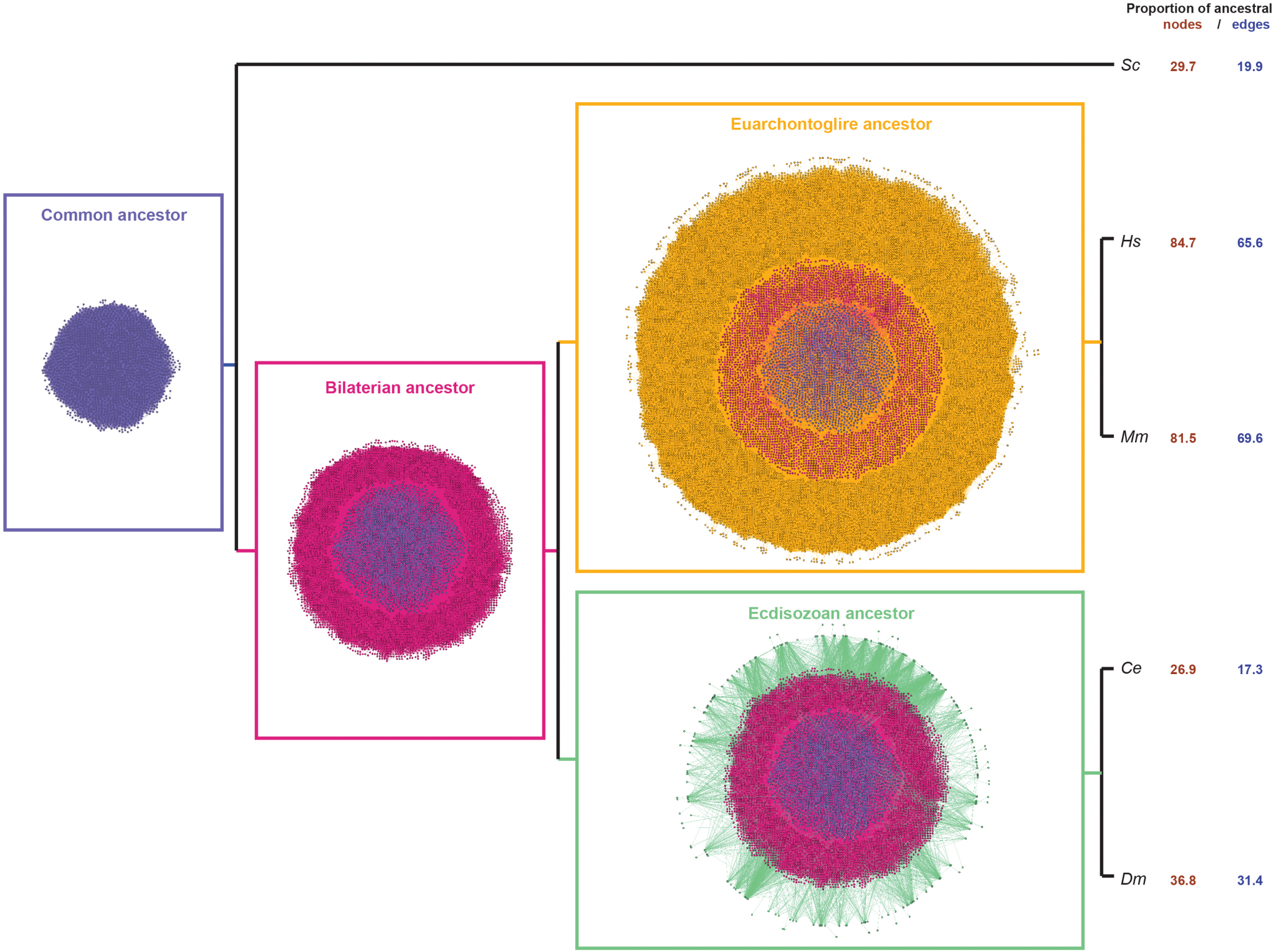
Proportion of ancestral
nodes / edges
Sc 29.7 19.9
Common ancestor
Bilaterian ancestor
Euarchontoglire ancestor
Hs 84.7 65.6
Mm 81.5 69.6
Ecdisozoan ancestor
Ce 26.9 17.3
Dm 36.8 31.4

Figure S9

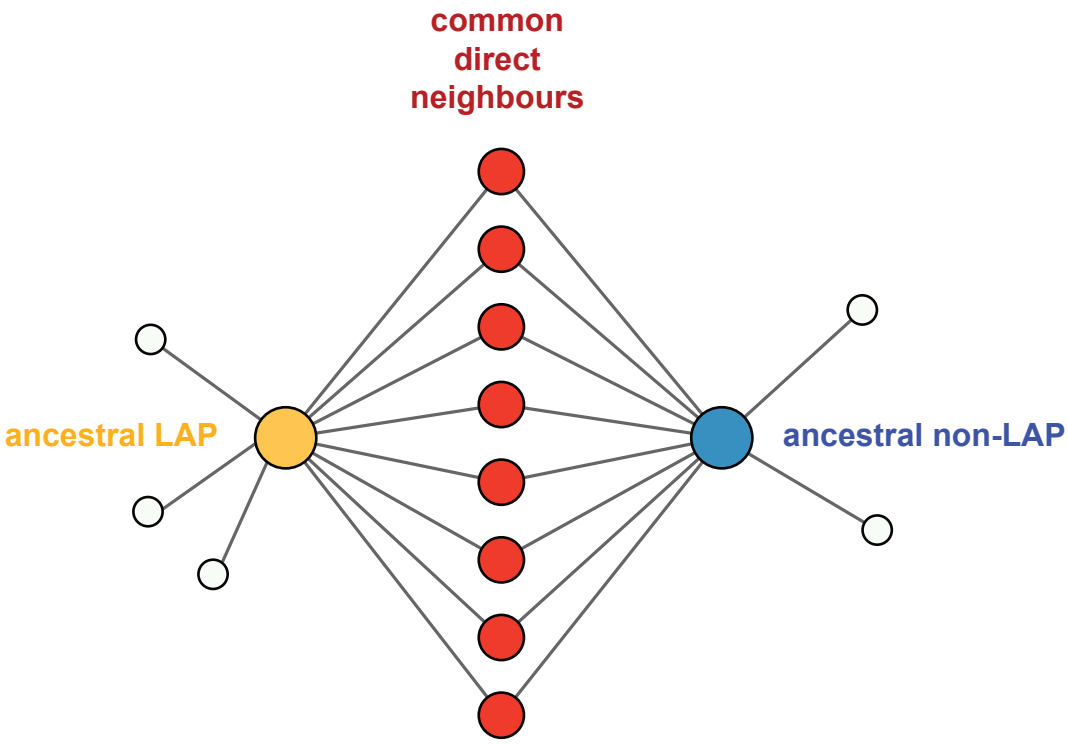

Number of common neighbours: 8
Total number of direct neighbours: 13

Jaccard index = 0.61 (8/13)

Figure S10

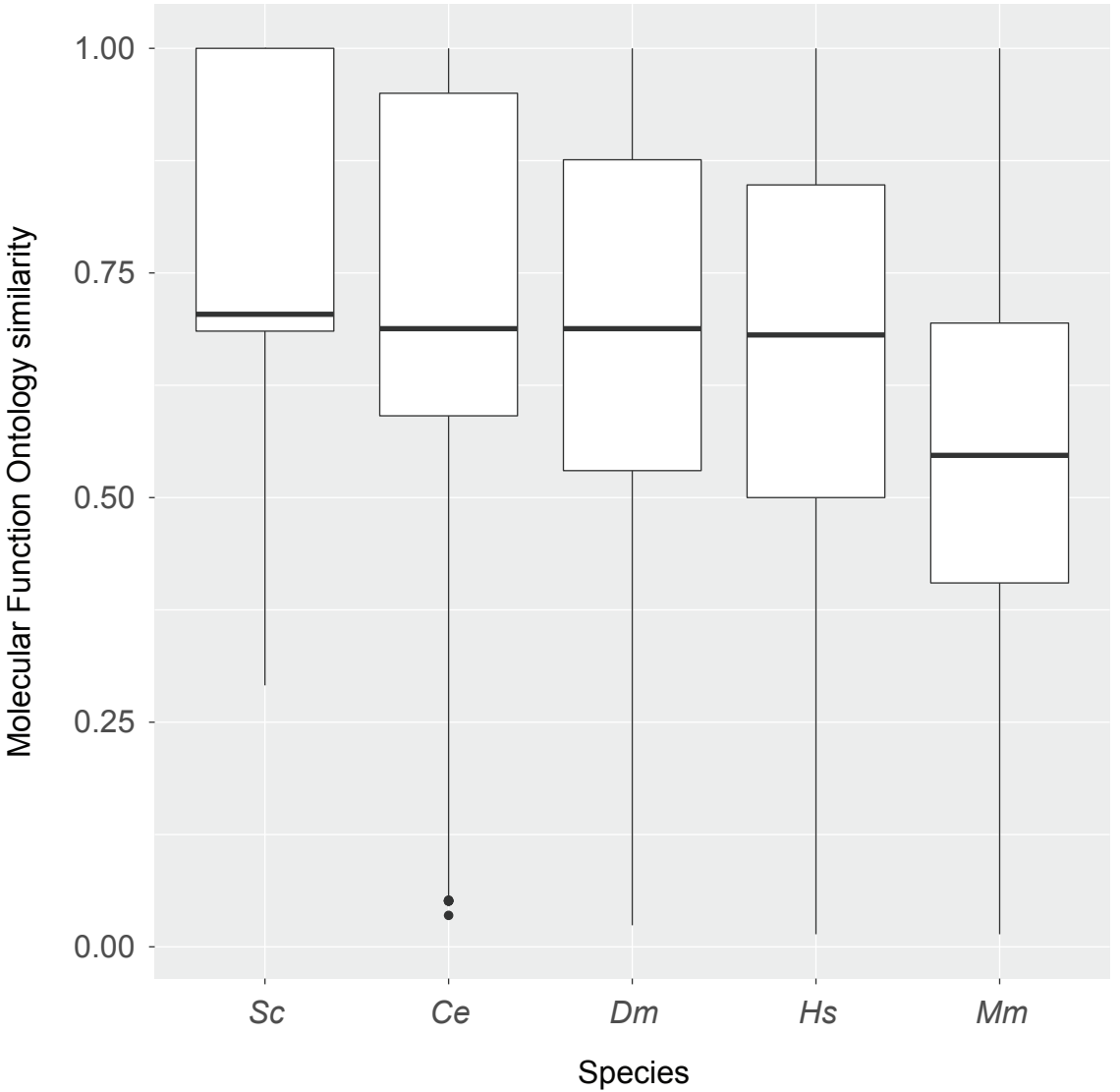
1.00
0.75
0.50
0.25
0.00
Molecular Function Ontology similarity
Sc
Ce
Dm
Hs
Mm
Species

Figure S11

A

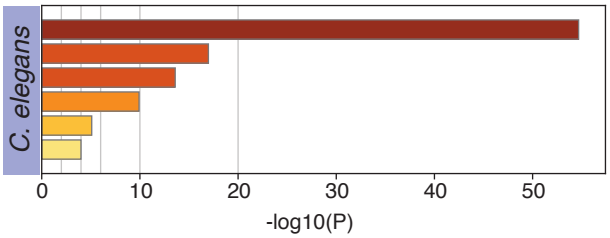

GO:0006412: translation
GO:0002181: cytoplasmic translation
GO:0022613: ribonucleoprotein complex biogenesis
GO:0010498: proteasomal protein catabolic process
GO:0042274: ribosomal small subunit biogenesis
GO:0010623: programmed cell death involved in cell development

B

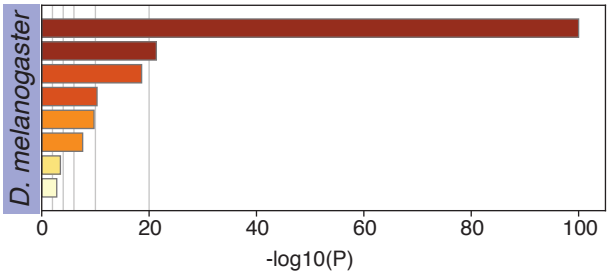

GO:0002181: cytoplasmic translation
GO:0022613: ribonucleoprotein complex biogenesis
GO:0043161: proteasome-mediated ubiquitin-dependent protein catabolic process
GO:0006413: translational initiation
GO:0042273: ribosomal large subunit biogenesis
GO:0006364: rRNA processing
GO:0042176: regulation of protein catabolic process
GO:0016199: axon midline choice point recognition

C

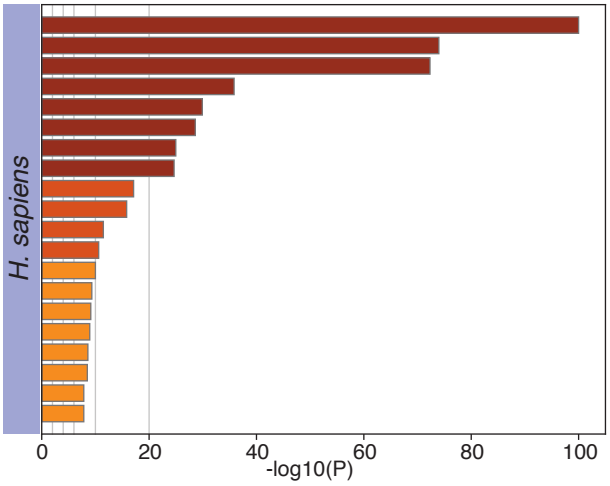

GO:0016567: protein ubiquitination
GO:0002181: cytoplasmic translation
GO:0000209: protein polyubiquitination
GO:0007188: adenylate cyclase-modulating G protein-coupled receptor signaling pathway
GO:0031146: SCF-dependent proteasomal ubiquitin-dependent protein catabolic process
GO:0070979: protein K11-linked ubiquitination
GO:0042176: regulation of protein catabolic process
GO:1903320: regulation of protein modification by small protein conjugation or removal
GO:0051865: protein autoubiquitination
GO:0045116: protein neddylation
GO:0010965: regulation of mitotic sister chromatid separation
GO:0007190: activation of adenylate cyclase activity
GO:1903047: mitotic cell cycle process
GO:0097646: calcitonin family receptor signaling pathway
GO:0006413: translational initiation
GO:0046058: cAMP metabolic process
GO:1904666: regulation of ubiquitin protein ligase activity
GO:0006974: cellular response to DNA damage stimulus
GO:0040008: regulation of growth
GO:0044703: multi-organism reproductive process

D

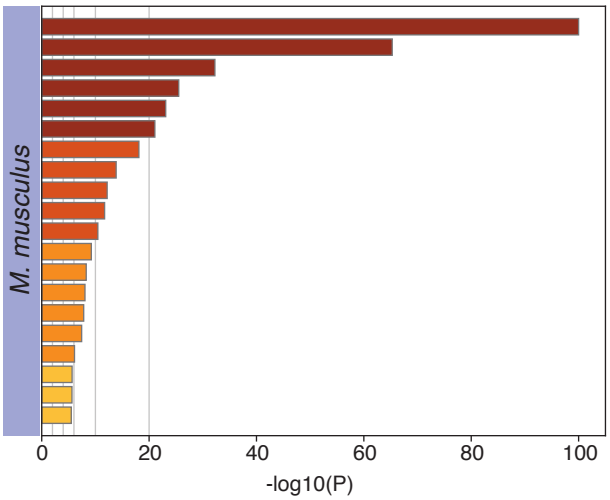

GO:0016567: protein ubiquitination
GO:0002181: cytoplasmic translation
GO:0007188: adenylate cyclase-modulating G protein-coupled receptor signaling pathway
GO:0031146: SCF-dependent proteasomal ubiquitin-dependent protein catabolic process
GO:0070936: protein K48-linked ubiquitination
GO:0070979: protein K11-linked ubiquitination
GO:0042176: regulation of protein catabolic process
GO:0051865: protein autoubiquitination
GO:1903320: regulation of protein modification by small protein conjugation or removal
GO:0043950: positive regulation of cAMP-mediated signaling
GO:0097646: calcitonin family receptor signaling pathway
GO:0007190: activation of adenylate cyclase activity
GO:0010965: regulation of mitotic sister chromatid separation
GO:0031648: protein destabilization
GO:0042273: ribosomal large subunit biogenesis
GO:0000338: protein deneddylation
GO:0045116: protein neddylation
GO:0006289: nucleotide-excision repair
GO:0044772: mitotic cell cycle phase transition
GO:0006974: cellular response to DNA damage stimulus

E

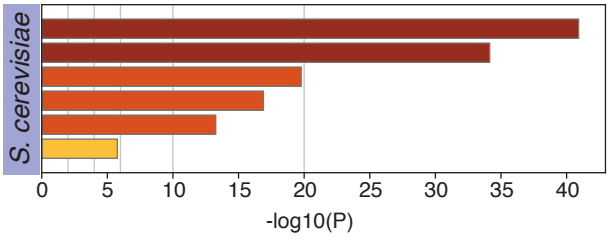

GO:0002181: cytoplasmic translation
GO:0006412: translation
GO:0042254: ribosome biogenesis
GO:0042255: ribosome assembly
GO:0006407: rRNA export from nucleus
GO:0006450: regulation of translational fidelity

Ancestor	GO-term	Description	Species used	Hits
common	GO:0006091	generation of precursor metabolites and energy	Hs	ATP5F1A|ATP5F1B|CAT|CYC1|DLAT|DLD|G6PD|GSK3B|IDH1|IDH3A|MDH2|MSH2|OGDH|SDHB|SOD2|TALDO1|SIRT3
common	GO:0043603	cellular amide metabolic process	Hs	DLAT|DLD|EEF2|EIF4A2|G6PD|IDH1|RPL10A|OGDH|RPL4|RPL9|RPL10|RPL19|RPS6|RPS12|SOD1|SOD2|LARS2
common	GO:0062197	cellular response to chemical stress	Hs	CAT|G6PD|HDAC2|MSRA|PRDX1|PRKAA2|SOD1|SOD2|LONP1|ATG5|ATG7
common	GO:0007005	mitochondrion organization	Hs	GSK3B|HSPA9|PHB1|SOD2|LONP1|ATG5|DNM1L|ATG7|PHB2|GABARAP
common	GO:0006790	sulfur compound metabolic process	Hs	DLAT|DLD|G6PD|HSPA9|IDH1|MSRA|OGDH|SOD1|SOD2
common	GO:0042743	hydrogen peroxide metabolic process	Hs	CAT|PRDX1|SOD1|SOD2
common	GO:0005975	carbohydrate metabolic process	Hs	DLAT|FBP1|G6PD|GSK3B|IDH1|IDH3A|OGDH|TALDO1
common	GO:0002262	myeloid cell homeostasis	Hs	G6PD|HSPA9|PRDX1|RPS6|SOD1
common	GO:0010506	regulation of autophagy	Hs	ATP6V0A1|GSK3B|PRKAA2|ATG5|DNM1L|RRAGB|ATG7
common	GO:0010332	response to gamma radiation	Hs	ATR|XRCC6|RAD51|SOD2
common	GO:0016570	histone modification	Hs	HDAC2|PHB1|PRKAA2|RAD51|RBBP5|WDR5|SIRT3
common	GO:0009725	response to hormone	Hs	ATP5F1A|CAT|CYC1|FBP1|GSK3B|IDH1|PHB1|PRKAA2|RBBP5
common	GO:0001649	osteoblast differentiation	Hs	ATP5F1B|CAT|PHB1|PSMC2
common	GO:0002639	positive regulation of immunoglobulin production	Hs	MSH2|PHB1|PHB2
common	GO:0097190	apoptotic signaling pathway	Hs	GSK3B|MSH2|SOD2|DNM1L|GABARAP
common	GO:1901699	cellular response to nitrogen compound	Hs	ATP5F1A|FBP1|GSK3B|HDAC2|RAD51|SOD1|RRAGB
common	GO:0021766	hippocampus development	Hs	GSK3B|OGDH|YWHAE
common	GO:0019216	regulation of lipid metabolic process	Hs	IDH1|SOD1|PHB2|SIRT3
common	GO:0048660	regulation of smooth muscle cell proliferation	Hs	XRCC6|PHB1|SOD2
common	GO:1903169	regulation of calcium ion transmembrane transport	Hs	G6PD|YWHAE|ATG5
bilaterian	GO:0015980	energy derivation by oxidation of organic compounds	Hs	ATP5F1A|ATP5F1B|CAT|CYC1|DLAT|DLD|FXN|MTOR|GSK3B|IDH1|IDH3A|MDH2|MSH2|OGDH|SDHB|SDHC|SOD2|SIRT3
bilaterian	GO:0062197	cellular response to chemical stress	Hs	APEX1|CAT|FXN|MTOR|G6PD|HDAC2|MSRA|PRDX1|PRKAA2|PRKCD|SOD1|SOD2|LONP1|ATG5|ATG7
bilaterian	GO:0043603	cellular amide metabolic process	Hs	DLAT|DLD|EEF2|EIF4A2|G6PD|GCLC|GCLM|IDH1|RPL10A|OGDH|RPL4|RPL9|RPL10|RPL19|RPS6|RPS12|SOD1|SOD2|LARS2
bilaterian	GO:0006099	tricarboxylic acid cycle	Hs	DLAT|IDH1|IDH3A|MDH2|OGDH|SDHB|SDHC
bilaterian	GO:0009725	response to hormone	Hs	APEX1|ATP5F1A|CAT|MAPK14|CYC1|FBP1|MTOR|GCLC|GCLM|GRB2|GSK3B|IDH1|PHB1|PRKAA2|PRKCD|RBBP5|RPS6KB1
bilaterian	GO:0031667	response to nutrient levels	Hs	CAT|MAPK14|MTOR|G6PD|GCLC|GCLM|PRKAA2|RPS6KB1|SOD1|SOD2|ATG5|RRAGB|ATG7|GABARAP
bilaterian	GO:0006790	sulfur compound metabolic process	Hs	DLAT|DLD|FXN|G6PD|GCLC|GCLM|HSPA9|IDH1|MSRA|OGDH|SOD1|SOD2
bilaterian	GO:0007005	mitochondrion organization	Hs	FXN|GCLC|GCLM|GSK3B|HSPA9|PHB1|SOD2|LONP1|ATG5|DNM1L|ATG7|PHB2|GABARAP
bilaterian	GO:0010212	response to ionizing radiation	Hs	ATR|MAPK14|XRCC6|GRB2|HRAS|MSH2|RAD51|SOD2
bilaterian	GO:0018105	peptidyl-serine phosphorylation	Hs	ATR|MAPK14|MTOR|GSK3B|PRKAA2|PRKCD|RPS6KB1|TOP1
bilaterian	GO:0019725	cellular homeostasis	Hs	APEX1|ATP5F1B|ATP6V0A1|DLD|FXN|GCLC|GCLM|PRDX1|PIK3CB|PRKAA2|SOD1|YWHAE
bilaterian	GO:2000377	regulation of reactive oxygen species metabolic process	Hs	MAPK14|G6PD|GRB2|PRKCD|SOD1|SOD2|ATG5
bilaterian	GO:0010506	regulation of autophagy	Hs	ATP6V0A1|MTOR|GSK3B|PIK3CB|PRKAA2|ATG5|DNM1L|RRAGB|ATG7
bilaterian	GO:0055093	response to hyperoxia	Hs	CAT|HDAC2|SOD2|ATG7
bilaterian	GO:0009975	carbohydrate metabolic process	Hs	MAPK14|DLAT|FBP1|G6PD|GCLC|GSK3B|IDH1|IDH3A|OGDH|TALDO1
bilaterian	GO:0009408	response to heat	Hs	MTOR|GCLC|HDAC2|RPS6KB1|SOD1|YWHAE
bilaterian	GO:0001775	cell activation	Hs	MAPK14|MTOR|GCLM|MSH2|PRDX1|PHB1|PIK3CB|PRKCD|RPS6|ATG5|PHB2
bilaterian	GO:0009896	positive regulation of catabolic process	Hs	MTOR|GCLC|GSK3B|PIK3CB|PRKAA2|PRKCD|PSMC2|ATG7|GABARAP|SIRT6
bilaterian	GO:0031400	negative regulation of protein modification process	Hs	G6PD|GCLC|GSK3B|HDAC2|PIK3CB|PRKAA2|PRKCD|YWHAE|ATG5|WDR5
bilaterian	GO:0016570	histone modification	Hs	HDAC2|PHB1|PRKAA2|PRKCD|RAD51|RBBP5|WDR5|SIRT3|SIRT6
ecdisozoan	GO:0008340	determination of adult lifespan	Ce	rpl-4|let-363|rpl-19|cyc-1|rps-6|frh-1|tag-1|raga-1|ctl-2|atp-2|clk-1|rpl-9|jnk-1|atq-7|atq-18|akt-1|unc-51|aak-2|mev-1
ecdisozoan	GO:0009060	aerobic respiration	Ce	cyc-1|dha-1|sdhb-1|atp-2|clk-1|mdh-2|oxph-1|idh-1|nuo-5|mev-1
ecdisozoan	GO:0044271	cellular nitrogen compound biosynthetic process	Ce	rpl-17|rpl-1|rpl-4|rpl-19|lars-2|cyc- 1|eef-2|rpl-31|rps-6|frh-1|rpl-10|ifg-1|cps-1|atp-2|rps-12|inf-1|rpl-9|unc-32|rpc-1|dat-1
ecdisozoan	GO:0000422	autophagy of mitochondrion	Ce	atg-5|phb-2|pgp-1|atg-3|atg-7|atg-18|unc-51
ecdisozoan	GO:0046034	ATP metabolic process	Ce	cyc-1|atp-2|clk-1|unc-32|oxph-1|nuo-5|dat-1|mev-1
ecdisozoan	GO:0006979	response to oxidative stress	Ce	phb-1|sod-2|frh-1|phb-2|gcs-1|ctl-2|pmk-1|mev-1
ecdisozoan	GO:0002119	nematode larval development	Ce	let-363|exo-3|pgs-1|pat-3|atp-2|unc-32|atg-7|let-60|atg-18|unc-51|sem-5|fti-2
ecdisozoan	GO:0009792	embryo development ending in birth or egg hatching	Ce	phb-1|rab-5|exo-3|phb-2|pat-4|unc-32|drp-1|atp-7|atg-18|unc-51
ecdisozoan	GO:0050793	regulation of developmental process	Ce	phb-1|phb-2|raga-1|pat-4|pat-3|clk-1|tpa-1|jnk-1|let-60|akt-1|unc-51|sem-5|aak-2
ecdisozoan	GO:0051128	regulation of cellular component organization	Ce	rab-5|tpa-1|pat-4|pat-3|tpa-1|nlk-1|ato-7|let-60|akt-1|unc-51|sem-5
ecdisozoan	GO:0009605	response to external stimulus	Ce	ato-5|eef-2|hda-3|tpa-1|raga-1|ato-2|unc-32|tpa-1|ato-7|ato-1|akt-1|unc-51|omk-1|mev-1
ecdisozoan	GO:0033554	cellular response to stress	Ce	ato-5|sod-2|exo-3|hda-3|kqo-1|raga-1|nlk-1|ato-7|hso-6|akt-1|omk-1
ecdisozoan	GO:0032879	regulation of localization	Ce	rab-5|rab-7|pat-4|pat-3|unc-32|let-60|unc-51|fth-2|aak-2|omk-1
ecdisozoan	GO:0019725	cellular homeostasis	Ce	frh-1|pat-4|bat-3|unc-32|dks-1
ecdisozoan	GO:0009893	positive regulation of metabolic process	Ce	let-363|kqo-1|sol-4|clk-1|tpa-1|ato-7|ato-1|lrs0t-1|unc-51|omk-1
ecdisozoan	GO:0010942	positive regulation of cell death	Ce	kqo-1|unc-32|nlk-1
euarchontoglire	GO:0006974	cellular response to DNA damage stimulus	Hs	PARP1|APEX1|ATM|ATR|BAX|BRCA1|CDK7|CDKN1A|MAPK14|ERCC1|ERCC2|ERCC4|FEN1|FOXM1|MTOR|XRCC6|GRB2|MIF|MSH2|POLG|RAD51|SOD2|TERF2|TP53|TP53BP1|TP73|XPA|XRCC5|PPM1D|TP63|CLOCK|ZMPSTE24|STUB1|CHEK2|SIRT1|SIRT7|SIRT6
euarchontoglire	GO:0071417	cellular response to organonitrogen compound	Hs	ADCY5|PARP1|AGTR1|AKT1|APEX1|BRCA1|CEBPB|MTOR|GHR|HRH|GCLC|GCLM|GRB2|GSK3A|GSK3B|HDAC2|IGF1R|GF1R|INSR|IRS1|PCK1|PPARG|PRKCD|RAD51|RPS6KB1|SHC1|SOD1|TP53|UCP2|IRS2|SOCS2|KLF|GF21
euarchontoglire	GO:0031667	response to nutrient levels	Hs	AKT1|APOE|CAT|CDKN1A|MAPK14|ERCC1|MTOR|GHR|HRH|GCLC|GCLM|IGF1R|PCK1|PPARG|RPS6KB1|SOD1|SOD2|TP53|UCP2|FGF23|PPM1D|KLIAT|GSISRT1|FGF21|RICTOR
euarchontoglire	GO:2001233	regulation of apoptotic signaling pathway	Hs	PARP1|AKT1|BAX|BRCA1|FXN|GCLC|GCLM|GSK3B|HTT|HELLS|IGF1L|MNA|MIF|SERPINE1|PIK3CB|PRKCD|PTEN|RPS6KB1|SOD1|SOD2|TERT|TP53|TP63|SIRT1
euarchontoglire	GO:0010564	regulation of cell cycle process	Hs	AKT1|APEX1|ATM|ATR|BRCA1|BUB1B|CDK7|CDKN1A|MAPK14|ERCC2|FEN1|IGF1|IGF1R|INSR|MSH2|PTEN|RAD51|TERF2|TERT|TP53|TP53BP1|RAE1|BUB3|CLOCK|ZMPSTE24|CHEK2|SIRT1
euarchontoglire	GO:0006979	response to oxidative stress	Hs	PARP1|AKT1|APEX1|APOE|ARNTL|CAT|ERCC1|ERCC2|FXN|GCLC|GCLM|GPX4|HDAC2|MSRA|PRDX1|PRKCD|SOD1|SOD2|TP53|UCP2|SIRT1
euarchontoglire	GO:0043549	regulation of kinase activity	Hs	AKT1|APOE|CDK7|CDKN1A|CEBPA|MTOR|XRCC6|GHR|HTT|HRAS|IGF1|IGF1R|INSR|IRS1|MIF|PIK3CB|PPARG|PRKCD|PTEN|SHC1|SOD1|XRCC5|IRS2|SOCS2|SIRT1|RICTOR
euarchontoglire	GO:1901214	regulation of neuron death	Hs	PARP1|AKT1|APOE|ATM|BAX|CEBPB|GHR|GCLC|GCLM|GRN|GSK3B|HRAS|MSH2|SOD1|SOD2|TERT|TP53|SIRT1|FGF21
euarchontoglire	GO:0009411	response to UV	Hs	PARP1|AKT1|ATR|BAX|CAT|CDKN1A|ERCC1|ERCC2|ERCC4|FEN1|MSH2|PRKCD|TP53|XPA|SIRT1
euarchontoglire	GO:0031331	positive regulation of cellular catabolic process	Hs	AKT1|APOE|ATM|BAX|CEBPA|MTOR|GCLC|GSK3A|GSK3B|HTT|IGF1|INSR|IRS1|PIK3CB|PRKCD|PTEN|IRS2|STUB1|SIRT1|FGF21|SIRT6
euarchontoglire	GO:0040008	regulation of growth	Hs	AGTR1|AKT1|APOE|CDKN1A|MAPK14|FXN|MTOR|GHR|GHRH|GSK3A|GSK3B|IGF1|INSR|TEN|RPS6KB1|SHC1|SOD1|TP53|TP73|SOCS2|ZMPSTE24|SIRT1|RICTOR
euarchontoglire	GO:0090398	cellular senescence	Hs	ARNTL|ATM|CDKN1A|MAPK14|HRAS|IGF1R|LMNA|PRKCD|TERF2|TP53|SIRT1
euarchontoglire	GO:0048732	gland development	Hs	AKT1|ATM|CEBPA|CEBPB|GHRH|INSR|PCK1|PCNU1F1|PROP1|PTEN|SOD1|SOD2|UCP2|TP63|IRS2|SOCS2|NCOR2|ZMPSTE24
euarchontoglire	GO:0097193	intrinsic apoptotic signaling pathway	Hs	ATM|BAX|BRCA1|CDKN1A|CEBPB|HRAS|MSH2|PRKCD|SOD2|TP53|TP73|TP63|CHEK2|SIRT1
euarchontoglire	GO:0046324	regulation of glucose import	Hs	AKT1|MAPK14|GSK3A|IGF1|INSR|IRS1|RPS6KB1|TERT|IRS2|FGF21|SIRT6
euarchontoglire	GO:0006468	protein phosphorylation	Hs	AKT1|ATM|ATR|BUB1B|CDK7|MAPK14|MTOR|GHR|GSK3A|GSK3B|IGF1R|INSR|PCK1|PIK3CB|PRKCD|RPS6KB1|TOP1|YWHAZ|PPM1D|SQSTM1|ZMPSTE24|CHEK2|RICTOR
euarchontoglire	GO:0042593	glucose homeostasis	Hs	AKT1|CEBPA|GHRH|GCLC|GCLM|IGF1R|INSR|IRS1|PCK1|PPARG|UCP2|IRS2|SIRT1|FGF21|SIRT6
euarchontoglire	GO:0032200	telomere organization	Hs	PARP1|APEX1|ATM|ATR|ERCC1|ERCC4|FEN1|XRCC6|RAD51|TERF2|TERT|XRCC5|SIRT6
euarchontoglire	GO:0019216	regulation of lipid metabolic process	Hs	AGTR1|AKT1|APOE|BRCA1|MTOR|IGF1R|IRS1|PCK1|PPARG|PRKCD|SOD1|IRS2|ZMPSTE24|STUB1|SIRT3|SIRT1|FGF21
euarchontoglire	GO:0010821	regulation of mitochondrion organization	Hs	AKT1|BAX|FXN|GCLC|GSK3A|GSK3B|HTT|IGF1L|MNA|PPARGI|TP53|SQSTM1|SIRT7

Protein	Com	Bilat	Euar	ADR_common	ADR_bilaterian	ADR_euarcho	Predictor	Pubmed_ID	Cellage	LongevityMap	ARD	Druggable	nb_drugs	FDA_approved_drugs	max_interaction_score
RPL21	2	2	2	46	58	160,5	9	0	0	0	0	0	NA	NA	NA
RPL6	2	2	2	60,8	74,2	166,2	9	0	0	0	0	0	NA	NA	NA
ETF1 *	2	2	0	56	97,2	175,7	4	0	0	0	0	0	NA	NA	NA
RPS23	2	2	0	17,2	20	78,5	7	0	0	0	0	0	NA	NA	NA
RPS18	2	2	0	17,8	14,3	76,8	8	0	0	0	0	1	1	NA	1,4
RPS3A	2	2	0	30,5	27,5	90,2	7	0	0	0	0	0	NA	NA	NA
RPL32 *	2	2	0	34,8	43,5	132,2	8	0	0	0	0	0	NA	NA	NA
RPS2 *	2	2	0	6	12,5	74,5	5	0	0	0	0	1	1	NA	0,79
RPL23A *	2	2	0	26,3	60	145,3	5	0	0	0	0	0	3	NA	2,1
RPL27A *	2	2	0	28,3	39,5	126,2	8	0	0	0	0	0	NA	NA	NA
RPL30	2	2	0	34	42,2	123	8	0	0	0	0	0	NA	NA	NA
RPL5 *	2	2	0	11,8	23,7	100	8	0	0	0	0	0	NA	NA	NA
RPLP2	2	2	0	70,3	88,3	185	8	0	0	0	0	0	NA	NA	NA
RPS28 *	2	2	0	35,3	30,5	101,7	5	0	0	0	0	1	1	NA	1,4
RPL35A *	2	2	0	44,2	52,7	140,3	9	0	0	0	0	0	NA	NA	NA
RPL12	2	2	0	39,3	43,8	144,2	8	0	0	0	0	0	NA	NA	NA
RPSA *	2	2	0	17,7	27,3	105	8	0	0	0	0	0	5	NA	11,36
RPS5	2	2	0	7	11,2	65,7	7	0	0	0	0	0	1	NA	1,4
RPS19 *	2	2	0	36,3	29	100,8	8	0	0	0	0	1	2	DEXAMETHASONE (unknown)	0,7
RPL35	2	2	0	39,8	41,3	145,5	7	0	0	0	0	1	1	NA	1,4
RPL36AL *	2	2	0	48,2	64,5	174,5	8	0	0	0	0	0	NA	NA	NA
RPL31 *	2	2	0	66,3	68	148,3	7	0	0	0	0	0	NA	NA	NA
RPS7	2	2	0	22,2	82,3	110,5	2	0	0	0	0	0	NA	NA	NA
RPL15 *	2	2	0	29,7	40,3	132,8	8	0	0	0	0	1	2	NA	3,16
RPS15	2	2	0	25,8	22,2	99,2	8	0	0	0	0	0	NA	NA	NA
RPS13 *	2	2	0	9,3	14	71,3	6	0	0	0	0	1	1	NA	1,4
RPL34	2	2	0	64	68	161	8	0	0	0	0	0	NA	NA	NA
RPS9 *	2	2	0	20,2	17,2	68,3	7	0	0	0	0	1	1	NA	1,4
RPS16 *	2	2	0	17,7	26,7	94,7	6	0	0	0	0	0	NA	NA	NA
RPL7A	2	2	0	34,8	53,5	160,7	8	0	0	0	0	0	NA	NA	NA
RPS15A	2	2	0	19,5	34,2	89,2	3	0	0	0	0	0	NA	NA	NA
RPL37A	2	2	0	44,3	48	128,2	6	0	0	0	0	0	NA	NA	NA
RPS20	2	2	0	25	19,2	88,5	7	0	0	0	0	0	NA	NA	NA
RPS8	2	2	0	11,5	19,3	82,8	6	0	0	0	0	1	1	NA	1,4
RPL11 *	2	2	0	29,8	31,7	106,3	8	0	0	0	0	1	2	NA	3,16
RPS14	2	2	0	12,3	24,2	70,5	7	0	0	0	0	0	NA	NA	NA
RPS11	2	2	0	12,5	11,3	67,8	6	0	0	0	0	0	NA	NA	NA
RPS25 *	2	2	0	45	38	106,7	7	0	0	0	0	0	NA	NA	NA
RPL18A	2	2	0	35,2	47,3	136	9	0	0	0	0	0	NA	NA	NA
RPS29 *	2	2	0	45,7	30,2	112,3	8	0	0	0	0	0	NA	NA	NA
RPLP0	2	2	0	26,5	37,7	129,2	9	0	0	0	0	0	NA	NA	NA
RPL13	2	2	0	58,7	59,5	150,8	8	0	0	0	0	1	2	2	1,58
RPS17 *	2	2	0	48,3	69,8	166	5	0	0	0	0	0	1	NA	1,4
RPL3	2	2	0	16	29,7	116	8	0	0	0	0	1	3	NA	6,31
GSPT2 *	2	2	0	64,5	110,7	245,8	3	0	0	0	0	0	NA	NA	NA
RPS3	2	2	0	5,8	8	59,3	7	0	0	0	0	0	NA	NA	NA
ATG4B	3	3	0	148,8	210,8	308,3	1	0	0	0	0	1	13	2	1,46
UBE2G1 *	0	2	2	NA	157	127,5	2	0	0	0	0	0	NA	NA	NA
UBE3A *	0	2	2	NA	149,8	111,2	2	0	0	0	0	0	NA	NA	NA
NEDD4 *	0	2	2	NA	138,5	105	2	0	0	0	0	0	1	NA	3,07
KEAP1	0	2	2	NA	147,8	81,3	2	32487458	0	0	0	1	3	DIMETHYL FUMARATE (inhibitor)	28,4
KLHL5 *	0	2	2	NA	166	108	2	0	0	0	0	0	NA	NA	NA
SPSB4 *	0	2	2	NA	138	104,2	2	0	0	0	0	0	NA	NA	NA
UBE3C *	0	2	2	NA	160,2	131,2	2	0	0	0	0	0	NA	NA	NA
TRIM9	0	2	2	NA	159	128,5	2	0	0	0	0	0	NA	NA	NA
ANAPC13 *	0	2	2	NA	167	119,2	2	0	0	0	0	0	NA	NA	NA
UBE2G2 *	0	2	2		135,2	132,2	116,5	2	0	0	0	0	0	NA	NA
UBR4 *	0	2	2	NA		133,6	57,8	2	0	0	0	0	0	NA	NA
RNF123 *	0	2	2	NA		164,6	124,8	2	0	0	0	0	0	NA	NA
FBXL15 *	0	2	2	NA		135,3	97,5	2	0	0	0	0	0	NA	NA
FBXL14 *	0	2	2	NA		137,2	103	2	0	0	0	0	0	NA	NA
UBA1 *	0	2	2		117,8	117,7	106,7	2	0	0	0	0	0	3	NA	37,87
UBR2 *	0	2	2	NA		162,8	135,8	2	0	0	0	0	0	NA	NA
UBE2K *	0	2	2		131,3	139,3	116,7	2	0	0	0	0	0	NA	NA
EIF5B	0	2	0		58	88,3	198,3	4	0	0	0	0	0	NA	NA
PSMA1 *	0	2	0		108,5	131,8	223	1	0	0	0	1	5	3	0,8
RPS10 *	0	2	0	NA		84,8	148,7	2	0	0	0	0	NA	NA	NA
NSA2 *	0	2	0		26,8	48,7	134,7	1	0	0	0	0	NA	NA	NA
RPL38 *	0	2	0		58,7	122,3	162,5	1	0	0	0	0	NA	NA	NA
EIF3G *	0	2	0		79,5	115,5	209,8	2	0	0	0	0	NA	NA	NA
RPL23	0	2	0	NA		57,3	111,8	6	0	0	0	0	2	NA	3,16
PSMD7 *	0	2	0		112,3	134	154	1	0	0	0	1	4	3	1
LIG1 *	0	2	0		94,7	127	206,3	1	0	0	1	1	1	1	BLEOMYCIN (inhibitor)	11,36
UBE2W *	0	2	0	NA		164,8	287,4	1	0	0	0	0	0	NA	NA
RPS21	0	2	0		69,2	41,2	117,3	6	0	0	0	0	0	NA	NA
RPL7	0	2	0	NA		75,3	147,8	2	0	0	0	0	0	NA	NA
RPL8 *	0	2	0	NA		58,5	107,8	5	0	0	0	0	2	NA	3,16
PSMD2 *	0	2	0		102,7	124,3	144,2	1	0	0	0	1	4	3	1
EIF5 *	0	2	0		111,8	136,2	241,8	1	0	0	0	0	NA	NA	NA
GNB2L1	0	2	0		20,7	49,8	128,7	6	0	0	0	0	NA	NA	NA
RPL36 *	0	2	0		65,5	101,3	180,2	6	0	0	0	0	NA	NA	NA
MRPL11 *	0	2	0		102,7	99,2	187	1	0	0	0	0	NA	NA	NA
PSMD6 *	0	2	0		110	133,5	150,5	1	0	0	0	1	4	3	1
EIF3A *	0	2	0		97	122,8	221,5	1	0	0	0	1	2	2	0,72
EIF3I *	0	2	0		66,7	99,5	206	5	0	0	0	0	NA	NA	NA
EIF3L *	0	2	0	NA		145,5	239,8	1	0	0	0	0	NA	NA	NA
PSMB2 *	0	2	0		110,3	137,7	149,3	1	0	0	0	1	8	3	7,1
RPL28 *	0	2	0	NA		113,3	192,7	2	0	0	0	0	NA	NA	NA
PSMB4 *	0	2	0		111,7	131,2	146,8	1	0	0	0	1	5	3	0,8
FBXL16 *	0	2	0	NA		148,8	103,3	1	0	0	0	0	NA	NA	NA
PSMB7 *	0	2	0		117	145,3	162,8	1	0	0	0	1	5	3	0,8
EIF2S1 *	0	2	0		68,8	92,3	191	1	0	0	0	1	1	NA	2,1
PSMD12 *	0	2	0		111	131,5	150,8	1	0	0	0	1	4	3	1
EIF2S2 *	0	2	0		101,5	127	226,2	2	0	0	0	0	NA	NA	NA
RPL27 *	0	2	0		59,5	123	182,3	1	0	0	0	0	NA	NA	NA
WDFY3	0	3	0	NA		217,5	312,2	1	0	0	0	0	NA	NA	NA
BARD1 *	0	0	1	NA	NA		233,5	2	0	0	0	1	1	5	4	1,14
RNF19A *	0	0	2	NA	NA		139,2	1	0	0	0	0	0	NA	NA	NA
MEPE *	0	0	2	NA	NA		274,2	1	0	0	0	0	0	NA	NA	NA
FEM1B	0	0	2	NA		215,8	213,5	1	0	0	0	0	0	NA	NA	NA
COMMD2 *	0	0	2	NA		184	186,2	1	0	0	0	0	0	NA	NA	NA
FBXO40 *	0	0	2	NA	NA		111,5	1	0	0	0	0	0	NA	NA	NA
WSB1 *	0	0	2	NA	NA		111	1	0	0	0	0	0	NA	NA	NA
FBXL18 *	0	0	2	NA	NA		116,4	1	0	0	0	0	0	NA	NA	NA
SPSB2 *	0	0	2	NA	NA		117,4	1	0	0	0	0	2	NA	56,81
UBE2O *	0	0	2	NA		164,4	133	1	0	0	0	0	0	NA	NA	NA
GAN *	0	0	2	NA	NA		110,5	1	0	0	0	0	0	NA	NA	NA
ASB14 *	0	0	2	NA	NA		116,6	1	0	0	0	0	0	NA	NA	NA
HRC *	0	0	2	NA	NA		277	1	0	0	0	0	0	NA	NA	NA
COMMD9 *	0	0	2	NA	NA		210,8	1	0	0	0	0	0	NA	NA	NA
FBXL3 *	0	0	2	NA	NA		102,3	1	0	0	0	0	0	NA	NA	NA
LRSAM1 *	0	0	2	NA	NA		147,8	1	0	0	0	0	0	NA	NA	NA
RNF182 *	0	0	2	NA	NA		150,4	1	0	0	0	0	0	NA	NA	NA
DCUN1D2	0	0	2	NA	NA		214,4	1	0	0	0	0	0	NA	NA	NA
SERPINB3 *	0	0	2	NA		264	303,6	1	0	0	0	1	2	NA	7,1
CDCA8 *	0	0	2	NA	NA		183	1	0	0	0	0	0	NA	NA	NA
KCTD6 *	0	0	2	NA	NA		115	1	0	0	0	0	0	NA	NA	NA
ADM *	0	0	2	NA	NA		272,2	3	0	0	0	1	0	7	NA	16,23

KLHL3 *	0	0	2	NA		NA		114,4	1		0	0	0	0	0	NA		NA			NA			
ADAM8 *	0	0	2	NA		NA		278,4	1		0	0	0	0	0	NA		NA			NA			
ASB18 *	0	0	2	NA		NA		117,6	1		0	0	0	0	0	NA		NA			NA			
GPR20 *	0	0	2	NA		NA		272,6	1		0	0	0	0	0	NA		NA			NA			
MIB2 *	0	0	2	NA			147,3	125	1		0	0	0	0	0	NA		NA			NA			
MAPK11	0	0	2		155,2		203,5	223,2	1		0	0	0	0	1		27			3			1,05	
ASB1 *	0	0	2	NA		NA		113,8	1		0	0	0	0	0	NA		NA			NA			
FBXO4 *	0	0	2	NA		NA		107	1		0	0	0	0	0	NA		NA			NA			
KRAS *	0	0	2	NA		NA		114,7	1		0	0	0	1	0		136	NA					1,25	
CHRNB4 *	0	0	2	NA		NA		272,6	1		0	0	0	0	1		18			5			3,16	
ASB4 *	0	0	2	NA		NA		111	1		0	0	0	0	0	NA		NA			NA			
UBE2J2 *	0	0	2		137,8		182,5	129,7	1		0	0	0	0	0	NA		NA			NA			
TRIM37 *	0	0	2	NA		NA		149,8	1		0	0	0	0	0	NA		NA			NA			
ASB9 *	0	0	2	NA		NA		116	1		0	0	0	0	0	NA		NA			NA			
UBA7 *	0	0	2	NA		NA		128	1		0	0	0	0	0	NA		NA			NA			
SLC15A4 *	0	0	2		164,8		245	300,6	1		0	0	0	0	0	NA		NA			NA			
TRIM71 *	0	0	2	NA		NA		138,2	1		0	0	0	0	0	NA		NA			NA			
ITCH *	0	0	2	NA		NA		84,7	1		0	0	0	0	0	NA		NA			NA			
HECTD2 *	0	0	2	NA		NA		141,8	1		0	0	0	0	0	NA		NA			NA			
COMMD3 *	0	0	2	NA			219,8	190,3	1		0	0	0	0	0	NA		NA			NA			
TRIP12 *	0	0	2		142		222,2	103,8	1		0	0	0	0	0	NA		NA			NA			
RNF41 *	0	0	2	NA			165	121,5	1		0	0	0	0	0	NA		NA			NA			
GPR45 *	0	0	2	NA		NA		273,2	1		0	0	0	0	0	NA		NA			NA			
FBXO10 *	0	0	2	NA		NA		115,6	1		0	0	0	0	0	NA		NA			NA			
KLHL21 *	0	0	2	NA		NA		116,8	1		0	0	0	0	0	NA		NA			NA			
RNF144B *	0	0	2	NA		NA		146,8	1		0	0	0	0	0	NA		NA			NA			
ASB7 *	0	0	2	NA		NA		114,6	1		0	0	0	0	0	NA		NA			NA			
GPR25 *	0	0	2	NA		NA		272,6	2		0	0	0	0	0	NA		NA			NA			
MEX3C *	0	0	2	NA		NA		148,4	1		0	0	0	0	0	NA		NA			NA			
HTR7 *	0	0	2	NA		NA		267,2	2		0	0	0	0	1		65			26			1,75	
KLHL11 *	0	0	2	NA		NA		110,8	1		0	0	0	0	0	NA		NA			NA			
COPS3	0	0	2	NA			161	153	1		0	0	0	0	0	NA		NA			NA			
ASB17 *	0	0	2	NA		NA		116,8	1		0	0	0	0	0	NA		NA			NA			
IAPP *	0	0	2	NA		NA		264	3		0	0	0	1	0		2	NA					0,39	
CD53 *	0	0	2	NA		NA		278,2	1		0	0	0	0	0	NA		NA			NA			
KLHL2 *	0	0	2	NA			146,2	101,5	1		0	0	0	0	0	NA		NA			NA			
AREL1 *	0	0	2	NA			165,6	138,2	1		0	0	0	0	0	NA		NA			NA			
ASB10 *	0	0	2	NA		NA		115,8	1		0	0	0	0	0	NA		NA			NA			
CALCRL *	0	0	2	NA			285	271,8	2		0	0	0	0	0		11	NA					15,49	
FBXW7 *	0	0	2	NA			189,8	87,7	1		0	0	0	0	0		8	NA					1,09	
UBE2H	0	0	2		136,2		145,2	126,5	1		0	0	1	0	0	NA		NA			NA			
UBE2Z *	0	0	2	NA		NA		147,2	1		0	0	0	0	0	NA		NA			NA			
KLHL42 *	0	0	2	NA		NA		115	1		0	0	0	0	0	NA		NA			NA			
ADCYAP1R1 *	0	0	2	NA		NA		269,4	2		0	0	0	0	0		4	NA					4,73	
DTX3L *	0	0	2	NA		NA		145,2	1		0	0	0	0	0	NA		NA			NA			
ADCY6 *	0	0	2	NA		NA		217,6	1		0	0	1	0	0	NA		NA			NA			
ASB2 *	0	0	2	NA		NA		108,8	1		0	0	0	0	0	NA		NA			NA			
CBLB *	0	0	2	NA		NA		110,5	1		0	0	0	0	1		2	FLUOROURACIL (unknown)					1,83	
UBA5 *	0	0	2	NA			141,5	122,7	1		0	0	0	0	0	NA		NA			NA			
ADCY3 *	0	0	2	NA			230	189,5	1		0	0	0	0	0	NA		NA			NA			
MMP25	0	0	2	NA		NA		296,6	1		0	0	0	0	1		3	NA					2,37	
TAAR2 *	0	0	2	NA		NA		273,8	3		0	0	0	0	0	NA		NA			NA			
GPR176 *	0	0	2	NA		NA		273,6	3		0	0	0	0	0	NA		NA			NA			
CRHR1 *	0	0	2	NA		NA		258,8	2	25541005	0	0	0	0	1		12			4			14,2	
RNF34 *	0	0	2	NA		NA		148,4	1		0	0	0	0	0	NA		NA			NA			
IFNA2 *	0	0	2	NA		NA		340,2	1		0	0	0	0	1		2	NA					28,4	
MYLIP *	0	0	2	NA			164,8	127,2	1		0	0	1	0	1		1	ATORVASTATIN (unknown)					1,78	
ASB16 *	0	0	2	NA		NA		117,8	1		0	0	0	0	0	NA		NA			NA			
MC4R *	0	0	2	NA		NA		229,2	2		0	0	0	1	1		18			13			3,16	
KLHL9 *	0	0	2	NA		NA		116,2	1		0	0	0	0	0	NA		NA			NA			
FBXO11 *	0	0	2	NA			129,7	95,2	1		0	0	0	0	0	NA		NA			NA			
PTH1R *	0	0	2	NA		NA		240,2	2		0	0	0	1	0		9	NA					15,78	
ADCYAP1 *	0	0	2	NA		NA		267,6	1		0	0	0	0	0		2	NA					2,99	
TRAF7 *	0	0	2	NA		NA		151	1		0	0	0	0	0	NA		NA			NA			
UBE2L6 *	0	0	2	NA		NA		117,2	1		0	0	0	0	0	NA		NA			NA			
COPS7B *	0	0	2	NA			163,8	160,2	1		0	0	0	0	0	NA		NA			NA			
COMMD1 *	0	0	2	NA		NA		206,6	1		0	0	0	0	0	NA		NA			NA			
TACR1 *	0	0	2	NA		NA		133,2	1		0	0	0	0	1		39			6			8,74	
KCTD7 *	0	0	2	NA		NA		111,6	1		0	0	0	0	0	NA		NA			NA			
FBXO9	0	0	2		154,2		135	97,8	1		0	0	0	0	0	NA		NA			NA			
FBXW2 *	0	0	2	NA		NA		109,5	1		0	0	0	0	0	NA		NA			NA			
ADCY8 *	0	0	2	NA			247	190,7	2		0	0	0	0	0	NA		NA			NA			
ANAPC1 *	0	0	2	NA			117	70,2	1		0	0	0	0	0	NA		NA			NA			
KBTBD13 *	0	0	2	NA		NA		111,4	1		0	0	0	0	0	NA		NA			NA			
PJA1 *	0	0	2	NA		NA		138,2	1		0	0	0	0	0	NA		NA			NA			
FBXL8 *	0	0	2	NA		NA		118	1		0	0	0	0	0	NA		NA			NA			
IGFBP4 *	0	0	2	NA		NA		273,2	1		0	0	1	0	0	NA		NA			NA			
KLHL20 *	0	0	2	NA			146,8	103,8	1		0	0	0	0	0	NA		NA			NA			
ADCY1	0	0	2	NA			229	213,8	2		0	0	0	0	1		5	NA					5,68	
BTBD6 *	0	0	2	NA		NA		113	1		0	0	0	0	0	NA		NA			NA			
PTHLH *	0	0	2	NA		NA		258,4	1		0	0	0	0	0		2	NA					28,4	
CALCB *	0	0	2	NA		NA		273,6	2		0	0	0	0	0		4	NA					10,65	
HECTD3 *	0	0	2	NA		NA		151,2	1		0	0	0	0	0	NA		NA			NA			
RAP2B *	0	0	2	NA		NA		282,8	1		0	0	0	0	0	NA		NA			NA			
ASB5 *	0	0	2	NA		NA		116,2	1		0	0	0	0	0	NA		NA			NA			
IL13RA2 *	0	0	2	NA		NA		309,3	1		0	0	0	0	1		3	NA					18,94	
FAM20C *	0	0	2	NA		NA		245	1		0	0	0	0	0	NA		NA			NA			
FBXL5 *	0	0	2	NA		NA		107,2	1		0	0	0	0	0	NA		NA			NA			
TRIM50 *	0	0	2	NA		NA		150,6	1		0	0	0	0	0	NA		NA			NA			
KLHL25 *	0	0	2	NA		NA		117	1		0	0	0	0	0	NA		NA			NA			
FBXW9 *	0	0	2	NA			213	113,6	1		0	0	0	0	0	NA		NA			NA			
MNAT1 *	0	0	2	NA			133,3	170,5	2		0	0	0	0	0	NA		NA			NA			
CCNH *	0	0	2		116,5		134	171	2		0	0	0	0	0	NA		NA			NA			
RAMP1 *	0	0	2	NA		NA		272,2	2		0	0	0	0	1		3			2			34,71	
CUL7 *	0	0	2	NA		NA		135,7	1		0	0	0	0	0	NA		NA			NA			
RXFP1 *	0	0	2	NA		NA		267	2		0	0	0	0	1		14	NA					4,06	
UBE2Q2 *	0	0	2	NA		NA		149,2	1		0	0	0	0	0	NA		NA			NA			
TAAR5 *	0	0	2	NA		NA		271,6	1		0	0	0	0	0	NA		NA			NA			
TRIM69 *	0	0	2	NA		NA		150,2	1		0	0	0	0	0	NA		NA			NA			
TRPM2	0	0	2	NA		NA		281,8	1		0	0	0	0	0		4	NA					7,1	
RCHY1 *	0	0	2	NA		NA		126,2	1		0	0	0	0	0	NA		NA			NA			
UBE2E2 *	0	0	2	NA		NA		147,6	1		0	0	0	0	0	NA		NA			NA			
PTH2R *	0	0	2	NA		NA		272,8	1	24378925	0	0	0	0	1		3			3			18,94	
RNF19B *	0	0	2	NA		NA		148,2	1		0	0	0	0	0	NA		NA			NA			
HTR4 *	0	0	2	NA		NA		272,2	2		0	0	0	0	0		34	NA					4,33	
HUWE1 *	0	0	2	NA			162,4	119,7	1		0	0	0	0	0	NA		NA			NA			
FBXW8 *	0	0	2	NA		NA		110,3	1		0	0	0	0	0	NA		NA			NA			
ASB11 *	0	0	2	NA		NA		116,8	1		0	0	0	0	0	NA		NA			NA			
MC2R *	0	0	2	NA		NA		267,6	1		0	0	0	0	1		9			6			63,12	
FBXO21 *	0	0	2	NA		NA		116,8	1		0	0	0	0	0	NA		NA			NA			
SIAH1 *	0	0	2	NA			150,2	123,7	1		0	0	0	0	1		1	NA					28,4	
WSB2 *	0	0	2	NA		NA		216,2	1		0	0	0	0	0	NA		NA			NA			
VIPR1 *	0	0	2	NA		NA		269,4	2		0	0	0	0	1		3	SECRETIN (agonist)					6,31	
AURKB *	0	0	2	NA		NA		92,8	2		0	0	0	0	1		64			6			2,66	
MC3R *	0	0	2	NA		NA		267	3		0	0	0	1	1		5			3			5,68	
GPR150	0	0	2	NA		NA		272,2	2		0	0	0	0	0	NA		NA			NA			
CDC26 *	0	0	2	NA		NA		85,8	1	34590680	0	0	0	0	0	NA		NA			NA			
RLIM *	0	0	2	NA		NA		136,3	1		0	0	0	0	0	NA		NA			NA			
KBTBD7 *	0	0	2	NA		NA		114,8	1		0	0	0	0	0	NA		NA			NA			

ZNRF2 *	0	0	2	NA		NA		143,4	1		0	0	0	0	0	NA		NA			NA				
PTGER2 *	0	0	2	NA		NA		271,4	2		0	0	0	0	1		17			5			6,68		
RNF25 *	0	0	2	NA		NA		141,3	1		0	0	0	0	0	NA		NA			NA				
UBOX5 *	0	0	2	NA			162,2	120,2	1		0	0	0	0	0	NA		NA			NA				
NUF2 *	0	0	2	NA		NA		214,6	1		0	0	0	0	0	NA		NA			NA				
WWP1 *	0	0	2	NA		NA		113,7	1		0	1	0	0	0	NA		NA			NA				
GLP1R *	0	0	2	NA		NA		268,4	2		0	0	0	0	1		152			23			7,47		
UBE2D2 *	0	0	2		126,8		195	66	1		0	0	0	0	0	NA		NA			NA				
LRR1 *	0	0	2	NA			147,8	98,6	1		0	0	0	0	0	NA		NA			NA				
SMURF2 *	0	0	2	NA		NA		85,2	1	29405587;24478790		1	0	0	0	NA		NA			NA				
PTGES2 *	0	0	2	NA			249,8	260,2	1		0	0	0	1	0	NA		NA			NA				
NUP214 *	0	0	2	NA			179,8	243,2	1		0	0	0	0	0	NA		NA			NA				
VPRBP *	0	0	2	NA			144,7	113,3	1		0	0	0	0	0	NA		NA			NA				
GTF2H1 *	0	0	2	NA			142,5	194,3	2		0	0	0	0	0	NA		NA			NA				
VHL *	0	0	2	NA		NA		67,2	1		0	0	0	0	1		17			10			3,34		
TAAR8 *	0	0	2	NA		NA		274,2	2		0	0	0	0	0	NA		NA			NA				
UBE3D *	0	0	2	NA		NA		145,8	1		0	0	0	0	0	NA		NA			NA				
RNF130 *	0	0	2	NA		NA		146,6	1		0	0	0	0	0	NA		NA			NA				
TRIM36 *	0	0	2	NA		NA		147,4	1		0	0	0	0	0	NA		NA			NA				
COMMD7 *	0	0	2	NA		NA		211	1		0	0	0	0	0	NA		NA			NA				
BUB1 *	0	0	2	NA			181,7	139,8	1		0	0	0	0	0	NA		NA			NA				
UBE2E3 *	0	0	2	NA			150,2	124,7	1		0	0	0	0	0	NA		NA			NA				
MAN2B1 *	0	0	2	NA			250,8	302	1		0	0	0	0	0	NA		NA			NA				
PIK3CD *	0	0	2	NA		NA		219,8	1	24165795		0	0	0	0		65	NA					1,75		
FBXO17 *	0	0	2	NA		NA		113,2	1		0	0	0	0	0	NA		NA			NA				
CHRDL1 *	0	0	2	NA		NA		275,8	1		0	0	0	0	0	NA		NA			NA				
TRIM63 *	0	0	2	NA		NA		137	1		0	0	0	0	0	NA		NA			NA				
CLEC5A *	0	0	2	NA		NA		251,3	1		0	0	0	0	0	NA		NA			NA				
RAMP3 *	0	0	2	NA		NA		271,8	3		0	0	0	0	0		3	NA					34,71		
CDKN1B *	0	0	2	NA		NA		222,5	1		0	1	1	1	1		12			10			1,18		
RAMP2 *	0	0	2	NA		NA		272	1		0	0	0	0	0		2	NA					42,6		
ASB15 *	0	0	2	NA		NA		111,4	1		0	0	0	0	0	NA		NA			NA				
FBXW5 *	0	0	2	NA			132,5	85,5	1		0	0	0	0	0	NA		NA			NA				
PARK2	0	0	2	NA			131,7	93,5	1		0	0	0	0	0	NA		NA			NA				
CUL2 *	0	0	2	NA			96,3	62,8	1		0	0	0	0	0	NA		NA			NA				
UBA3 *	0	0	2		131,7		130	111,8	1		0	0	0	0	1		1	NA					28,4		
NHLRC3 *	0	0	2	NA		NA		305	1		0	0	0	0	0	NA		NA			NA				
FBXO27 *	0	0	2	NA		NA		113,2	1		0	0	0	0	0	NA		NA			NA				
GTF2H3 *	0	0	2		113,8		137,3	190,8	2		0	0	0	0	0	NA		NA			NA				
UBE4A	0	0	2		133		137,2	117,8	1		0	0	0	0	0	NA		NA			NA				
SOCS5 *	0	0	2	NA		NA		208,8	1		0	0	0	0	0	NA		NA			NA				
UBAC1 *	0	0	2	NA		NA		135,7	1		0	0	0	0	0	NA		NA			NA				
LTN1 *	0	0	2	NA			152	118,8	1		0	0	0	0	0	NA		NA			NA				
FEM1A *	0	0	2	NA		NA		241,8	1		0	0	0	0	0	NA		NA			NA				
SMURF1 *	0	0	2	NA			141,3	103	1		0	0	0	0	0	NA		NA			NA				
RNF115 *	0	0	2	NA		NA		139,5	1		0	0	0	0	0	NA		NA			NA				
ATP11A *	0	0	2	NA		NA		281,2	1		0	0	0	0	0	NA		NA			NA				
KLHL13 *	0	0	2	NA		NA		115	1		0	0	0	0	0	NA		NA			NA				
LHCGR *	0	0	2	NA		NA		263,8	2		0	0	0	1	1		14			6			16,23		
FBXO7 *	0	0	2	NA		NA		109,4	1		0	0	0	0	0	NA		NA			NA				
ANAPC10 *	0	0	2	NA			117,8	73	1		0	0	0	0	0	NA		NA			NA				
ADCY4 *	0	0	2	NA			245,8	214,4	2		0	0	0	0	0	NA		NA			NA				
DET1 *	0	0	2	NA			161,8	120,6	1		0	0	0	0	0	NA		NA			NA				
RNF6 *	0	0	2	NA		NA		149,6	1		0	0	0	0	0	NA		NA			NA				
HTR6 *	0	0	2	NA		NA		243,7	1		0	0	0	1	1		51			22			6,68		
FBXL4 *	0	0	2	NA			147,4	103,2	1		0	0	0	0	0	NA		NA			NA				
XRCC1 *	0	0	2	NA			194,6	276,2	2		0	0	1	1	1		10			8			0,81		
ANO8 *	0	0	2	NA		NA		277,8	1		0	0	0	0	0	NA		NA			NA				
ATP8B4 *	0	0	2	NA		NA		284	2		0	0	0	0	0	NA		NA			NA				
CRHR2 *	0	0	2	NA			295	238,8	1		0	0	0	0	1		5			3			5,68		
DCUN1D3 *	0	0	2	NA		NA		240,8	1		0	0	0	0	0	NA		NA			NA				
UBE3B *	0	0	2	NA			152,7	131,2	1		0	0	0	0	0	NA		NA			NA				
CYBA *	0	0	2	NA		NA		233,2	1	23755540;17307262		0	0	1	1		3			3			2,63		
UBE2V2 *	0	0	2	NA		NA		106,5	1		0	0	0	0	0	NA		NA			NA				
CSF1 *	0	0	2	NA		NA		212,7	1		0	0	0	0	1		2	PEXIDARTINIB (unknown)					14,2		
PTH *	0	0	2	NA		NA		239,8	1		0	0	0	0	1		17			14			3,34		
NUP93 *	0	0	2		141,7		180,7	253,5	1		0	0	0	0	0	NA		NA			NA				
SCAMP1 *	0	0	2	NA		NA		302,6	1		0	0	0	0	0	NA		NA			NA				
TRIM21 *	0	0	2	NA		NA		135	1		0	0	0	0	0	NA		NA			NA				
TRAIP *	0	0	2	NA		NA		137,3	1		0	0	0	0	0	NA		NA			NA				
CCNF *	0	0	2	NA		NA		85,8	1		0	0	0	0	0	NA		NA			NA				
COPS4	0	0	2	NA			157,2	152,5	1		0	0	0	0	0	NA		NA			NA				
ADCY7 *	0	0	2	NA		NA		216,6	2		0	0	0	0	0	NA		NA			NA				
FZR1 *	0	0	2	NA			110,5	66	1		0	0	0	0	0	NA		NA			NA				
BPIFB2 *	0	0	2	NA		NA		275,8	2		0	0	0	0	0	NA		NA			NA				
MC5R *	0	0	2	NA		NA		272	2		0	0	0	0	1		4			3			4,73		
FSTL1 *	0	0	2	NA		NA		271,6	2		0	0	0	0	0	NA		NA			NA				
GPR83 *	0	0	2	NA		NA		270,6	2		0	0	0	0	1		2	HYDROCHLOROTHIAZIDE (unkno					3,16		
FBXO15 *	0	0	2	NA		NA		109,5	1		0	0	0	0	0	NA		NA			NA				
CNTFR *	0	0	2	NA		NA		303,8	1		0	0	0	0	0		1	NA					56,81		
GPBAR1 *	0	0	2	NA		NA		267,2	2		0	0	0	0	0		5	NA					34,08		
ADRB1 *	0	0	2	NA		NA		265,6	2		0	0	0	1	1		126			65			5,41		
HERC2 *	0	0	2	NA			148,8	105	1		0	0	0	0	1		1	NERATINIB (unknown)					10,33		
MSH6	0	0	2		116,7		172,2	248,8	1	24357391		0	1	1	1		2			2			9,47		
ALDH3B1 *	0	0	2	NA		NA		282	1		0	0	0	0	0		1	NA					1,18		
SCT *	0	0	2	NA		NA		267,4	2		0	0	0	0	0	NA		NA			NA				
FBXL12 *	0	0	2	NA		NA		114,8	1		0	0	0	0	0	NA		NA			NA				
HERC3 *	0	0	2	NA			217,6	148	1	33565151		0	0	0	0	NA		NA			NA				
TNC	0	0	2	NA		NA		266,8	2	33217999		0	0	0	1		5	NA					11,36		
FSHB *	0	0	2	NA		NA		260,4	2		0	0	0	1	0	NA		NA			NA				
ANAPC7 *	0	0	2	NA			117,2	70,2	1		0	0	0	0	0	NA		NA			NA				
ANAPC5 *	0	0	2	NA			118,8	74,3	1		0	0	0	0	0	NA		NA			NA				
ARIH2	0	0	2		138,5		143,5	131	1	24486325		0	0	0	0	NA		NA			NA				
RBBP6 *	0	0	2	NA			209,8	131	1		0	0	0	0	0	NA		NA			NA				
ANKRD9 *	0	0	2	NA		NA		235,4	1		0	0	0	0	0	NA		NA			NA				
PTGDR *	0	0	2	NA		NA		272,8	2		0	0	0	0	1		14			4			8,12		
GTF2H4 *	0	0	2		109,5		132,3	183,7	2		0	0	0	0	0	NA		NA			NA				
ADRB3 *	0	0	2	NA		NA		266,8	2		0	0	0	1	1		52			22			4,37		
ANAPC4 *	0	0	2	NA			124,4	69,4	1		0	0	0	0	0	NA		NA			NA				
PTH2 *	0	0	2	NA		NA		272,4	1		0	0	0	0	0	NA		NA			NA				
SHISA5 *	0	0	2	NA		NA		275,6	1		0	0	0	0	0	NA		NA			NA				
OLR1 *	0	0	2	NA		NA		276,4	2		0	0	0	1	0	NA		NA			NA				
UFL1 *	0	0	2	NA			144	126,7	1		0	0	0	0	0	NA		NA			NA				
FBXO2 *	0	0	2	NA		NA		107,3	1		0	0	0	0	0	NA		NA			NA				
PGRMC1 *	0	0	2	NA			229,2	288,4	1		0	0	0	0	1		3	NA					2,37		
PJA2 *	0	0	2	NA		NA		140,8	1		0	0	0	0	0	NA		NA			NA				
ASB12 *	0	0	2	NA		NA		115	1		0	0	0	0	0	NA		NA			NA				
BTBD1 *	0	0	2	NA		NA		112,4	1		0	0	0	0	0	NA		NA			NA				
FBXO31 *	0	0	2	NA		NA		112,8	1		0	1	0	0	0	NA		NA			NA				
UBA6 *	0	0	2	NA		NA		137,8	1		0	0	0	0	0	NA		NA			NA				
ADORA2B *	0	0	2	NA		NA		256	2		0	0	0	0	1		39			10			2,91		
UBE2F *	0	0	2	NA		NA		121,4	1		0	0	0	0	0	NA		NA			NA				
NUP50	0	0	2	NA		NA		266,2	1		0	0	0	0	1		1	TENIPOSIDE (unknown)					14,2		
FBXL19 *	0	0	2	NA		NA		95,8	1		0	0	0	0	0	NA		NA			NA				
MGRN1 *	0	0	2	NA		NA		134,5	1		0	0	0	0	0	NA		NA			NA				
SPARCL1 *	0	0	2	NA		NA		245,3	1	29154276		0	0	0	0	NA		NA			NA				
TRIM32 *	0	0	2	NA		NA		132,5	1		0	0	0	0	0	NA		NA			NA				
FGFR2 *	0	0	2	NA		NA		301,8	1		0	0	1	0	1		55			18			3,1		
LAMTOR2 *	0	0	2	NA			196,4	210,3	1		0	0	1	0	0	NA		NA			NA				

TRIM41 *	0	0	2	NA		NA		150,6	1		0	0	0	0	0	NA		NA		NA				
GPR27 *	0	0	2	NA		NA		273	2		0	0	0	0	0	NA		NA		NA				
TAAR1 *	0	0	2	NA		NA		272	1		0	0	0	0	1		31		11				3,66	
ASB13 *	0	0	2	NA		NA		117,6	1		0	0	0	0	0	NA		NA		NA				
PCSK9 *	0	0	2	NA		NA		254	1		0	0	0	1	1		6		3				28,4	
LIFR *	0	0	2	NA		NA		299,7	1		0	0	0	0	1		1	NA					113,61	
TAAR9 *	0	0	2	NA		NA		274,4	2		0	0	0	0	0	NA		NA		NA				
CISH *	0	0	2	NA		NA		204,2	1		0	0	0	0	1		1	EPOETIN ALFA (unknown)					5,98	
CCNB2 *	0	0	2	NA		NA		141,8	1		0	0	0	0	0	NA		NA		NA				
FBXW11 *	0	0	2	NA		NA		92,2	1		0	0	0	0	0	NA		NA		NA				
FBXL13 *	0	0	2	NA		NA		114,6	1		0	0	0	0	0	NA		NA		NA				
SERPINB6 *	0	0	2	NA		NA		316,6	1		0	0	0	0	0	NA		NA		NA				
CRH *	0	0	2	NA		NA		245,6	2		0	0	0	0	1		5	NALOXONE (unknown)					11,36	
FBXO41 *	0	0	2	NA		NA		116,4	1		0	0	0	0	0		1	NA					2,14	
CSF2RB *	0	0	2	NA		NA		281,3	1		0	0	0	0	0		5	NA					15,91	
KLHL22 *	0	0	2	NA		NA		112,8	1		0	0	0	0	0	NA		NA		NA				
ESPL1 *	0	0	2	NA		NA		184,8	1	32574725		0	0	0	0	NA		NA		NA				
TAAR6 *	0	0	2	NA		NA		273,6	2		0	0	0	0	1		1	ARIPIPRAZOLE (unknown)					2,42	
SOCS1 *	0	0	2	NA		NA		102,5	1		0	1	1	0	1		2	INSULIN (unknown)					2,18	
SERPIND1 *	0	0	2	NA		NA		261,2	1		0	0	0	0	1		5	NA					22,72	
SIAH2 *	0	0	2	NA		NA		131,3	1		0	0	0	0	0	NA		NA		NA				
SPSB3 *	0	0	2	NA		NA		240,8	1		0	0	0	0	0	NA		NA		NA				
RBCK1 *	0	0	2	NA		NA		120,2	1		0	0	0	0	0	NA		NA		NA				
RNF138 *	0	0	2	NA		NA		141,5	1		0	0	0	0	0	NA		NA		NA				
KBTBD8 *	0	0	2	NA		NA		115,2	1		0	0	0	0	0	NA		NA		NA				
DZIP3 *	0	0	2	NA		NA		137,3	1		0	0	1	0	0	NA		NA		NA				
FBXL20 *	0	0	2	NA			141,8	101,5	1		0	0	0	0	0	NA		NA		NA				
HMOX2 *	0	0	2	NA		NA		289,4	2		0	0	0	0	1		4		2				49,7	
CAND1 *	0	0	2	NA			185	203	1		0	0	0	0	0	NA		NA		NA				
RNF114 *	0	0	2	NA		NA		149,8	1		0	0	0	0	0	NA		NA		NA				
STC2 *	0	0	2	NA		NA		277,6	2		0	0	0	0	0	NA		NA		NA				
SOCS3 *	0	0	2	NA		NA		69,3	1		0	0	0	0	0	NA		NA		NA				
RNF4 *	0	0	2	NA		NA		134,2	1		0	0	0	0	0	NA		NA		NA				
IFNGR2 *	0	0	2	NA		NA		297,5	1		0	0	0	0	0		1	NA					170,42	
GPS1 *	0	0	2	NA			180	157,8	1		0	0	0	0	0	NA		NA		NA				
SCTR *	0	0	2	NA		NA		273,6	2		0	0	0	0	1		4		3				37,87	
TMEM132A *	0	0	2	NA		NA		277,2	2		0	0	0	0	0	NA		NA		NA				
ZNRF1 *	0	0	2	NA		NA		141,2	1		0	0	0	0	0	NA		NA		NA				
ORMDL3 *	0	0	2		163		223,8	290,6	1		0	0	0	0	0	NA		NA		NA				
APLP2 *	0	0	2	NA		NA		240,3	1		0	0	0	0	1		2	NA					0,59	
SLC2A3 *	0	0	2	NA			226,4	275,6	1		0	0	0	0	1		3	INSULIN (unknown)					2,37	
SCG2 *	0	0	2	NA		NA		273	1		0	0	0	0	0	NA		NA		NA				
IL10RA *	0	0	2	NA		NA		336,6	1		0	0	0	0	1		1	NA					11,36	
PLAUR *	0	0	2	NA		NA		248	1		0	0	0	0	1		6		3				7,57	
ASB6 *	0	0	2	NA		NA		112	1		0	0	0	0	0	NA		NA		NA				
CLEC4D *	0	0	2	NA		NA		284,6	1		0	0	0	0	0	NA		NA		NA				
TMC6 *	0	0	2	NA		NA		284,4	2		0	0	0	0	0	NA		NA		NA				
UBE2R2 *	0	0	2	NA			159,4	130,8	1		0	0	0	0	0	NA		NA		NA				
UBE2A *	0	0	2		120		119,2	108,2	1		0	0	0	0	0	NA		NA		NA				
COMMD10 *	0	0	2	NA		NA		210,6	1		0	0	0	0	0	NA		NA		NA				
GPR15 *	0	0	2	NA		NA		273,6	1		0	0	0	0	0	NA		NA		NA				
TNFRSF12A *	0	0	2	NA		NA		317,8	1		0	0	0	0	1		1	NA					113,61	
SOCS6 *	0	0	2	NA		NA		210,3	1		0	0	0	0	1		1	INSULIN (unknown)					2,23	
DCUN1D4 *	0	0	2	NA		NA		211,8	1		0	0	0	0	0	NA		NA		NA				
COPS7A *	0	0	2	NA		NA		161,7	1		0	0	0	0	0	NA		NA		NA				
SPSB1 *	0	0	2	NA		NA		114,6	1		0	0	0	0	0	NA		NA		NA				
PDIA6 *	0	0	2	NA			197,5	226,5	1		0	0	0	0	0	NA		NA		NA				
BIRC5 *	0	0	2	NA		NA		183,8	1		0	0	0	0	1		38		25				4,48	
MAGED2 *	0	0	2	NA		NA		315,2	1		0	0	0	0	0	NA		NA		NA				
CD47 *	0	0	2	NA		NA		270,8	1		0	0	0	0	1		3	NA					18,94	
NFKBIB *	0	0	2	NA		NA		274,2	1		0	0	0	0	1		1	GEFITINIB (unknown)					1,67	
SERPINC1 *	0	0	2	NA		NA		235,2	1		0	0	0	0	1		29		17				7,84	
TSPAN14 *	0	0	2	NA		NA		283,2	1		0	0	0	0	0	NA		NA		NA				
GPHA2 *	0	0	2	NA		NA		273,6	1		0	0	0	0	0	NA		NA		NA				
ANAPC2 *	0	0	2	NA			116,7	71,3	1		0	0	0	0	0	NA		NA		NA				
WFS1 *	0	0	2	NA			237	236,3	1		0	0	1	1	0	NA		NA		NA				
COMMD6 *	0	0	2	NA		NA		192,2	1		0	0	0	0	0	NA		NA		NA				
GLMN *	0	0	2	NA		NA		130,2	1		0	0	0	0	0	NA		NA		NA				
VGF *	0	0	2	NA		NA		274,6	1		0	0	0	0	0	NA		NA		NA				
HECW2 *	0	0	2	NA		NA		151,2	1	21782286		0	1	0	0	NA		NA		NA				
MCEMP1	0	0	2	NA		NA		281,2	1		0	0	0	0	0	NA		NA		NA				
TMBIM1 *	0	0	2	NA		NA		299,6	1		0	0	0	0	0	NA		NA		NA				
SPP1 *	0	0	2	NA		NA		224,2	1		0	0	0	1	1		6		4				9,47	
RELB *	0	0	2	NA		NA		267	1		0	0	0	0	0	NA		NA		NA				
TARM1 *	0	0	2	NA		NA		285	1		0	0	0	0	0	NA		NA		NA				
CDC23 *	0	0	2		147,8		111	66,8	1		0	0	0	0	0	NA		NA		NA				
DMP1 *	0	0	2	NA		NA		271,8	1		0	0	0	0	0	NA		NA		NA				
AMBN *	0	0	2	NA		NA		271	1		0	0	0	0	0	NA		NA		NA				
HVCN1 *	0	0	2	NA		NA		301,8	1		0	0	0	0	0	NA		NA		NA				
FBXW4 *	0	0	2	NA			263,3	107,2	1		0	0	0	0	0	NA		NA		NA				
GOLM1 *	0	0	2	NA		NA		276,8	2		0	0	0	0	0	NA		NA		NA				
IGFBP1 *	0	0	2	NA		NA		267,6	2	23009592		1	1	1	1		9		7				6,31	
DRD5 *	0	0	2	NA		NA		265,4	1		0	0	0	0	1		37		19				2,3	
CDC27 *	0	0	2	NA			110,5	61,8	1		0	0	0	0	0	NA		NA		NA				
APOA1 *	0	0	2	NA		NA		196,8	1		0	0	1	1	0		11	NA					10,33	
FAM20A *	0	0	2	NA		NA		243,8	1		0	0	0	0	0	NA		NA		NA				
LTBP1 *	0	0	2	NA		NA		273	1		0	0	0	0	0	NA		NA		NA				
SCG3 *	0	0	2	NA		NA		275	1		0	0	0	1	0	NA		NA		NA				
RNF7 *	0	0	2	NA			128,5	88,2	1		0	0	0	0	0	NA		NA		NA				
GNAS	0	0	2	NA			234,8	207	2		0	0	0	1	0		37	NA					1,54	
GTF2H5 *	0	0	2	NA			137	187	2		0	0	0	0	0	NA		NA		NA				
NOTUM *	0	0	2	NA		NA		260,8	1		0	0	0	0	0	NA		NA		NA				
COPS8 *	0	0	2	NA		NA		161	1		0	0	0	0	0	NA		NA		NA				
PLK1	0	0	2		126,8		118	45,5	1		0	0	0	0	1		176		18				0,95	
GLP2R *	0	0	2	NA		NA		272	2		0	0	0	0	1		4	TEDUGLUTIDE (agonist)					71,01	
PTGIR *	0	0	2	NA		NA		242,7	2		0	0	0	0	1		18		9				18,94	
PRKCSH *	0	0	2	NA			203,7	234,5	1		0	0	0	0	0	NA		NA		NA				
MXRA8 *	0	0	2	NA		NA		275,8	1		0	0	0	0	0	NA		NA		NA				
FSTL3 *	0	0	2	NA		NA		272	2		0	0	0	0	0	NA		NA		NA				
TRIM39 *	0	0	2	NA		NA		152	1		0	0	0	0	0	NA		NA		NA				
NUP62 *	0	0	2		139		177,5	250,3	1		0	0	0	0	0	NA		NA		NA				
ADM2 *	0	0	2	NA		NA		273,2	1		0	0	0	0	0	NA		NA		NA				
LAMB1 *	0	0	2	NA		NA		218,8	1		0	0	0	0	0		2	NA					1,67	
GIPR *	0	0	2	NA		NA		273	1		0	0	0	0	1		2	OLANZAPINE (unknown)					9,47	
UBE2B *	0	0	2	NA		NA		102	1		0	0	0	0	0	NA		NA		NA				
FBXO30 *	0	0	2	NA		NA		116,8	1		0	0	0	0	0	NA		NA		NA				
SERPINA10 *	0	0	2	NA		NA		265,8	1		0	0	0	0	0	NA		NA		NA				
FBXO32 *	0	0	2	NA		NA		98,8	1		0	0	0	0	0	NA		NA		NA				
IGFBP5 *	0	0	2	NA		NA		268,8	1		0	1	1	0	1		1	NA					4,94	
TSHB *	0	0	2	NA		NA		266,8	1	19158193		0	1	0	1		11		7				1,48	
GPHB5 *	0	0	2	NA		NA		274	1		0	0	0	0	0	NA		NA		NA				
KCNAB2 *	0	0	2	NA		NA		218,2	1		0	0	0	0	0	NA		NA		NA				
NDC1	0	0	2	NA		NA		302,4	1		0	0	0	0	0	NA		NA		NA				
LNX1 *	0	0	2	NA		NA		133,3	1		0	0	0	0	0	NA		NA		NA				
MSLN *	0	0	2	NA		NA		223,8	1		0	0	0	0	1		1	NA					227,22	
HERC1 *	0	0	2	NA		NA		140,3	1		0	0	0	0	0	NA		NA		NA				
TRIM11 *	0	0	2	NA		NA		139,8	1		0	0	0	0	0	NA		NA		NA				
GPR97 *	0	0	2	NA		NA		303,4	1		0	0	0	0	0	NA		NA		NA				
EVA1A *	0	0	2	NA		NA		276,2	1		0	0	0	0	0	NA		NA		NA				

NFKBIE *	0	0	2	NA	NA		280,5	1	0	0	0	0	0	NA	NA	NA		
GIP *	0	0	2	NA	NA		264,6	1	0	0	0	0	0	NA	NA	NA		
HERC6 *	0	0	2	NA	NA		141,4	1	0	0	0	0	0	NA	NA	NA		
CUL5 *	0	0	2	NA		125,7	84,3	1	0	0	0	0	0	NA	NA	NA		
TULP4	0	0	2	NA		215	236	1	0	0	0	0	0	NA	NA	NA		
RLN2 *	0	0	2	NA	NA		273,2	1	0	0	0	0	1		1	NEOMYCIN (unknown)		18,94
MATN3 *	0	0	2	NA	NA		270,4	1	0	0	0	0	0	NA	NA	NA	NA	
MKRN1 *	0	0	2	NA	NA		144	1	31476350	0	0	0	0	NA	NA	NA	NA	
P2RX1 *	0	0	2	NA	NA		289,4	1	0	0	0	0	1		2	NA		14,2
STK10 *	0	0	2	NA	NA		302,6	1	0	0	0	0	1		3	BOSUTINIB (inhibitor)		0,82
MAPKAP1	0	0	3	NA		216,3	308,8	1	0	0	0	0	0		3	NA		1,89
CCDC88A	0	0	3	NA	NA		325,2	1	0	0	0	0	0	NA	NA	NA	NA	

Protein	Comi	Bilate	Ecdis	ADR_common	ADR_bilaterian	ADR_ecdisozo	Predictors	Pubmed_ID	Wormbase
RPS-18	2	2	2	17,8	14,3	14	8	0	0
RPS-1	2	2	2	30,5	27,5	24,5	7	0	0
RPL-32 *	2	2	2	34,8	43,5	44,5	8	0	0
RPS-2 *	2	2	2	6	12,5	12,5	8	0	0
RPS-24	2	2	2	26,8	54,5	42	8	0	0
RPL-25.2 *	2	2	2	26,3	60	104,8	5	0	0
Y37E3.8 *	2	2	2	28,3	39,5	38,7	8	0	0
RPL-5 *	2	2	2	11,8	23,7	27,2	8	0	0
RLA-2	2	2	2	70,3	88,3	91	8	0	0
RPS-28 *	2	2	2	35,3	30,5	28,7	8	0	0
RPL-33 *	2	2	2	44,2	52,7	51,8	9	0	0
RPL-21	2	2	2	46	58	58	9	0	0
RPL-12	2	2	2	39,3	43,8	42,8	8	0	0
RPL-26	2	2	2	52	115,3	75	7	0	0
RPS-19 *	2	2	2	36,3	29	27,8	8	0	0
RPL-35	2	2	2	39,8	41,3	40,2	10	0	0
W01D2.1	2	2	2	58,7	96,3	89,2	6	0	0
RPL-41 *	2	2	2	48,2	64,5	56,7	8	0	0
RPL-15 *	2	2	2	29,7	40,3	41,3	8	0	0
RPS-13 *	2	2	2	9,3	14	14,8	8	0	0
RPL-34	2	2	2	64	68	64,2	8	0	0
RPS-7 *	2	2	2	30,2	90,3	51,5	7	0	0
RPS-9 *	2	2	2	20,2	17,2	16,3	8	0	1
RPL-43	2	2	2	44,3	48	48	8	0	0
RPL-11.2 *	2	2	2	29,8	31,7	30,5	8	0	0
RPL-20	2	2	2	35,2	47,3	49,3	9	0	0
RPS-29 *	2	2	2	45,7	30,2	26,8	8	0	1
RPS-27	2	2	2	64,3	128,3	83,3	3	0	1
RPL-13	2	2	2	58,7	59,5	54,2	9	0	0
RPS-17 *	2	2	2	48,3	69,8	68,2	6	0	0
RPL-18 *	2	2	2	49,8	77,8	66	7	0	0
ERFA-3 *	2	2	2	64,5	110,7	111,6	4	0	0
RPL-6	2	2	2	60,8	74,2	73,2	8	0	1
IFFB-1	0	2	2	58	88,3	90	8	0	0
RPL-16 *	0	2	2	48,5	111,5	66	7	0	0
RPN-8 *	0	2	2	112,3	134	88,2	1	0	1
RPL-29	0	2	2	53,7	98,3	78,8	6	0	0
UBC-16 *	0	2	2	NA	164,8	159	1	0	0
RPS-21	0	2	2	69,2	41,2	35,7	7	0	1
RPL-2 *	0	2	2	NA	58,5	41,8	8	0	0
RPN-1 *	0	2	2	102,7	124,3	84,7	1	0	1
C37C3.2 *	0	2	2	111,8	136,2	129,2	1	0	0
RPL-24.1 *	0	2	2	66,3	130,3	89,5	8	0	0
RPL-36 *	0	2	2	65,5	101,3	115	6	0	0
MRPL-11 *	0	2	2	102,7	99,2	93,8	2	0	0
RPL-11.1 *	0	2	2	71,6	147,4	144,8	3	15687263	1
EIF-3.I *	0	2	2	66,7	99,5	94,3	6	0	0
EIF-3.L *	0	2	2	NA	145,5	123,3	2	27690135	1
RPL-14 *	0	2	2	84,4	160,4	157,8	2	0	0
EIF-2ALPHA *	0	2	2	68,8	92,3	87	2	33723245	0
PAS-6 *	0	2	0	108,5	131,8	122	1	0	1
UBC-7 *	0	2	0	NA	157	150,6	1	0	0
W09C5.1 *	0	2	0	26,8	48,7	44	1	0	0
Y92H12A.2	0	2	0	NA	138,5	126,8	1	0	0
LIG-1 *	0	2	0	94,7	127	133	1	0	0
SPSB-2	0	2	0	NA	138	129,2	1	0	0
UBC-14 *	0	2	0	135,2	132,2	124	1	0	0
RPN-7 *	0	2	0	110	133,5	125,2	1	25093668	1

PBS-7 *	0	2	0		111,7		131,2	120,7	1	0	1
UBA-1	0	2	0		117,8		117,7	109	1	23354069	1
RPN-5 *	0	2	0		111		131,5	90	1	0	0
RPS-25 *	0	2	0		79,8		155,4	152,8	1	0	0
WDFY-3	0	3	3	NA			217,5	205,3	1	0	0
PBS-6 *	0	0	2		110,5		134	88,7	1	25093668	1
PAS-5 *	0	0	2		104,3		123,2	80,8	1	0	1
RPN-3 *	0	0	2		111,5		132,3	90,2	1	0	1
C48B6.2 *	0	0	2		35,2		40,2	32,7	1	0	0
F21D5.7 *	0	0	2		80,5		109,2	110	3	0	0
EIF-3.E *	0	0	2	NA			129,7	106,5	6	0	1
RPL-27 *	0	0	2	NA		NA		128	2	0	0
RPL-38 *	0	0	2	NA		NA		128	3	0	0
PAS-2 *	0	0	2		107,2		128,5	85,3	1	0	0
EIF-3.C *	0	0	2		80,8		97,2	82	1	0	0
TRX-2	0	0	3	NA			217,8	209	1	0	0

Protein	Comi	Bilate	Ecdis	ADR_common	ADR_bilaterian	ADR_ecdisozo	Predictors	Pubmed_ID	Flybase
RpS23	2	2	2	17,2	20	19,5	8	0	0
RpS18	2	2	2	17,8	14,3	14	8	0	0
RpS3A	2	2	2	30,5	27,5	24,5	7	0	0
RpL32 *	2	2	2	34,8	43,5	44,5	8	0	0
RpS2 *	2	2	2	6	12,5	12,5	8	0	0
RpS24	2	2	2	26,8	54,5	42	8	0	0
RpL27A *	2	2	2	28,3	39,5	38,7	8	0	0
RpL30	2	2	2	34	42,2	45	8	0	0
RpL5 *	2	2	2	11,8	23,7	27,2	8	0	0
RpLP2	2	2	2	70,3	88,3	91	8	0	0
RpS28b *	2	2	2	35,3	30,5	28,7	8	0	0
RpL35A *	2	2	2	44,2	52,7	51,8	9	0	0
RpL21	2	2	2	46	58	58	9	0	0
RpL12	2	2	2	39,3	43,8	42,8	8	0	0
sta *	2	2	2	17,7	27,3	34,2	8	0	0
RpS5a	2	2	2	7	11,2	14,7	8	0	0
RpL26	2	2	2	52	115,3	75	7	0	0
RpS19a *	2	2	2	36,3	29	27,8	8	0	0
RpL35	2	2	2	39,8	41,3	40,2	10	0	0
RpL37a	2	2	2	58,7	96,3	89,2	6	0	0
RpL36A *	2	2	2	48,2	64,5	56,7	8	0	0
RpL31 *	2	2	2	66,3	68	75,8	7	0	0
RpL15 *	2	2	2	29,7	40,3	41,3	8	0	0
RpS15	2	2	2	25,8	22,2	19,2	8	0	0
RpS13 *	2	2	2	9,3	14	14,8	8	0	0
RpL34a	2	2	2	64	68	64,2	8	0	0
RpS7 *	2	2	2	30,2	90,3	51,5	7	0	0
RpS9 *	2	2	2	20,2	17,2	16,3	8	0	0
RpS16 *	2	2	2	17,7	26,7	34,8	8	0	0
RpL7A	2	2	2	34,8	53,5	57,3	8	0	0
RpS15Aa	2	2	2	19,5	34,2	42,7	8	0	0
RpL37A	2	2	2	44,3	48	48	8	0	0
RpS20	2	2	2	25	19,2	18	8	0	0
RpS8	2	2	2	11,5	19,3	21	7	0	0
RpL11 *	2	2	2	29,8	31,7	30,5	8	0	0
RpS14a	2	2	2	12,3	24,2	36,2	7	0	0
RpS11	2	2	2	12,5	11,3	13	6	0	0
RpS25 *	2	2	2	45	38	44	7	0	0
RpL18A	2	2	2	35,2	47,3	49,3	9	0	0
RpS29 *	2	2	2	45,7	30,2	26,8	8	0	0
RpS27	2	2	2	64,3	128,3	83,3	3	0	0
RpLP0	2	2	2	26,5	37,7	40,2	9	0	0
RpL13	2	2	2	58,7	59,5	54,2	9	0	0
RpS17 *	2	2	2	48,3	69,8	68,2	6	0	0
RpL3	2	2	2	16	29,7	28,2	8	0	0
RpL18 *	2	2	2	49,8	77,8	66	7	0	0
Elf *	2	2	2	64,5	110,7	111,6	4	0	0
RpL6	2	2	2	60,8	74,2	73,2	8	0	0
RpS3	2	2	2	5,8	8	8,2	8	30947023	0
eRF1 *	2	2	0	56	97,2	103,5	4	0	0
Atg4a	3	3	3	148,8	210,8	202,8	1	0	0
eIF5B	0	2	2	58	88,3	90	8	0	0
RpS10a	0	2	2	57,7	121,5	86,5	7	0	0
RpS10b *	0	2	2	NA	84,8	75,3	2	0	0
RpL13A *	0	2	2	48,5	111,5	66	7	0	0
RpL23	0	2	2	NA	57,3	39,3	8	0	0
Rpn8 *	0	2	2	112,3	134	88,2	1	0	0

RpL29	0	2	2		53,7	98,3	78,8	6	0	0
CG7220 *	0	2	2	NA		164,8	159	1	0	0
RpS26	0	2	2		52,3	115,8	78,3	7	0	0
RpS21	0	2	2		69,2	41,2	35,7	7	0	1
RpL7	0	2	2	NA		75,3	55,8	7	0	0
RpL8 *	0	2	2	NA		58,5	41,8	8	0	0
Rpn1 *	0	2	2		102,7	124,3	84,7	1	29615416	0
eIF5 *	0	2	2		111,8	136,2	129,2	1	0	1
RpL24 *	0	2	2		66,3	130,3	89,5	8	0	0
Rack1	0	2	2		20,7	49,8	52,7	9	24277934	1
mRpL11 *	0	2	2		102,7	99,2	93,8	2	0	1
Trip1 *	0	2	2		66,7	99,5	94,3	6	0	0
eIF3l *	0	2	2	NA		145,5	123,3	2	0	0
RpL28 *	0	2	2	NA		113,3	105,7	6	0	0
eIF-2alpha *	0	2	2		68,8	92,3	87	2	0	0
Prosalpha6 *	0	2	0		108,5	131,8	122	1	0	0
CG40045 *	0	2	0	NA		157	150,6	1	0	0
Ip259 *	0	2	0		26,8	48,7	44	1	0	0
eIF3g1 *	0	2	0		79,5	115,5	123,3	2	0	0
Ube3a *	0	2	0	NA		149,8	141,7	1	0	0
Nedd4	0	2	0	NA		138,5	126,8	1	0	0
DNA-ligI *	0	2	0		94,7	127	133	1	0	0
CG17754 *	0	2	0	NA		166	163,4	1	0	0
gus	0	2	0	NA		138	129,2	1	0	0
CG3356 *	0	2	0	NA		160,2	157,6	1	0	0
Trim9	0	2	0	NA		159	152	1	0	0
CG33981 *	0	2	0	NA		167	164,4	1	0	0
Ubc7 *	0	2	0		135,2	132,2	124	1	0	0
RpS19b *	0	2	0		70,8	146	143,4	1	0	0
Rpn7 *	0	2	0		110	133,5	125,2	1	0	1
RpS28a *	0	2	0		50,6	125,2	122,6	1	0	0
RpL36 *	0	2	0		73,3	137,8	132,2	2	0	0
poe *	0	2	0	NA		133,6	131	1	0	0
Kpc1 *	0	2	0	NA		164,6	162	1	0	0
eIF3-S10 *	0	2	0		97	122,8	122,3	1	0	0
jet *	0	2	0	NA		135,3	127,2	1	0	0
Ppa *	0	2	0	NA		137,2	129	1	0	0
Prosbeta4 *	0	2	0		110,3	137,7	139	1	0	0
Prosbeta7 *	0	2	0		111,7	131,2	120,7	1	0	1
Uba1	0	2	0		117,8	117,7	109	1	23382794	1
CG32085 *	0	2	0	NA		148,8	146,2	1	0	0
Ubr1 *	0	2	0	NA		162,8	160,2	1	0	0
Prosbeta2 *	0	2	0		117	145,3	143,3	1	0	0
Ubc4 *	0	2	0		131,3	139,3	137	1	0	0
Rpn5 *	0	2	0		111	131,5	90	1	0	0
eIF-2beta *	0	2	0		101,5	127	126,2	2	0	0
RpS4	0	2	0		33,7	96,7	91	1	0	0
Iru *	0	2	0	NA		170,2	167,6	1	0	0
Prosbeta6 *	0	0	2		110,5	134	88,7	1	0	0
Prosalpha5 *	0	0	2		104,3	123,2	80,8	1	0	0
Rpn3 *	0	0	2		111,5	132,3	90,2	1	0	1
CG4866 *	0	0	2		35,2	40,2	32,7	1	0	0
Srp54k *	0	0	2		80,5	109,2	110	3	0	0
Int6 *	0	0	2	NA		129,7	106,5	6	0	0
RpL27 *	0	0	2	NA	NA		128	2	0	0
RpL38 *	0	0	2	NA	NA		128	3	0	0
Prosalpha2 *	0	0	2		107,2	128,5	85,3	1	0	0
eIF3-S8 *	0	0	2		80,8	97,2	82	1	0	0

eIF3-S9	0	0	2		63,5	86,3	74,5	1	0	0
Srp14 *	0	0	2	NA		178	175,4	1	0	0
Glo1	0	0	3	NA		217,8	209,7	1	34734976	1
CG8993	0	0	3	NA		217,8	209	1	0	0

Protein	Com	Bilate	Euar	ADR_common	ADR_bilaterian	ADR_euarchoı	Predictors	Pubmed_ID
Rpl21	2	2	2	46	58	160,5	9	0
Rpl6	2	2	2	60,8	74,2	166,2	9	0
Etf1 *	2	2	0	56	97,2	175,7	4	0
Rps23	2	2	0	17,2	20	78,5	7	0
Rps18	2	2	0	17,8	14,3	76,8	8	0
Rps3a1	2	2	0	30,5	27,5	90,2	7	0
Rpl32 *	2	2	0	34,8	43,5	132,2	8	0
Rps2 *	2	2	0	6	12,5	74,5	5	34103648
Rps24	2	2	0	26,8	54,5	190,5	6	0
Rpl23a *	2	2	0	26,3	60	145,3	5	0
Rpl27a *	2	2	0	28,3	39,5	126,2	8	0
Rpl30	2	2	0	34	42,2	123	8	0
Rpl5 *	2	2	0	11,8	23,7	100	8	0
Rplp2	2	2	0	70,3	88,3	185	8	0
Rps28 *	2	2	0	35,3	30,5	101,7	5	0
Rpl35a *	2	2	0	44,2	52,7	140,3	9	0
Rpl12	2	2	0	39,3	43,8	144,2	8	0
Rpsa *	2	2	0	17,7	27,3	105	8	0
Rps5	2	2	0	7	11,2	65,7	7	0
Rps19 *	2	2	0	36,3	29	100,8	8	0
Rpl35	2	2	0	39,8	41,3	145,5	7	0
Rpl37	2	2	0	58,7	96,3	220,5	5	0
Rpl36al *	2	2	0	48,2	64,5	174,5	8	0
Rpl31 *	2	2	0	66,3	68	148,3	7	0
Rps7	2	2	0	22,2	82,3	110,5	2	0
Rpl15 *	2	2	0	29,7	40,3	132,8	8	0
Rps15	2	2	0	25,8	22,2	99,2	8	31921849
Rps13 *	2	2	0	9,3	14	71,3	6	0
Rpl34	2	2	0	64	68	161	8	0
Rps9 *	2	2	0	20,2	17,2	68,3	7	0
Rps16 *	2	2	0	17,7	26,7	94,7	6	0
Rpl7a	2	2	0	34,8	53,5	160,7	8	0
Rps15a	2	2	0	19,5	34,2	89,2	3	0
Rpl37a	2	2	0	44,3	48	128,2	6	0
Rps20	2	2	0	25	19,2	88,5	7	0
Rps8	2	2	0	11,5	19,3	82,8	6	0
Rpl11 *	2	2	0	29,8	31,7	106,3	8	0
Rps14	2	2	0	12,3	24,2	70,5	7	0
Rps11	2	2	0	12,5	11,3	67,8	6	0
Rps25 *	2	2	0	45	38	106,7	7	0
Rpl18a	2	2	0	35,2	47,3	136	9	0
Rps29 *	2	2	0	45,7	30,2	112,3	8	0
Rplp0	2	2	0	26,5	37,7	129,2	9	0
Rpl13	2	2	0	58,7	59,5	150,8	8	0
Rps17 *	2	2	0	48,3	69,8	166	5	0
Rpl3	2	2	0	16	29,7	116	8	0
Rpl18 *	2	2	0	49,8	77,8	204,7	6	0
Rps3	2	2	0	5,8	8	59,3	7	0
Atg4b	3	3	0	148,8	210,8	308,3	1	0
Ube2g1 *	0	2	2	nan	157	127,5	2	0
Ube3a *	0	2	2	nan	149,8	111,2	2	0
Nedd4 *	0	2	2	nan	138,5	105	2	0
Keap1	0	2	2	nan	147,8	81,3	2	32590331;32487458;33318486
Klhl5 *	0	2	2	nan	166	108	2	0
Spsb4 *	0	2	2	nan	138	104,2	2	0
Ube3c *	0	2	2	nan	160,2	131,2	2	0
Trim9	0	2	2	nan	159	128,5	2	0
Anapc13 *	0	2	2	nan	167	119,2	2	0
Ube2g2 *	0	2	2	135,2	132,2	116,5	2	0
Ubr4 *	0	2	2	nan	133,6	57,8	2	0
Rnf123 *	0	2	2	nan	164,6	124,8	2	0

Fbxl15 *	0	2	2	nan		135,3	97,5	2	0
Fbxl14 *	0	2	2	nan		137,2	103	2	0
Uba1 *	0	2	2		117,8	117,7	106,7	2	0
Ubr2 *	0	2	2	nan		162,8	135,8	2	0
Ube2k *	0	2	2		131,3	139,3	116,7	2	0
Eif5b	0	2	0		58	88,3	198,3	4	0
Psma1 *	0	2	0		108,5	131,8	223	1	0
Rps10 *	0	2	0	nan		84,8	148,7	2	0
Nsa2 *	0	2	0		26,8	48,7	134,7	1	0
Rpl38 *	0	2	0		58,7	122,3	162,5	1	0
Eif3g *	0	2	0		79,5	115,5	209,8	2	0
Rpl23	0	2	0	nan		57,3	111,8	6	0
Psmd7 *	0	2	0		112,3	134	154	1	0
Lig1 *	0	2	0		94,7	127	206,3	1	0
Rpl29	0	2	0		53,7	98,3	274	5	0
Rps21	0	2	0		69,2	41,2	117,3	6	0
Rpl7	0	2	0	nan		75,3	147,8	2	0
Rpl8 *	0	2	0	nan		58,5	107,8	5	0
Psmd2 *	0	2	0		102,7	124,3	144,2	1	0
Eif5 *	0	2	0		111,8	136,2	241,8	1	0
Gnb2l1	0	2	0		20,7	49,8	128,7	6	0
Rpl36 *	0	2	0		65,5	101,3	180,2	6	0
Mrpl11 *	0	2	0		102,7	99,2	187	1	0
Psmd6 *	0	2	0		110	133,5	150,5	1	0
Eif3a *	0	2	0		97	122,8	221,5	1	0
Eif3i *	0	2	0		66,7	99,5	206	5	0
Eif3l *	0	2	0	nan		145,5	239,8	1	0
Psmb2 *	0	2	0		110,3	137,7	149,3	1	0
Rpl28 *	0	2	0	nan		113,3	192,7	2	0
Psmb4 *	0	2	0		111,7	131,2	146,8	1	0
Fbxl16 *	0	2	0	nan		148,8	103,3	1	0
Psmb7 *	0	2	0		117	145,3	162,8	1	0
Eif2s1 *	0	2	0		68,8	92,3	191	1	0
Psmd12 *	0	2	0		111	131,5	150,8	1	0
Eif2s2 *	0	2	0		101,5	127	226,2	2	0
Rnf126	0	2	0	nan		170,2	292,8	1	0
Rpl27 *	0	2	0		59,5	123	182,3	1	0
Wdfy3	0	3	0	nan		217,5	312,2	1	0
Blm	0	0	1	nan	nan		236,8	2	0
Bard1 *	0	0	1	nan	nan		233,5	2	0
Rnf19a *	0	0	2	nan	nan		139,2	1	0
Mepe *	0	0	2	nan	nan		274,2	1	0
Fem1b	0	0	2	nan		215,8	213,5	1	0
Commd2 *	0	0	2	nan		184	186,2	1	0
Fbxo40 *	0	0	2	nan	nan		111,5	1	0
Wsb1 *	0	0	2	nan	nan		111	1	0
Fbxl18 *	0	0	2	nan	nan		116,4	1	0
Spsb2 *	0	0	2	nan	nan		117,4	1	0
Ube2o *	0	0	2	nan		164,4	133	1	0
Gan *	0	0	2	nan	nan		110,5	1	0
Asb14 *	0	0	2	nan	nan		116,6	1	0
Hrc *	0	0	2	nan	nan		277	1	0
Commd9 *	0	0	2	nan	nan		210,8	1	0
Fbxl3 *	0	0	2	nan	nan		102,3	1	0
Lrsam1 *	0	0	2	nan	nan		147,8	1	0
Ercc3	0	0	2		107	123,5	179,7	2	0
Rnf182 *	0	0	2	nan	nan		150,4	1	0
Dcun1d2	0	0	2	nan	nan		214,4	1	0
Serpinb3a *	0	0	2	nan		264	303,6	1	0
Cdca8 *	0	0	2	nan	nan		183	1	0
Kctd6 *	0	0	2	nan	nan		115	1	0
Adm *	0	0	2	nan	nan		272,2	3	29187812

Klhl3 *	0	0	2	nan		nan		114,4	1	0
Adam8 *	0	0	2	nan		nan		278,4	1	0
Asb18 *	0	0	2	nan		nan		117,6	1	0
Gpr20 *	0	0	2	nan		nan		272,6	1	0
Mib2 *	0	0	2	nan			147,3	125	1	0
Mapk11	0	0	2		155,2		203,5	223,2	1	0
Asb1 *	0	0	2	nan		nan		113,8	1	0
Fbxo4 *	0	0	2	nan		nan		107	1	0
Kras *	0	0	2	nan		nan		114,7	1	0
Chrnb4 *	0	0	2	nan		nan		272,6	1	0
Asb4 *	0	0	2	nan		nan		111	1	0
Ube2j2 *	0	0	2		137,8		182,5	129,7	1	0
Trim37 *	0	0	2	nan		nan		149,8	1	0
Asb9 *	0	0	2	nan		nan		116	1	0
Uba7 *	0	0	2	nan		nan		128	1	0
Slc15a4 *	0	0	2		164,8		245	300,6	1	0
Trim71 *	0	0	2	nan		nan		138,2	1	0
Itch *	0	0	2	nan		nan		84,7	1	0
Hectd2 *	0	0	2	nan		nan		141,8	1	0
Commd3 *	0	0	2	nan			219,8	190,3	1	0
Trip12 *	0	0	2		142		222,2	103,8	1	0
Rnf41 *	0	0	2	nan			165	121,5	1	0
Gpr45 *	0	0	2	nan		nan		273,2	1	0
Fbxo10 *	0	0	2	nan		nan		115,6	1	0
Klhl21 *	0	0	2	nan		nan		116,8	1	0
Rnf144b *	0	0	2	nan		nan		146,8	1	0
Asb7 *	0	0	2	nan		nan		114,6	1	0
Gpr25 *	0	0	2	nan		nan		272,6	2	0
Mex3c *	0	0	2	nan		nan		148,4	1	0
Htr7 *	0	0	2	nan		nan		267,2	2	0
Klhl11 *	0	0	2	nan		nan		110,8	1	0
Cops3	0	0	2	nan			161	153	1	0
Asb17 *	0	0	2	nan		nan		116,8	1	0
Iapp *	0	0	2	nan		nan		264	3	0
Cd53 *	0	0	2	nan		nan		278,2	1	0
Klhl2 *	0	0	2	nan			146,2	101,5	1	0
Arel1 *	0	0	2	nan			165,6	138,2	1	0
Asb10 *	0	0	2	nan		nan		115,8	1	0
Calcrl *	0	0	2	nan			285	271,8	2	0
Fbxw7 *	0	0	2	nan			189,8	87,7	1	0
Ube2h	0	0	2		136,2		145,2	126,5	1	0
Ube2z *	0	0	2	nan		nan		147,2	1	0
Klhl42 *	0	0	2	nan		nan		115	1	0
Adcyap1r1 *	0	0	2	nan		nan		269,4	2	0
Dtx3l *	0	0	2	nan		nan		145,2	1	0
Adcy6 *	0	0	2	nan		nan		217,6	1	0
Asb2 *	0	0	2	nan		nan		108,8	1	0
Cblb *	0	0	2	nan		nan		110,5	1	0
Uba5 *	0	0	2	nan			141,5	122,7	1	0
Adcy3 *	0	0	2	nan			230	189,5	1	0
Mmp25	0	0	2	nan		nan		296,6	1	0
Taar2 *	0	0	2	nan		nan		273,8	3	0
Gpr176 *	0	0	2	nan		nan		273,6	3	0
Crhr1 *	0	0	2	nan		nan		258,8	2	0
Rnf34 *	0	0	2	nan		nan		148,4	1	0
Ifna2 *	0	0	2	nan		nan		340,2	1	0
Mylip *	0	0	2	nan			164,8	127,2	1	0
Asb16 *	0	0	2	nan		nan		117,8	1	0
Mc4r *	0	0	2	nan		nan		229,2	2	0
Klhl9 *	0	0	2	nan		nan		116,2	1	0
Fbxo11 *	0	0	2	nan			129,7	95,2	1	0
Pth1r *	0	0	2	nan		nan		240,2	2	0

Adcyap1 *	0	0	2	nan		nan		267,6	1	29774542;16505386
Traf7 *	0	0	2	nan		nan		151	1	0
Ube2l6 *	0	0	2	nan		nan		117,2	1	0
Cops7b *	0	0	2	nan			163,8	160,2	1	0
Commd1 *	0	0	2	nan		nan		206,6	1	0
Tacr1 *	0	0	2	nan		nan		133,2	1	0
Kctd7 *	0	0	2	nan		nan		111,6	1	0
Fbxo9	0	0	2		154,2		135	97,8	1	0
Fbxw2 *	0	0	2	nan		nan		109,5	1	0
Adcy8 *	0	0	2	nan			247	190,7	2	0
Anapc1 *	0	0	2	nan			117	70,2	1	0
Kbtbd13 *	0	0	2	nan		nan		111,4	1	0
Pja1 *	0	0	2	nan		nan		138,2	1	0
Fbxl8 *	0	0	2	nan		nan		118	1	0
Igfbp4 *	0	0	2	nan		nan		273,2	1	32223893
Klhl20 *	0	0	2	nan			146,8	103,8	1	0
Adcy1	0	0	2	nan			229	213,8	2	0
Btbd6 *	0	0	2	nan		nan		113	1	0
Pthlh *	0	0	2	nan		nan		258,4	1	0
Calca *	0	0	2	nan		nan		273,6	2	0
Hectd3 *	0	0	2	nan		nan		151,2	1	0
Rap2b *	0	0	2	nan		nan		282,8	1	0
Asb5 *	0	0	2	nan		nan		116,2	1	0
Il13ra2 *	0	0	2	nan		nan		309,3	1	0
Fam20c *	0	0	2	nan		nan		245	1	0
Fbxl5 *	0	0	2	nan		nan		107,2	1	0
Trim50 *	0	0	2	nan		nan		150,6	1	0
Klhl25 *	0	0	2	nan		nan		117	1	0
Fbxw9 *	0	0	2	nan			213	113,6	1	0
Mnat1 *	0	0	2	nan			133,3	170,5	2	0
Ccnh *	0	0	2		116,5		134	171	2	0
Ramp1 *	0	0	2	nan		nan		272,2	2	0
Cul7 *	0	0	2	nan		nan		135,7	1	0
Rxfp1 *	0	0	2	nan		nan		267	2	0
Ube2q2 *	0	0	2	nan		nan		149,2	1	0
Taar5 *	0	0	2	nan		nan		271,6	1	0
Trim69 *	0	0	2	nan		nan		150,2	1	0
Trpm2	0	0	2	nan		nan		281,8	1	30999030
Rchy1 *	0	0	2	nan		nan		126,2	1	0
Ube2e2 *	0	0	2	nan		nan		147,6	1	0
Pth2r *	0	0	2	nan		nan		272,8	1	0
Rnf19b *	0	0	2	nan		nan		148,2	1	0
Htr4 *	0	0	2	nan		nan		272,2	2	0
Huwe1 *	0	0	2	nan			162,4	119,7	1	22187431
Fbxw8 *	0	0	2	nan		nan		110,3	1	0
Asb11 *	0	0	2	nan		nan		116,8	1	0
Mc2r *	0	0	2	nan		nan		267,6	1	0
Fbxo21 *	0	0	2	nan		nan		116,8	1	0
Siah1a *	0	0	2	nan			150,2	123,7	1	0
Wsb2 *	0	0	2	nan		nan		216,2	1	0
Vipr1 *	0	0	2	nan		nan		269,4	2	0
Aurkb *	0	0	2	nan		nan		92,8	2	0
Mc3r *	0	0	2	nan		nan		267	3	0
Gpr150	0	0	2	nan		nan		272,2	2	0
Cdc26 *	0	0	2	nan		nan		85,8	1	34590680
Rlim *	0	0	2	nan		nan		136,3	1	0
Kbtbd7 *	0	0	2	nan		nan		114,8	1	0
Znrf2 *	0	0	2	nan		nan		143,4	1	0
Ptger2 *	0	0	2	nan		nan		271,4	2	0
Rnf25 *	0	0	2	nan		nan		141,3	1	0
Ubox5 *	0	0	2	nan			162,2	120,2	1	0
Nuf2 *	0	0	2	nan		nan		214,6	1	0

Wwp1 *	0	0	2	nan		nan		113,7	1	0
Glp1r *	0	0	2	nan		nan		268,4	2	0
Ube2d2a *	0	0	2		126,8		195	66	1	0
Lrr1 *	0	0	2	nan			147,8	98,6	1	0
Smurf2 *	0	0	2	nan		nan		85,2	1	28387615;24494704
Ptges2 *	0	0	2	nan			249,8	260,2	1	0
Nup214 *	0	0	2	nan			179,8	243,2	1	0
Vprbp *	0	0	2	nan			144,7	113,3	1	32730228
Gtf2h1 *	0	0	2	nan			142,5	194,3	2	0
Vhl *	0	0	2	nan		nan		67,2	1	23999831
Taar8b *	0	0	2	nan		nan		274,2	2	0
Ube2cbp *	0	0	2	nan		nan		145,8	1	0
Rnf130 *	0	0	2	nan		nan		146,6	1	0
Trim36 *	0	0	2	nan		nan		147,4	1	0
Commd7 *	0	0	2	nan		nan		211	1	0
Gtf2h2	0	0	2		108,7		128,5	189,3	2	0
Bub1 *	0	0	2	nan			181,7	139,8	1	0
Ube2e3 *	0	0	2	nan			150,2	124,7	1	0
Man2b1 *	0	0	2	nan			250,8	302	1	0
Pik3cd *	0	0	2	nan		nan		219,8	1	0
Fbxo17 *	0	0	2	nan		nan		113,2	1	0
Chrdl1 *	0	0	2	nan		nan		275,8	1	0
Trim63 *	0	0	2	nan		nan		137	1	29717119
Clec5a *	0	0	2	nan		nan		251,3	1	0
Ramp3 *	0	0	2	nan		nan		271,8	3	0
Cdkn1b *	0	0	2	nan		nan		222,5	1	0
Ramp2 *	0	0	2	nan		nan		272	1	0
Asb15 *	0	0	2	nan		nan		111,4	1	0
Fbxw5 *	0	0	2	nan			132,5	85,5	1	0
Park2	0	0	2	nan			131,7	93,5	1	0
Cul2 *	0	0	2	nan			96,3	62,8	1	0
Uba3 *	0	0	2		131,7		130	111,8	1	0
Ercc5	0	0	2		118,5		168	253,8	2	0
Nhlrc3 *	0	0	2	nan		nan		305	1	0
Fbxo27 *	0	0	2	nan		nan		113,2	1	0
Gtf2h3 *	0	0	2		113,8		137,3	190,8	2	0
Ube4a	0	0	2		133		137,2	117,8	1	0
Socs5 *	0	0	2	nan		nan		208,8	1	0
Ubac1 *	0	0	2	nan		nan		135,7	1	0
Ltn1 *	0	0	2	nan			152	118,8	1	0
Fem1a *	0	0	2	nan		nan		241,8	1	0
Smurf1 *	0	0	2	nan			141,3	103	1	0
Rnf115 *	0	0	2	nan		nan		139,5	1	0
Atp11a *	0	0	2	nan		nan		281,2	1	0
Klhl13 *	0	0	2	nan		nan		115	1	0
Lhcgr *	0	0	2	nan		nan		263,8	2	0
Fbxo7 *	0	0	2	nan		nan		109,4	1	0
Anapc10 *	0	0	2	nan			117,8	73	1	0
Adcy4 *	0	0	2	nan			245,8	214,4	2	0
Det1 *	0	0	2	nan			161,8	120,6	1	0
Rnf6 *	0	0	2	nan		nan		149,6	1	0
Htr6 *	0	0	2	nan		nan		243,7	1	0
Fbxl4 *	0	0	2	nan			147,4	103,2	1	0
Xrcc1 *	0	0	2	nan			194,6	276,2	2	0
Ano8 *	0	0	2	nan		nan		277,8	1	0
Atp8b4 *	0	0	2	nan		nan		284	2	0
Crhr2 *	0	0	2	nan			295	238,8	1	0
Dcun1d3 *	0	0	2	nan		nan		240,8	1	0
Ube3b *	0	0	2	nan			152,7	131,2	1	0
Cyba *	0	0	2	nan		nan		233,2	1	0
Ube2v2 *	0	0	2	nan		nan		106,5	1	0
Csf1 *	0	0	2	nan		nan		212,7	1	0

Pth *	0	0	2	nan		nan		239,8	1	0
Nup93 *	0	0	2		141,7		180,7	253,5	1	0
Scamp1 *	0	0	2	nan		nan		302,6	1	0
Trim21 *	0	0	2	nan		nan		135	1	0
Traip *	0	0	2	nan		nan		137,3	1	0
Ccnf *	0	0	2	nan		nan		85,8	1	0
Cops4	0	0	2	nan			157,2	152,5	1	0
Adcy7 *	0	0	2	nan		nan		216,6	2	0
Fzr1 *	0	0	2	nan			110,5	66	1	19160489
Bpifb2 *	0	0	2	nan		nan		275,8	2	0
Mc5r *	0	0	2	nan		nan		272	2	0
Fstl1 *	0	0	2	nan		nan		271,6	2	27426744
Gpr83 *	0	0	2	nan		nan		270,6	2	0
Fbxo15 *	0	0	2	nan		nan		109,5	1	0
Cntfr *	0	0	2	nan		nan		303,8	1	0
Gpbar1 *	0	0	2	nan		nan		267,2	2	0
Adrb1 *	0	0	2	nan		nan		265,6	2	0
Herc2 *	0	0	2	nan			148,8	105	1	0
Msh6	0	0	2		116,7		172,2	248,8	1	0
Aldh3b1 *	0	0	2	nan		nan		282	1	0
Sct *	0	0	2	nan		nan		267,4	2	0
Fbxl12 *	0	0	2	nan		nan		114,8	1	0
Herc3 *	0	0	2	nan			217,6	148	1	33565151
Tnc	0	0	2	nan		nan		266,8	2	33217999
Fshb *	0	0	2	nan		nan		260,4	2	0
Anapc7 *	0	0	2	nan			117,2	70,2	1	0
Anapc5 *	0	0	2	nan			118,8	74,3	1	0
Igfbp3	0	0	2	nan		nan		257,6	1	0
Arih2	0	0	2		138,5		143,5	131	1	0
Rbbp6 *	0	0	2	nan			209,8	131	1	0
Ankrd9 *	0	0	2	nan		nan		235,4	1	0
Ptgdr *	0	0	2	nan		nan		272,8	2	0
Gtf2h4 *	0	0	2		109,5		132,3	183,7	2	0
Adrb3 *	0	0	2	nan		nan		266,8	2	0
Anapc4 *	0	0	2	nan			124,4	69,4	1	0
Pth2 *	0	0	2	nan		nan		272,4	1	0
Shisa5 *	0	0	2	nan		nan		275,6	1	0
Olr1 *	0	0	2	nan		nan		276,4	2	0
Ufl1 *	0	0	2	nan			144	126,7	1	0
Fbxo2 *	0	0	2	nan		nan		107,3	1	0
Pgrmc1 *	0	0	2	nan			229,2	288,4	1	28005395
Pja2 *	0	0	2	nan		nan		140,8	1	0
Asb12 *	0	0	2	nan		nan		115	1	0
Btbd1 *	0	0	2	nan		nan		112,4	1	0
Fbxo31 *	0	0	2	nan		nan		112,8	1	0
Uba6 *	0	0	2	nan		nan		137,8	1	0
Adora2b *	0	0	2	nan		nan		256	2	34138843
Ncor1	0	0	2	nan		nan		204,8	1	0
Ube2f *	0	0	2	nan		nan		121,4	1	0
Nup50	0	0	2	nan		nan		266,2	1	0
Fbxl19 *	0	0	2	nan		nan		95,8	1	0
Mgrn1 *	0	0	2	nan		nan		134,5	1	0
Sparcl1 *	0	0	2	nan		nan		245,3	1	0
Trim32 *	0	0	2	nan		nan		132,5	1	0
Fgfr2 *	0	0	2	nan		nan		301,8	1	0
Lamtor2 *	0	0	2	nan			196,4	210,3	1	0
Trim41 *	0	0	2	nan		nan		150,6	1	0
Gpr27 *	0	0	2	nan		nan		273	2	0
Taar1 *	0	0	2	nan		nan		272	1	0
Asb13 *	0	0	2	nan		nan		117,6	1	0
Pcsk9 *	0	0	2	nan		nan		254	1	0
Lifr *	0	0	2	nan		nan		299,7	1	0

Taar9 *	0	0	2	nan		nan		274,4	2	0
Cish *	0	0	2	nan		nan		204,2	1	0
Ccnb2 *	0	0	2	nan		nan		141,8	1	0
Fbxw11 *	0	0	2	nan		nan		92,2	1	0
Fbxl13 *	0	0	2	nan		nan		114,6	1	0
Serpinb6a *	0	0	2	nan		nan		316,6	1	0
Crh *	0	0	2	nan		nan		245,6	2	0
Fbxo41 *	0	0	2	nan		nan		116,4	1	0
Csf2rb *	0	0	2	nan		nan		281,3	1	0
Klhl22 *	0	0	2	nan		nan		112,8	1	0
Espl1 *	0	0	2	nan		nan		184,8	1	0
Taar6 *	0	0	2	nan		nan		273,6	2	0
Socs1 *	0	0	2	nan		nan		102,5	1	0
Serpind1 *	0	0	2	nan		nan		261,2	1	0
Siah2 *	0	0	2	nan		nan		131,3	1	0
Spsb3 *	0	0	2	nan		nan		240,8	1	0
Rbck1 *	0	0	2	nan		nan		120,2	1	0
Rnf138 *	0	0	2	nan		nan		141,5	1	0
Kbtbd8 *	0	0	2	nan		nan		115,2	1	0
Dzip3 *	0	0	2	nan		nan		137,3	1	0
Fbxl20 *	0	0	2	nan			141,8	101,5	1	0
Hmox2 *	0	0	2	nan		nan		289,4	2	0
Cand1 *	0	0	2	nan			185	203	1	0
Rnf114 *	0	0	2	nan		nan		149,8	1	0
Stc2 *	0	0	2	nan		nan		277,6	2	0
Socs3 *	0	0	2	nan		nan		69,3	1	0
Rnf4 *	0	0	2	nan		nan		134,2	1	0
Ifngr2 *	0	0	2	nan		nan		297,5	1	0
Gps1 *	0	0	2	nan			180	157,8	1	0
Sctr *	0	0	2	nan		nan		273,6	2	0
Tmem132a *	0	0	2	nan		nan		277,2	2	0
Znrf1 *	0	0	2	nan		nan		141,2	1	0
Ormdl3 *	0	0	2		163		223,8	290,6	1	0
Aplp2 *	0	0	2	nan		nan		240,3	1	0
Slc2a3 *	0	0	2	nan			226,4	275,6	1	0
Scg2 *	0	0	2	nan		nan		273	1	0
Il10ra *	0	0	2	nan		nan		336,6	1	0
Plaur *	0	0	2	nan		nan		248	1	0
Asb6 *	0	0	2	nan		nan		112	1	0
Clec4d *	0	0	2	nan		nan		284,6	1	0
Tmc6 *	0	0	2	nan		nan		284,4	2	0
Ube2r2 *	0	0	2	nan			159,4	130,8	1	0
Ube2a *	0	0	2		120		119,2	108,2	1	0
Commd10 *	0	0	2	nan		nan		210,6	1	0
Gpr15 *	0	0	2	nan		nan		273,6	1	0
Tnfrsf12a *	0	0	2	nan		nan		317,8	1	0
Socs6 *	0	0	2	nan		nan		210,3	1	0
Dcun1d4 *	0	0	2	nan		nan		211,8	1	0
Cops7a *	0	0	2	nan		nan		161,7	1	0
Spsb1 *	0	0	2	nan		nan		114,6	1	0
Pdia6 *	0	0	2	nan			197,5	226,5	1	0
Birc5 *	0	0	2	nan		nan		183,8	1	0
Maged2 *	0	0	2	nan		nan		315,2	1	0
Cd47 *	0	0	2	nan		nan		270,8	1	32679764;29042481
Nfkbib *	0	0	2	nan		nan		274,2	1	0
Serpinc1 *	0	0	2	nan		nan		235,2	1	0
Tspan14 *	0	0	2	nan		nan		283,2	1	0
Gpha2 *	0	0	2	nan		nan		273,6	1	0
Anapc2 *	0	0	2	nan			116,7	71,3	1	0
Wfs1 *	0	0	2	nan			237	236,3	1	0
Commd6 *	0	0	2	nan		nan		192,2	1	0
Glmn *	0	0	2	nan		nan		130,2	1	0

Vgf *	0	0	2	nan		nan		274,6	1	0
Hecw2 *	0	0	2	nan		nan		151,2	1	0
Mcemp1	0	0	2	nan		nan		281,2	1	0
Tmbim1 *	0	0	2	nan		nan		299,6	1	0
Spp1 *	0	0	2	nan		nan		224,2	1	29500246;28254837
Relb *	0	0	2	nan		nan		267	1	0
Tarm1 *	0	0	2	nan		nan		285	1	0
Cdc23 *	0	0	2		147,8		111	66,8	1	0
Dmp1 *	0	0	2	nan		nan		271,8	1	0
Ambn *	0	0	2	nan		nan		271	1	0
Hvcn1 *	0	0	2	nan		nan		301,8	1	0
Fbxw4 *	0	0	2	nan			263,3	107,2	1	0
Golm1 *	0	0	2	nan		nan		276,8	2	0
Igfbp1 *	0	0	2	nan		nan		267,6	2	0
Drd5 *	0	0	2	nan		nan		265,4	1	0
Cdc27 *	0	0	2	nan			110,5	61,8	1	0
Apoa1 *	0	0	2	nan		nan		196,8	1	0
Fam20a *	0	0	2	nan		nan		243,8	1	0
Ltbp1 *	0	0	2	nan		nan		273	1	0
Scg3 *	0	0	2	nan		nan		275	1	0
Rnf7 *	0	0	2	nan			128,5	88,2	1	0
Gnas	0	0	2	nan			234,8	207	2	0
Gtf2h5 *	0	0	2	nan			137	187	2	0
Notum *	0	0	2	nan		nan		260,8	1	0
Cops8 *	0	0	2	nan		nan		161	1	0
Plk1	0	0	2		126,8		118	45,5	1	0
Glp2r *	0	0	2	nan		nan		272	2	0
Prkdc	0	0	2	nan		nan		260,8	1	24740260;17072335;15105825
Ptgir *	0	0	2	nan		nan		242,7	2	0
Prkcsh *	0	0	2	nan			203,7	234,5	1	0
Mxra8 *	0	0	2	nan		nan		275,8	1	0
Fstl3 *	0	0	2	nan		nan		272	2	0
Trim39 *	0	0	2	nan		nan		152	1	0
Nup62 *	0	0	2		139		177,5	250,3	1	0
Adm2 *	0	0	2	nan		nan		273,2	1	32229709
Lamb1 *	0	0	2	nan		nan		218,8	1	0
Gipr *	0	0	2	nan		nan		273	1	31003779
Ube2b *	0	0	2	nan		nan		102	1	0
Fbxo30 *	0	0	2	nan		nan		116,8	1	0
Serpina10 *	0	0	2	nan		nan		265,8	1	0
Fbxo32 *	0	0	2	nan		nan		98,8	1	0
Igfbp5 *	0	0	2	nan		nan		268,8	1	0
Tshb *	0	0	2	nan		nan		266,8	1	0
Gphb5 *	0	0	2	nan		nan		274	1	0
Kcnab2 *	0	0	2	nan		nan		218,2	1	0
Ndc1	0	0	2	nan		nan		302,4	1	0
Lnx1 *	0	0	2	nan		nan		133,3	1	0
Msln *	0	0	2	nan		nan		223,8	1	0
Herc1 *	0	0	2	nan		nan		140,3	1	0
Trim11 *	0	0	2	nan		nan		139,8	1	0
Agpat2	0	0	2		159		239,2	264,6	1	0
Gpr97 *	0	0	2	nan		nan		303,4	1	0
Eva1a *	0	0	2	nan		nan		276,2	1	0
Nfkbie *	0	0	2	nan		nan		280,5	1	0
Gip *	0	0	2	nan		nan		264,6	1	31977316
Herc6 *	0	0	2	nan		nan		141,4	1	0
Cul5 *	0	0	2	nan			125,7	84,3	1	0
Tulp4	0	0	2	nan			215	236	1	0
Rln1 *	0	0	2	nan		nan		273,2	1	0
Matn3 *	0	0	2	nan		nan		270,4	1	0
Mkrn1 *	0	0	2	nan		nan		144	1	0
P2rx1 *	0	0	2	nan		nan		289,4	1	0

Stk10 *	0	0	2	nan	nan		302,6	1	0
Mapkap1	0	0	3	nan		216,3	308,8	1	0
Ccdc88a	0	0	3	nan	nan		325,2	1	0
Terf1	0	0	3	nan	nan		286	1	30452555

Sc_predictions

Protein	Com	ADR_common	Predictors	Pubmed	Database
RPS9B *	2	20,2	3	0	0
RPS15	2	25,8	5	0	0
RPS18A	2	17,8	3	17174052	0
RPL32 *	2	34,8	4	0	0
RPS2 *	2	6	2	0	0
RPL25 *	2	26,3	2	0	0
RPL28 *	2	28,3	6	0	0
RPL30	2	34	5	0	0
RPL5 *	2	11,8	5	0	0
RPS28B *	2	35,3	4	0	0
RPL33A *	2	44,2	4	0	0
RPS0A *	2	17,7	1	0	0
RPS5	2	7	2	0	0
RPS19A *	2	36,3	2	0	0
RPL42B *	2	48,2	2	0	0
RPL31B *	2	66,3	3	0	0
RPS13 *	2	9,3	2	0	0
SUP45 *	2	56	1	0	0
RPS7B *	2	30,2	1	0	0
RPS3	2	5,8	2	0	0
RPS11B	2	12,5	2	0	0
RPS16A *	2	17,7	3	0	0
RPL8A	2	34,8	5	0	0
RPS22A	2	19,5	1	0	0
RPS20	2	25	5	0	0
RPS8A	2	11,5	3	0	0
RPL11A *	2	29,8	6	0	0
RPL15A *	2	29,7	4	0	0
RPS14B	2	12,3	6	0	0
RPS23A	2	17,2	5	0	0
RPS29B *	2	45,7	3	0	0
RPP0	2	26,5	6	0	0
RPS17B *	2	48,3	2	0	0
RPL3	2	16	3	0	0
RPL18A *	2	49,8	5	0	0
SUP35 *	2	64,5	1	28910422	0
RPS25A *	2	45	3	0	0
ATG4	3	148,8	1	0	0

Table_S11

Predicted LAP	ADR	Cellular senescence-association	Longevity-association	ARD-association	Druggability
PLK1	61,2	-	-	-	druggable
UBE2D2	92,2	-	-	-	-
RPS2	101,3	-	-	-	druggable
RPS3	102,2	-	-	-	-
VHL	105,3	-	-	-	druggable
RPS14	109,3	-	-	-	-
CDC27	114,8	-	-	-	-
SOCS3	117,3	-	-	-	-
RPS18	118	-	-	-	druggable
RPS9	119	-	-	-	druggable
KRAS	121,7	-	-	associated	-
FBXW7	123	-	-	-	-
RPS5	123,8	-	-	-	-
ITCH	124	-	-	-	-
RPS11	124,3	-	-	-	-
CUL2	124,5	-	-	-	-
FZR1	126	-	-	-	-
UBR4	127,3	-	-	-	-
RPS13	128,2	-	-	-	druggable
CDC23	128,8	-	-	-	-
AURKB	129	-	-	-	druggable
RPSA	129,2	-	-	-	-
RPS8	130,2	-	-	-	druggable
RPL11	131,5	-	-	-	druggable
RPS7	132,5	-	-	-	-
FBXW11	133	-	-	-	-
ADCY3	133	-	-	-	-
UBE2V2	133,3	-	-	-	-
RPL5	135,2	-	-	-	-
RPS20	135,2	-	-	-	-
RPS15A	135,2	-	-	-	-
ADCY8	135,8	-	-	-	-
SMURF2	136,5	associated	-	-	-
RPS3A	137,3	-	-	-	-
RPS16	137,5	-	-	-	-
ANAPC1	138,3	-	-	-	-
ADCY7	140,2	-	-	-	-
PARK2	140,2	-	-	-	-
ADCY1	140,2	-	-	-	druggable
ADCY6	140,8	-	associated	-	-
RPL8	141	-	-	-	-
ANAPC7	142,3	-	-	-	-
ADCY4	142,5	-	-	-	-
RPS15	143,2	-	-	-	-
ANAPC4	144,3	-	-	-	-
RPS23	144,3	-	-	-	-
ANAPC2	144,8	-	-	-	-
ANAPC10	146	-	-	-	-
RPL23A	146,3	-	-	-	-
ANAPC5	147,7	-	-	-	-
KEAP1	148,5	-	-	-	druggable
CUL5	150,2	-	-	-	-
RPL23	151,7	-	-	-	-
SMURF1	151,8	-	-	-	-
WWP1	152,3	associated	-	-	-
UBE3A	152,7	-	-	-	-
RPLP0	154,5	-	-	-	-
CDC26	155,3	-	-	-	-
FBXL19	155,7	-	-	-	-
RPS19	157,2	-	-	-	druggable
RPS28	157,3	-	-	-	druggable
SOCS1	158,2	associated	associated	-	druggable
FBXW5	159,7	-	-	-	-
FBXO7	160,7	-	-	-	-
NEDD4	163,2	-	-	-	-
UBA1	164,3	-	-	-	-
HUWE1	165,2	-	-	-	-
UBE2B	165,3	-	-	-	-

HERC2	165,5	-	-	-	druggable
CCNF	165,5	-	-	-	-
UBE2A	166	-	-	-	-
TRIM21	166,8	-	-	-	-
RPL30	167,2	-	-	-	-
GNB2L1	168	-	-	-	-
UBA3	168,8	-	-	-	druggable
RPL15	169	-	-	-	druggable
RPS29	169,2	-	-	-	-
RNF7	169,2	-	-	-	-
RPL3	170,3	-	-	-	druggable
RPS25	170,3	-	-	-	-
RPL37A	171,5	-	-	-	-
CBLB	172	-	-	-	druggable
RPL12	173	-	-	-	-
RPL18A	173,7	-	-	-	-
FBXO32	174,3	-	-	-	-
RPL27A	176,3	-	-	-	-
FBXL3	177	-	-	-	-
RPS21	177,2	-	-	-	-
RNF4	178	-	-	-	-
FBXL5	178,2	-	-	-	-
RPL35	178,5	-	-	-	druggable
FBXW4	178,7	-	-	-	-
UBE2L6	180,5	-	-	-	-
RPL7	180,8	-	-	-	-
RPL6	180,8	-	-	-	-
RPL32	181,7	-	-	-	-
FBXO4	182,7	-	-	-	-
FBXW2	183	-	-	-	-
TRIP12	183,5	-	-	-	-
KLHL2	185	-	-	-	-
RPS17	185,8	-	-	-	-
FBXO11	186	-	-	-	-
RPS10	186,2	-	-	-	-
RPL27	186,7	-	-	-	-
ASB6	186,8	-	-	-	-
RPL31	187	-	-	-	-
FBXO2	187,2	-	-	-	-
FBXW8	187,3	-	-	-	-
RPL13	188	-	-	-	druggable
GAN	188,3	-	-	-	-
FBXL15	188,8	-	-	-	-
UBE2K	189,2	-	-	-	-
RPL38	189,8	-	-	-	-
LRR1	190,2	-	-	-	-
ASB7	190,2	-	-	-	-
KLHL22	190,5	-	-	-	-
CUL7	191,2	-	-	-	-
BTBD1	191,2	-	-	-	-
FBXO9	191,3	-	-	-	-
VPRBP	191,5	-	-	-	-
RPL7A	191,7	-	-	-	-
FBXL13	191,7	-	-	-	-
ASB4	192,2	-	-	-	-
LNX1	192,2	-	-	-	-
ASB2	192,3	-	-	-	-
SIAH1	193,2	-	-	-	druggable
KLHL13	193,2	-	-	-	-
KCTD6	193,3	-	-	-	-
FBXO31	193,5	associated	-	-	-
KCTD7	193,5	-	-	-	-
KBTBD7	193,5	-	-	-	-
FBXL12	194	-	-	-	-
FBXO17	194	-	-	-	-
FBXW9	194	-	-	-	-
KLHL3	194,2	-	-	-	-
KLHL9	194,7	-	-	-	-
KLHL42	194,8	-	-	-	-

ASB15	195	-	-	-	-
WSB1	195,3	-	-	-	-
KLHL20	195,3	-	-	-	-
ASB9	195,3	-	-	-	-
LTN1	195,5	-	-	-	-
ASB1	195,5	-	-	-	-
FBXO27	195,8	-	-	-	-
FBXL4	196	-	-	-	-
FBXL14	196,2	-	-	-	-
SPSB1	196,2	-	-	-	-
FBXO15	196,3	-	-	-	-
ASB11	196,3	-	-	-	-
ASB10	196,3	-	-	-	-
RBCK1	196,3	-	-	-	-
ASB12	196,5	-	-	-	-
KBTBD13	196,7	-	-	-	-
BTBD6	197,2	-	-	-	-
FBXL18	197,3	-	-	-	-
FBXO40	197,5	-	-	-	-
KBTBD8	197,5	-	-	-	-
FBXO10	198	-	-	-	-
FBXL20	198,2	-	-	-	-
FBXO21	198,3	-	-	-	-
FBXL16	198,5	-	-	-	-
DET1	198,5	-	-	-	-
FBXO30	198,5	-	-	-	-
KLHL11	198,7	-	-	-	-
KLHL21	198,8	-	-	-	-
ASB14	199,3	-	-	-	-
ASB5	199,5	-	-	-	-
SPSB2	199,5	-	-	-	-
ASB16	199,7	-	-	-	-
RPL21	200	-	-	-	-
SPSB4	200,2	-	-	-	-
ASB13	200,5	-	-	-	-
ASB17	200,5	-	-	-	-
ASB18	200,7	-	-	-	-
FBXO41	200,7	-	-	-	-
KLHL25	200,7	-	-	-	-
FBXL8	201	-	-	-	-
PSMD2	201,8	-	-	-	druggable
KLHL5	202	-	-	-	-
ANAPC13	202	-	-	-	-
UBE2F	202	-	-	-	-
CCNB2	202	-	-	-	-
RCHY1	202,2	-	-	-	-
RPL35A	202,5	-	-	-	-
UBE2E3	203,8	-	-	-	-
RPL36	204	-	-	-	-
SIAH2	204,7	-	-	-	-
RBBP6	204,7	-	-	-	-
UBA7	206,5	-	-	-	-
TRIM32	206,7	-	-	-	-
TRIM63	207,2	-	-	-	-
UBA6	207,8	-	-	-	-
UBE4A	208	-	-	-	-
TACR1	208,8	-	-	-	druggable
UBE2H	209	-	associated	-	-
RPL34	209,3	-	-	-	-
UBE2G2	209,7	-	-	-	-
UBE2E2	209,7	-	-	-	-
GLMN	211	-	-	-	-
RNF41	211,2	-	-	-	-
HECW2	212	-	associated	-	-
UBA5	212,3	-	-	-	-
UBE2O	212,7	-	-	-	-
PSMA1	212,8	-	-	-	druggable
UBAC1	214,8	-	-	-	-
BUB1	214,8	-	-	-	-

PJA1	215,2	-	-	-	-
MIB2	215,3	-	-	-	-
HERC6	215,3	-	-	-	-
MEX3C	216	-	-	-	-
DTX3L	216,7	-	-	-	-
UBOX5	217	-	-	-	-
RPLP2	217,2	-	-	-	-
UBE3C	217,5	-	-	-	-
UBE2W	218,3	-	-	-	-
LRSAM1	218,5	-	-	-	-
MGRN1	218,7	-	-	-	-
TRIM37	219,2	-	-	-	-
RLIM	219,5	-	-	-	-
UBE2J2	219,8	-	-	-	-
RNF123	220	-	-	-	-
TRAIP	220	-	-	-	-
DZIP3	220,7	-	associated	-	-
TRIM39	220,8	-	-	-	-
RNF115	221	-	-	-	-
MKRN1	221,3	-	-	-	-
UBE2G1	221,5	-	-	-	-
ZNRF2	221,8	-	-	-	-
UBE2Z	222,2	-	-	-	-
RNF114	222,7	-	-	-	-
TRIM41	222,7	-	-	-	-
UBR2	222,7	-	-	-	-
MYLIP	223,7	-	associated	-	druggable
TRIM69	223,8	-	-	-	-
UBE2R2	224,3	-	-	-	-
TRIM11	224,3	-	-	-	-
RNF19B	224,5	-	-	-	-
TRIM50	224,5	-	-	-	-
HERC1	224,7	-	-	-	-
UBE3D	225,2	-	-	-	-
ARIH2	225,2	-	-	-	-
TRIM9	225,3	-	-	-	-
TRIM36	225,3	-	-	-	-
RNF144B	225,5	-	-	-	-
RNF130	225,7	-	-	-	-
RNF34	225,8	-	-	-	-
HERC3	226	-	-	-	-
UFL1	226,3	-	-	-	-
TRAF7	226,7	-	-	-	-
RNF19A	226,8	-	-	-	-
AREL1	227	-	-	-	-
TRIM71	227,2	-	-	-	-
UBE2Q2	227,2	-	-	-	-
RNF6	227,7	-	-	-	-
PJA2	227,8	-	-	-	-
HECTD3	228,3	-	-	-	-
BIRC5	228,7	-	-	-	druggable
RNF138	229,2	-	-	-	-
ZNRF1	229,8	-	-	-	-
UBE3B	229,8	-	-	-	-
RNF25	230,5	-	-	-	-
RNF182	231,2	-	-	-	-
PSMD12	231,7	-	-	-	druggable
RPL28	231,8	-	-	-	-
NSA2	231,8	-	-	-	-

TableS11

Homology code	STRING identifier	Alliance identifier	Protein symbol
--H1	4932.YDL075W	SGD:S000002233	RPL31A
--H1	6239.W09C5.6a	WB:WBGene00004445	RPL-31
--H2	6239.F35G12.10.1	WB:WBGene00000206	ASB-1
--H2	6239.F02E8.1.3	WB:WBGene00000207	ASB-2
--H3	6239.Y24D9A.4a	WB:WBGene00004419	RPL-7A
--H3	4932.YLL045C	SGD:S000003968	RPL8B
--H4	6239.R04A9.4	WB:WBGene00002060	IFE-2
--H4	6239.F53A2.6a	WB:WBGene00002059	IFE-1
--H5	4932.YOR089C	SGD:S000005615	VPS21
--H5	6239.F26H9.6	WB:WBGene00004268	RAB-5
--H6	6239.H28O16.1a	WB:WBGene00010419	H28O16.1
--H6	4932.YBL099W	SGD:S000000195	ATP1
--H7	7227.FBpp0082682	FB:FBgn0010379	Akt1
--H7	4932.YKL126W	SGD:S000001609	YPK1
--H7	4932.YHR205W	SGD:S000001248	SCH9
--H7	6239.C12D8.10b	WB:WBGene00000102	AKT-1
--H7	6239.Y47D3A.16	WB:WBGene00012929	RSKS-1
--H7	10090.ENSMUSP00000001780	MGI:87986	Akt1
--H7	7227.FBpp0305462	FB:FBgn0283472	S6k
--H7	9606.ENSP00000451828	HGNC:391	AKT1
--H8	4932.YER020W	SGD:S000000822	GPA2
--H8	6239.C34D1.3	WB:WBGene00003850	ODR-3
--H9	6239.Y47D3A.4	WB:WBGene00000519	CKU-70
--H9	9606.ENSP00000352257	HGNC:4055	XRCC6
--H10	6239.C15F1.7a	WB:WBGene00004930	SOD-1
--H10	7227.FBpp0305736	WB:WBGene00004930	Sod
--H10	4932.YJR104C	SGD:S000003865	SOD1
--H10	9606.ENSP00000270142	HGNC:11179	SOD1
--H11	10090.ENSMUSP00000017290	MGI:104537	Brca1
--H11	9606.ENSP00000418960	HGNC:1100	BRCA1
--H12	4932.YGL180W	SGD:S000003148	ATG1
--H12	7227.FBpp0289788	FB:FBgn0260945	Atg1
--H13	6239.B0285.1b	WB:WBGene00007135	CDTL-7
--H13	4932.YKL139W	SGD:S000001622	CTK1
--H14	9606.ENSP00000263253	HGNC:3373	EP300
--H14	9606.ENSP00000262367	HGNC:2348	CREBBP
--H15	9606.ENSP00000289153	HGNC:8976	PIK3CB
--H15	6239.B0334.8	WB:WBGene00000090	AGE-1
--H15	9606.ENSP00000263967	HGNC:8975	PIK3CA
--H16	9606.ENSP00000362649	HGNC:4852	HDAC1
--H16	9606.ENSP00000430432	HGNC:4853	HDAC2
--H16	4932.YNL330C	SGD:S000005274	RPD3
--H17	4932.YDR500C	SGD:S000002908	RPL37B
--H17	4932.YLR185W	SGD:S000004175	RPL37A
--H18	6239.C32D5.9	WB:WBGene00002980	LGG-1
--H18	4932.YBL078C	SGD:S000000174	ATG8
--H19	4932.YOR369C	SGD:S000005896	RPS12
--H19	6239.F54E7.2.3	WB:WBGene00004481	RPS-12
--H20	10090.ENSMUSP00000106278	MGI:1351320	Trp53bp1
--H20	4932.YDR217C	SGD:S000002625	RAD9
--H20	9606.ENSP00000371475	HGNC:11999	TP53BP1
--H21	4932.YGR108W	SGD:S000003340	CLB1
--H21	4932.YPR119W	SGD:S000006323	CLB2
--H22	9606.ENSP00000376345	HGNC:4566	GRB2
--H22	6239.C14F5.5	WB:WBGene00004774	SEM-5

--H23	4932.YML073C	SGD:S000004538	RPL6A
--H23	4932.YLR448W	SGD:S000004440	RPL6B
--H24	6239.F43C1.2b	WB:WBGene00003401	MPK-1
--H24	4932.YGR040W	SGD:S000003272	KSS1
--H24	9606.ENSP00000263025	HGNC:6877	MAPK3
--H25	4932.YHR021C	SGD:S000001063	RPS27B
--H25	4932.YKL156W	SGD:S000001639	RPS27A
--H26	4932.YCR005C	SGD:S000000598	CIT2
--H26	4932.YNR001C	SGD:S000005284	CIT1
--H27	7227.FBpp0288669	FB:FBgn0283499	InR
--H27	6239.Y55D5A.5a	WB:WBGene00000898	DAF-2
--H27	9606.ENSP00000268035	WB:WBGene00000898	IGF1R
--H28	4932.YDL066W	SGD:S000002224	IDP1
--H28	4932.YLR174W	SGD:S000004164	IDP2
--H28	6239.F59B8.2b	WB:WBGene00010317	IDH-1
--H29	9606.ENSP00000351777	HGNC:12666	VCP
--H29	6239.C06A1.1	WB:WBGene00007352	CDC-48.1
--H30	9606.ENSP00000287820	HGNC:9236	PPARG
--H30	6239.F11A1.3a	WB:WBGene00000908	DAF-12
--H30	10090.ENSMUSP00000000450	MGI:97747	Pparg
--H31	9606.ENSP00000372023	HGNC:16627	CHEK2
--H31	10090.ENSMUSP00000066679	MGI:1355321	Chek2
--H31	4932.YDL101C	SGD:S000002259	DUN1
--H32	10090.ENSMUSP00000028610	MGI:88271	Cat
--H32	4932.YGR088W	SGD:S000003320	CTT1
--H32	4932.YDR256C	SGD:S000002664	CTA1
--H32	7227.FBpp0074825	FB:FBgn0000261	Cat
--H32	9606.ENSP00000241052	HGNC:1516	CAT
--H33	6239.D1007.6.2	WB:WBGene00004479	RPS-10
--H33	4932.YMR230W	SGD:S000004843	RPS10B
--H34	6239.F40F11.1.2	WB:WBGene00004480	RPS-11
--H34	4932.YDR025W	SGD:S000002432	RPS11A
--H35	4932.YHR171W	SGD:S000001214	ATG7
--H35	7227.FBpp0085891	FB:FBgn0034366	Atg7
--H35	6239.M7.5	WB:WBGene00010882	ATG-7
--H36	7227.FBpp0080003	FB:FBgn0021796	Tor
--H36	6239.B0261.2a	WB:WBGene00002583	LET-363
--H36	10090.ENSMUSP00000099510	MGI:1928394	Mtor
--H36	9606.ENSP00000354558	HGNC:3942	MTOR
--H36	4932.YJR066W	SGD:S000003827	TOR1
--H37	9606.ENSP00000344456	HGNC:2514	CTNNB1
--H37	6239.C54D1.6	WB:WBGene00000238	BAR-1
--H37	4932.YEL013W	SGD:S000000739	VAC8
--H38	9606.ENSP00000360266	HGNC:6204	JUN
--H38	4932.YEL009C	SGD:S000000735	GCN4
--H39	9606.ENSP00000378974	HGNC:6881	MAPK8
--H39	6239.B0478.1a	WB:WBGene00002178	JNK-1
--H39	7227.FBpp0079676	FB:FBgn0000229	bsk
--H39	7227.FBpp0080111	FB:FBgn0024846	p38b
--H39	9606.ENSP00000229795	HGNC:6876	MAPK14
--H40	10090.ENSMUSP00000022971	MGI:97250	Myc
--H40	9606.ENSP00000479618	MGI:97250	MYC
--H40	7227.FBpp0303995	FB:FBgn0262656	dm
--H41	6239.F10B5.1.2	WB:WBGene00004421	RPL-10
--H41	4932.YLR075W	SGD:S000004065	RPL10
--H42	10090.ENSMUSP00000104298	MGI:98834	Trp53

--H42	9606.ENSP00000269305	HGNC:11998	TP53
--H43	6239.B0041.4	WB:WBGene00004415	RPL-4
--H43	4932.YBR031W	SGD:S000000235	RPL4A
--H44	6239.C26E6.9c	WB:WBGene00004782	SET-2
--H44	4932.YHR119W	SGD:S000001161	SET1
--H45	4932.YDL082W	SGD:S000002240	RPL13A
--H45	4932.YMR142C	SGD:S000004750	RPL13B
--H46	4932.YEL024W	SGD:S000000750	RIP1
--H46	6239.F42G8.12	WB:WBGene00002162	ISP-1
--H47	4932.YLR048W	SGD:S000004038	RPS0B
--H47	6239.B0393.1.1	WB:WBGene00004469	RPS-0
--H48	4932.YOR065W	SGD:S000005591	CYT1
--H48	6239.C54G4.8	WB:WBGene00000869	CYC-1
--H49	4932.YJR121W	SGD:S000003882	ATP2
--H49	6239.C34E10.6.1	WB:WBGene00000229	ATP-2
--H50	9606.ENSP00000355759	HGNC:270	PARP1
--H50	10090.ENSMUSP00000027777	MGI:1340806	Parp1
--H51	6239.Y48G8AL.8a	WB:WBGene00004429	RPL-17
--H51	4932.YJL177W	SGD:S000003713	RPL17B
--H52	10090.ENSMUSP00000113388	MGI:107202	Atm
--H52	9606.ENSP00000278616	HGNC:795	ATM
--H53	9606.ENSP00000407586	HGNC:5173	HRAS
--H53	6239.ZK792.6	WB:WBGene00002335	LET-60
--H53	4932.YNL098C	SGD:S000005042	RAS2
--H54	9606.ENSP00000306245	HGNC:3796	FOS
--H54	9606.ENSP00000387699	HGNC:2345	CREB1
--H55	4932.YHR203C	SGD:S000001246	RPS4B
--H55	4932.YJR145C	SGD:S000003906	RPS4A
--H56	4932.YLR362W	SGD:S000004354	STE11
--H56	4932.YJL095W	SGD:S000003631	BCK1
--H57	6239.R13A5.8	WB:WBGene00004420	RPL-9
--H57	4932.YGL147C	SGD:S000003115	RPL9A
--H57	4932.YNL067W	SGD:S000005011	RPL9B
--H58	4932.YIL052C	SGD:S000001314	RPL34B
--H58	4932.YER056C-A	SGD:S000002135	RPL34A
--H59	9606.ENSP00000361021	HGNC:9588	PTEN
--H59	7227.FBpp0088843	FB:FBgn0026379	Pten
--H59	10090.ENSMUSP00000013807	MGI:109583	Pten
--H59	6239.T07A9.6	WB:WBGene00000913	DAF-18
--H60	9606.ENSP00000385824	HGNC:3821	FOXO3
--H60	7227.FBpp0293589	FB:FBgn0038197	foxo
--H60	6239.R13H8.1h	WB:WBGene00000912	DAF-16
--H60	9606.ENSP00000368880	HGNC:3819	FOXO1
--H61	4932.YJR045C	SGD:S000003806	SSC1
--H61	6239.C37H5.8	WB:WBGene00002010	HSP-6
--H62	4932.YPL120W	SGD:S000006041	VPS30
--H62	6239.T19E7.3	WB:WBGene00000247	BEC-1
--H63	9606.ENSP00000293328	HGNC:11367	STAT5B
--H63	9606.ENSP00000264657	HGNC:11364	STAT3
--H64	4932.YOR374W	SGD:S000005901	ALD4
--H64	4932.YMR169C	SGD:S000004779	ALD3
--H64	4932.YPL061W	SGD:S000005982	ALD6
--H65	7227.FBpp0077451	FB:FBgn0000490	dpp
--H65	6239.B0412.2	WB:WBGene00000903	DAF-7
--H66	4932.YLL039C	SGD:S000003962	UBI4
--H66	9606.ENSP00000304697	HGNC:12463	UBB

--H67	4932.YKL166C	SGD:S000001649	TPK3
--H67	4932.YPL203W	SGD:S000006124	TPK2
--H67	4932.YJL164C	SGD:S000003700	TPK1
--H68	6239.F39B2.6.2	WB:WBGene00004495	RPS-26
--H68	4932.YER131W	SGD:S000000933	RPS26B
--H69	9606.ENSP00000269571	HGNC:3430	ERBB2
--H69	6239.ZK1067.1c	WB:WBGene00002299	LET-23
--H69	9606.ENSP00000275493	HGNC:3236	EGFR
--H70	6239.C52E4.4.1	WB:WBGene00004501	RPT-1
--H70	4932.YKL145W	SGD:S000001628	RPT1
--H71	4932.YBL027W	SGD:S000000123	RPL19B
--H71	6239.C09D4.5.1	WB:WBGene00004431	RPL-19
--H71	4932.YBR084C-A	SGD:S000002156	RPL19A
--H72	4932.YDR477W	SGD:S000002885	SNF1
--H72	6239.T01C8.1b	WB:WBGene00020142	AAK-2
--H73	4932.YBL045C	SGD:S000000141	COR1
--H73	6239.F56D2.1	WB:WBGene00018963	UCR-1
--H74	10090.ENSMUSP00000007012	MGI:98352	Sod2
--H74	6239.F10D11.1.2	WB:WBGene00004931	SOD-2
--H74	7227.FBpp0086226	FB:FBgn0010213	Sod2
--H74	9606.ENSP00000446252	HGNC:11180	SOD2
--H74	4932.YHR008C	SGD:S000001050	SOD2
--H75	6239.Y53C10A.12	WB:WBGene00002004	HSF-1
--H75	4932.YHR206W	SGD:S000001249	SKN7
--H76	9606.ENSP00000372088	HGNC:9817	RAD51
--H76	4932.YER095W	SGD:S000000897	RAD51
--H77	4932.YPL079W	SGD:S000006000	RPL21B
--H77	4932.YBR191W	SGD:S000000395	RPL21A
--H78	6239.F53G12.10.1	WB:WBGene00004418	RPL-7
--H78	4932.YGL076C	SGD:S000003044	RPL7A
--H79	7227.FBpp0080015	FB:FBgn0024291	Sir2
--H79	6239.R11A8.4a	WB:WBGene00004800	SIR-2.1
--H79	9606.ENSP00000212015	HGNC:14929	SIRT1
--H79	4932.YDL042C	SGD:S000002200	SIR2
--H79	10090.ENSMUSP00000101082	MGI:2135607	Sirt1
--H79	4932.YOL068C	SGD:S000005429	HST1
--H80	7227.FBpp0082147	FB:FBgn0013277	Hsp70Ba
--H80	9606.ENSP00000364802	HGNC:5232	HSPA1A
--H80	9606.ENSP00000432083	HGNC:5241	HSPA8
--H81	4932.YKL085W	SGD:S000001568	MDH1
--H81	4932.YOL126C	SGD:S000005486	MDH2
--H81	6239.F20H11.3	WB:WBGene00003162	MDH-2
--H82	4932.YDR099W	SGD:S000002506	BMH2
--H82	4932.YER177W	SGD:S000000979	BMH1
--H82	9606.ENSP00000379287	HGNC:12855	YWHAZ
--H83	4932.YPL090C	SGD:S000006011	RPS6A
--H83	6239.Y71A12B.1a	WB:WBGene00004475	RPS-6
--H84	4932.YER040W	SGD:S000000842	GLN3
--H84	9606.ENSP00000329357	HGNC:11205	SP1
--H84	4932.YDR146C	SGD:S000002553	SWI5
--H85	4932.YGL049C	SGD:S000003017	TIF4632
--H85	4932.YGR162W	SGD:S000003394	TIF4631
--H85	6239.M110.4a	WB:WBGene00002066	IFG-1
--H86	6239.F25H5.4a.1	WB:WBGene00001167	EEF-2
--H86	4932.YOR133W	SGD:S000005659	EFT1
--H86	4932.YDR385W	SGD:S000002793	EFT2

--H87	4932.YDR069C	SGD:S000002476	DOA4
--H87	4932.YMR223W	SGD:S000004836	UBP8
--H88	4932.YCL040W	SGD:S000000545	GLK1
--H88	4932.YGL253W	SGD:S000003222	HXK2
--H89	4932.YBR245C	SGD:S000000449	ISW1
--H89	4932.YOR304W	SGD:S000005831	ISW2
--H90	9606.ENSP00000302665	HGNC:5464	IGF1
--H90	10090.ENSMUSP00000056668	MGI:96432	Igf1
--H91	4932.YML001W	SGD:S000004460	YPT7
--H91	6239.W03C9.3.2	WB:WBGene00004271	RAB-7